SYNTHESIS AND CHARACTERIZATION OF CdSe QUANTUM DOTS FOR SOLAR CELL APPLICATIONS

MASTER OF SCIENCE DISSERTATION

BY

SINOVUYO MAKINANA
(201101763)

A dissertation submitted to University of Fort Hare Faculty of Science and Agriculture in fulfilment of the requirement for the degree of Master of Science in Chemistry

Supervisor: Doctor Raymond Taziwa
Co-Supervisors: Professor Edson L. Meyer
Professor Omobola Okoh

DECLARATION

I, ***SINOVUYO MAKINANA*** declare that where due acknowledgement has been made, the work presented herein is that of the author alone; submitted in fulfilment for a Master of Science (MSc) degree in department of Pure & Applied Chemistry and Fort Hare institute of Technology (FHIT) at the University of Fort Hare.

I, therefore, certify that the work has not been submitted before, in whole or in part to qualify for any other academic award; the content of the dissertation is the result of the work carried out since the authorised commencement date of the approved research project; any editorial work carried out by a third party is acknowledged; and ethics procedures and conditions have been followed.

Signature…… Date……..…..

DEDICATION

This work is dedicated to my late mother, Xoliswa Gloria Makinana, my father Lungani Ted Makinana, my daughter Alunamida Sinogcobo Makinana and my siblings (Odwa and Mahlubi Makinana).

ACKNOWLEDGEMENTS

Above all, I would like to thank God for blessing me with the gift of life, for giving me this opportunity and giving me the strength to complete this research.

I owe my deepest gratitude to my supervisors, Prof. E. L Meyer, Fort Hare Institute of Technology (FHIT), Dr R. T Taziwa, Department of Chemistry and Fort Hare Institute of Technology (FHIT) and Prof O. Okoh, Department of Chemistry for their guidance, encouragements, and support during the course of this work. Without their tireless efforts and constant help this research would not have been possible.

I would also like to express my deep appreciation to the Fort Hare Institute of Technology and Chemistry Department for providing chemicals needed to complete my Masters in Science in Chemistry. Many thanks also to all research group members (PV research group) at Fort Hare Institute of Technology for their support.

Many thanks to Doctor Raymond Taziwa (UFH) for helping with Confocal Raman Microscopy, Mr Mcako (UFH) for his assistance with UV-Vis and FTIR measurements and Miranda Waldron (UCT) for the helping with XRD and HRTEM analysis. I say to all of them, thank you.

I am grateful for the financial support rendered by National Research Foundation (NRF) and Govan Mbeki Research and Development Centre (GMRDC) of the University of Fort Hare.

A special gratitude and love goes to my family for their unfailing love and support.

ABSTRACT

This study shows a detailed report on the ***morphological***, ***structural*** and ***optical*** properties of CdSe QDs synthesised by the ***hot injection method***. Cadmium acetate dihydrate and Se powder were used as cadmium and selenide precursors, respectively. Various QD sizes were achieved by synthesizing in temperature range of 150ºC, 175ºC, 200ºC, 225ºC, 250ºC, 275ºC and 300ºC, respectively. The as synthesized QDs by the hot injection method were cross-examined for their ***morphological***, ***structural*** and ***optical*** using HRTEM, FTIR, XRD, RS, and UV-Vis spectroscopy techniques respectively. FTIR analysis has revealed vibrations at 738, 738, 738, 738, 735, 735 and 733 cm^{-1} for the QDs synthesized at various temperatures of 150, 175, 200, 225, 250, 275, and 300℃, respectively. The presence of the above mentioned peaks confirms the presence of Cd-Se bond in our samples. XRD analysis of CdSe QDs revealed diffraction peaks at 2θ angles of 16.66°, 25.20°, 34.77°, 40.9°, 45.39° and 49.10° for 150°C; 17.40°, 25.22°, 34.85°, 41.7°, 44.45° and 47.5° for the QDs synthesized at various temperatures of 175°C; 17.07°, 25.19°, 34.85°, 41.34°, 44.41° and 48.86° for 200°C; 16.34°, 25.20°, 34.76°, 40.6°, 44.74° and 49.48° for 225°C; 17.44°, 25.17°, 34.19°, 41.70°, 44.45°, 49.24° for 250°C; 16.70°, 25.16°, 34.85°, 40.32°, 45.10° and 49.1°7 for 275°C;and 17.35°, 25.18°, 35.13°, 41.63°, 45.70°, 49.48° for 300°C . These XRD peaks relate to crystal planes of (100), (002), (102), (220), (103) and (112) which belong to hexagonal Wurtzite CdSe crystal structure. Additionally XRD analysis has revealed a general peak shift to higher 2θ values was observed for CdSe QDs. HRTEM analysis showed that the synthesised CdSe QDs have a spherical shape and are monodispersed. Moreover, HRTEM analysis has revealed CdSe QDs modal crystallite size of 1.79 nm, 1.81 nm, 2.06 nm, 2.08 nm, 2.11 nm, 3.10 nm and 3.12 nm for the QDs synthesized at various temperatures of 150ºC, 175ºC, 200ºC, 225ºC, 250ºC, 275ºC and 300ºC, respectively. HRTEM results were in mutual agreement with XRD results. Additionally, the SAED images showed intense electron diffraction rings, which confirmed that the as-synthesised CdSe QDs have a Wurtzite crystal structure. RS analysis

showed that CdSe QDs have LO and 2LO vibrational modes which are characteristic peaks for CdSe. The presence of these peaks in Raman spectra further supports our previous observation from XRD analysis and HRTEM analysis that the synthesized CdSe QDs have a Wurtzite crystal structure. The effect of synthesis temperature Raman peak shift, FHWH and peak intensity has been cross examined in this work, Moreover, the effect of increasing temperature on the peak shift, FWHM and peak intensity is discussed in detail below. UV-Vis analysis revealed an absorbance of CdSe QDs in higher wavelengths as temperature was increased. Furthermore, the Yu et al 2003 relation was used to calculate QD size and band gap energy of CdSe QDs. The results showed that QD size increases with increasing synthesis temperature, which is in agreement with HRTEM and XRD results.

Keywords: Morphological, Structural and Optical properties; hot injection method; CdSe, Quantum Dots

PREFACE

The supply of secure, clean and sustainable energy while limiting the global temperature increase is the biggest challenge of the 21st century. Fossil fuels cover approximately 95 % of the total energy demand worldwide. However, the major shortcomings of fossil fuel-based energy are drastic depletion of fossil fuels, emission of CO_2 which is a greenhouse gas and pose a threat to the environment. It is thus imperative to find solutions that can ensure the supply of energy with low greenhouse emissions for future generations. To achieve this goal, it is mandatory to seek alternative renewable energy sources. Solar energy is a promising alternative source of energy because it is pollution free and readily available. Solar energy technologies have emerged as superior candidates for eliminating greenhouse gas emission while at the same time providing a cost effective sustainable renewable energy resource.

Use of solar cells has attracted world-wide attention. Although the monocrystalline Silicon solar cell has achieved the highest photon conversion efficiency, their relatively high manufacturing cost has inhibited commercialization. Several new photovoltaic systems have been presented including dye-sensitized solar cells (DSSCs) (which was invented by Michael Gratzel and Brian O'Regan in 1991), multi-junction solar cells and organic solar cells. As a promising alternative to Si-based solar cells, DSSCs have played a promising role in the development of renewable energy. DSSCs are made from low-cost materials and do not require any elaborate or complicated machinery to operate. Also, they can be engineered into flexible sheets and are resilient.

DSSCs are limited by how many photons the dye can absorb. The photons that do not get absorbed are the ones that produce energy. The rate at which the photons are absorbed depends on the overlap between the absorption spectrum of the TiO_2 and the entire flux spectrum. Additionally, the major problems associated with using expensive dyes to sensitise solar cells is

still not worthwhile. Therefore, this study aims to replace these expensive molecular dyes by synthesizing CdSe QDs of various sizes to broaden the spectral response of QDSSC devices. The use of nano-sized narrow band gap semiconductor QDS as sensitizers instead of molecular dyes is preferred as an effective and favourable alternative due to a number of factors presented above.

CdSe QD is a low cost semiconducting material that presents remarkable unique properties such as tuneable band gaps achievable by changing their sizes and compositions, sharp absorption onset, large absorption coefficients and hence higher absorption. Additionally, CdSe QDs can produce more than one exciton from one high energy photon of sunlight, referred to as multiple exciton generation (MEG). CdSe QDs increase the efficiency and reduce the cost of today's typical Si PV cells. This makes them better candidates for development.

Table of Contents

LIST OF SYMBOLS

eV	Electron volts
nm	Nanometre
ml	Millilitres
g	Grams
cm	Centimetre
mm	Millimetre
λ	Wavelength
ε	Molar absorptivity constant
d	Distance
k	Shape factor
β	Beta
θ	Theta
LO	Longitudinal optical
2LO	Second (2^{nd}) mode longitudinal optical
E_g	Band gap energy
h	Planck's constant
c	Speed of light
I	Intensity of light

ACRONYMS

QD	Quantum dot
TiO_2	Titanium Dioxide
HOMO	Highest occupied molecular orbital
LUMO	Lowest unoccupied molecular orbital
DSSC	Dye sensitised solar cell
QDSSC	Quantum dot sensitised solar cell
CdSe	Cadmium selenide
PV	Photovoltaic
FTIR	Flourier transform infrared spectroscopy
HRTEM	High-resolution transmission electron microscopy
XRD	X-ray diffraction
RS	Raman spectroscopy
UV-Vis	Ultraviolet-visible spectroscopy
I-V	Current-voltage
βME	2-mercaptoethanol
FWHM	Full width at half maximum
SAED	Selected area electron diffraction
CIGS	Copper Indium Gallium Selenide
ACS	American Chemical Society
FFT	Fast Fourier Transformation

Chapter 1
Overview

1.1 Why Solar Energy?

It is predicted that by the year 2040 the rate of global energy consumption will increase by 93% and triple by the end of the century compared to the world's primary consumption in 2010, which was about 20.2 Terawatts. It is evident that the carbon rich sources such as coal, oil, uranium and natural gas are not the solution for the tremendous increase of energy demand due to their negative impact such as CO_2 emission, that affect both the environment (climate changes & pollution) and the society. Nuclear power could be a feasible way to meet the energy demand, but the problem is it has major safety issues.

On the other hand, solar energy is the most sustainable, clean and environmentally friendly source of energy that provides the earth with about 120 000 Terawatts of radiation, making solar energy an attractive source for green, sustainable and efficient energy conversion devices, such as solar cells that can be eventually combined with hydrogen fuel cells and storage devices such as batteries. These devices, solar cells in particular, are potential candidates to address the energy issues. Regardless of this, it still remains a huge challenge to find energy technologies that harvest solar energy in a cost effective manner.

Solar cells are photovoltaic devices that directly convert solar energy into electrical energy. The first p-n junction solar cell design was published by Bell Laboratories in 1954 with an efficiency of 6 % [1]. The innovation by Bell Labs produced the first viable commercial solar cell, which transformed the photovoltaic industry. Since then, major developments have been made to give photovoltaics more accessibility in the global energy market. The utmost efficient devices are currently achieving at least 43 % photoconversion efficiency [2]. The cost of these types of solar

cells is still relatively high and combine several devices into one solar cell along with the concentration of incoming light to achieve the high efficiency. Lower-cost, more easily manufactured devices have also been developed at the expense of photoconversion efficiency. Hence is its desirable to fabricate cost effective solar cells that are able to compete on the global energy market.

1.2. Photovoltaic Solar cells

The photovoltaics field deals with the conversion of light into electricity. The term "photovoltaic" was derived from the combination of "phos" (Greek work for light) and "volt" (unit for electrical voltage named after the Italian physicist Alessandro Volta). The first experimental observation of the photovoltaic effect was discovered in 1839 by Alexandre Edmond Becquerel, who established the foundations of the field. In his experiments, he detected current between two platinum electrodes immersed into an electrolyte with metal halide salts when illuminated by sunlight [3]. Since then, numerous different kinds of photovoltaic and photoelectrochemical solar cell devices have been developed [4, 5, 6], and great progress has been made in understanding the basics and operation principle of solar cells. Currently, a wide range of materials is used to fabricate solar cells and photoelectric conversion effects as high as approximately 45% have been achieved with modern day devices [7]. Fig. 1.1 shows the current best research efficiency for solar cells.

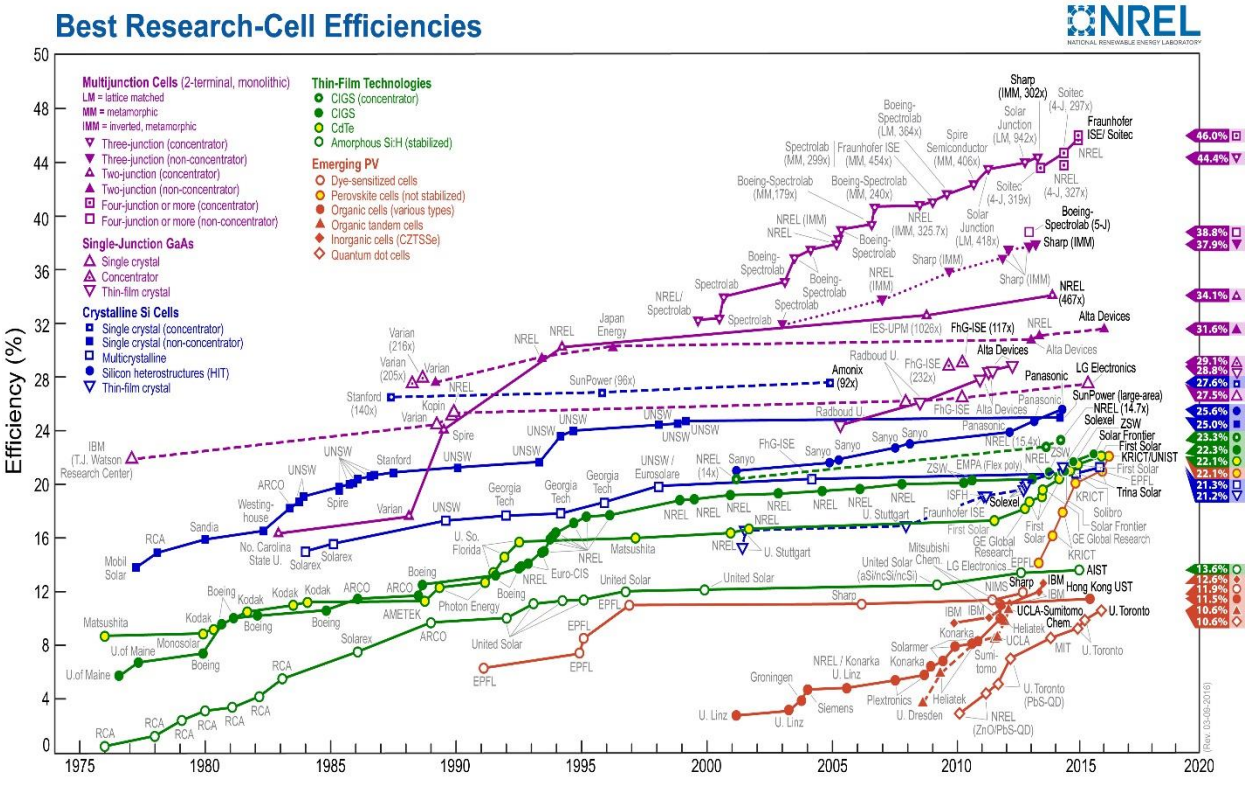

Figure 1.1: *Current efficiencies for the best research solar cells [NREL] [7].*

Generally, photovoltaic devices can be grouped into three categories- first, second and third generation solar cells- based on the nature of the materials, supreme achievable performances, production and installation costs [8]. First generation solar cells such as single junction crystalline GaAs and Si solar cells use high purity and high quality materials such as crystals. The principle these solar cells use is based on the separation of photodegraded electron-hole pairs at the interface between n-doped (electron rich) and p-doped (electron-poor) semiconductors. When n-type (Fermi level closer to conduction band) and p-type (Fermi level closer to valence band) semiconductors are brought together, electrons migrate from the n-type section into the p-type section so as to equilibrate the Fermi level (in the dark). The negative and positive space charge assembled at the vicinity of p-type and n-type materials results in the formation of a depletion layer in the p-n junction, with the electric field directed towards the p-type from the n-type

material [8]. Under radiance, the Fermi level at the p-n junction divides into two quasi-fermi levels in the p-type and n-type sections, respectively. The difference between the p-type and n-type quasi-Fermi levels gives the open circuit voltage. In the neutral regions both Quasi-Fermi levels become the same as the majority-fermi level. Currently, first generation solar cells produce the highest efficiencies both in single and multijunction devices (fig 1.1). Nevertheless, due to high production and installation costs these cells exceed the cost of R14.36/watt photoelectric power conversion [8].

Second generation solar cells, also known as thin film solar cells use less materials and low cost production, which helps to bring down the price for photoelectric power conversion to less than R14.36/watt [8]. CdTe and CIGS are typical examples of second generation solar cells [20, 21 and 22]. These solar cells produce high efficiencies e.g. 23.3% for CIGS relative to the 27.6% of single crystal Si solar cells [7]. Regardless of these very good efficiencies, issues such as the use of rare In and toxic element remain.

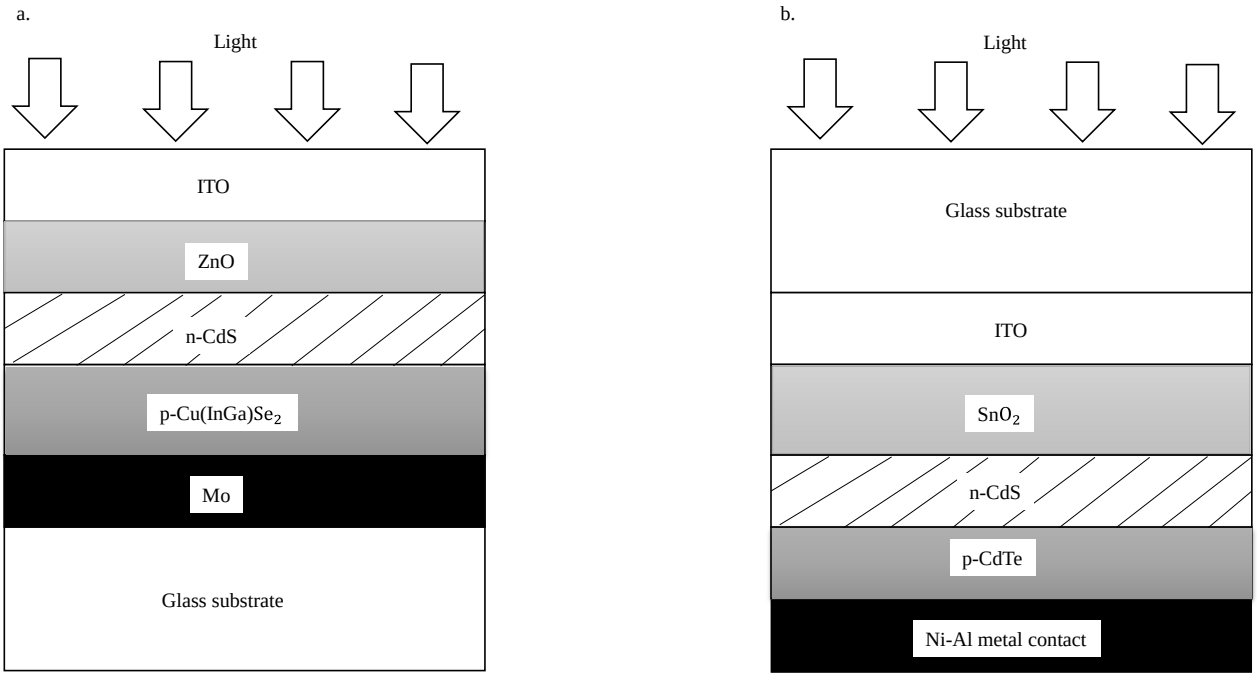

Figure 1.2: *Schematic cross-section view of thin film (a) CIGS and (b) CdTe solar cells*

In 1961, William Shockley and Hans-Joachim Queisser developed a theoretical framework for determining the limiting efficiency of a single junction solar cell based on the principle of detailed balance equating the incoming and outgoing fluxes of photons for a device at open-circuit conditions [23]. The limit is one of the most important factors for solar energy production, and is considered to be one of the most important contributions in the field [24]. They calculated the maximum theoretical efficiency for single p-n junction solar cells and found it to be 30% for an energy gap of 1.1 eV under 1 sun illumination [23]. From their analysis, it was found that this limit was due to loss mechanisms such as non-usage of the photon energies smaller than the bandgap and thermalisation of photon energies higher than the bandgap [8].

Several approaches have been suggested to overcome the Shockley-Queisser limit. One of these approaches is the up and down conversion, whereby the use of a material that can absorb more than one low energy photon and emit one photon with energy above the bandgap (also referred to as anti-stokes optical process) is proposed in the case of up conversion [8, 26]. Moreover, the multiple exciton generation (MEG) is another approach under investigation. This approach involves the use of photons with energies at least twice greater than the bandgap energy to generate and split two excitons out of one absorbed energetic photon. Additionally, the extraction of "hot" charge carriers before they thermalize is also a way to make use of energetic photons and thus increase the voltage of the cells. In light of these developments, it has been foreseen that the successful application of these methods to decrease the nonradiative losses will break the Shockley-Queisser limit for single junction solar cells. Solar cell devices that follow these approaches are known as third generation solar cells. Strictly speaking, it should be known that only quantum dot sensitised solar cells satisfy some of the criteria for a third generation solar cells. If successful, these devices promise to curb the cost for photoelectric power conversion to less than R7.18/watt [8].

In 1991, Gratzel and O'Regan pioneered in the development of dye sensitised solar cells (DSSCs) [25]. Even though they are not as good as the crystalline Si or CIGS solid state solar cells in terms of efficiency, DSSCs have been immensely studied as the next-generation solar cells because of their simple structure, light weight, and their promise to be relatively inexpensive. The recorded efficiency values of the best DSSCs with liquid and solid hole transporting materials (HTM) are about 13% and 7.2%, respectively [30, 31]. DSSCs are comprised of a mesoporous TiO_2 anode sensitised with a light absorbing dye layer and permeated by a liquid redox couple or solid HTM [32]. Under radiant light, the dye molecule absorbs a photon and becomes excited by the transfer of an electron from the highest occupied molecular orbital (HOMO) to lowest unoccupied molecular orbital (LUMO). This excited electron is rapidly injected into the conduction band of TiO_2 and travels to one of the solar cell electrodes by hopping from particle to particle. The positively charged dye undergoes an electrochemical reaction with I^- in the electrolyte to form I3- which shuttles the hole to the counter electrode where it is reduced back to I^- to repeat the cycles. DSSCs have proven to be a promising emerging photovoltaic technology; however, DSSCs have low stability, low spectral absorption inherently caused by dye complexes, high electron recombination rate and poor mechanism of transport of generated electrons from the sensitizers [25]. For these reasons, it is risky to adapt the materials to be not only cost effective but also long lasting. Additionally, so far no dye has been found that injects electrons in the whole visible and near infrared of the solar spectrum.

1.3 Quantum dots (QDs)

As already mentioned, the sensitizers commonly employed in DSSCs uses organic dyes of ruthenium polypyridine complexes. To increase the light harvesting efficiency in the visible region many efforts have been made to synthesize organic dyes of ruthenium complexes with improved visible light absorption. It has always been a challenge to obtain an ideal organic/inorganic dye sensitizer (rainbow dye) that matches the entire visible section of the solar spectrum (400-1800 nm). For this reason, narrow band-gap semiconductors such as quantum dots (QDs), have been used as photo-sensitizers instead of organic/inorganic dye as sensitizers. QDS are small crystals of semiconducting materials whose exciton undergoes quantum confinement in three spatial dimensions and is composed of about a hundred to a few thousand atoms [10]. They are made up of atoms of periodic groups of II-VI, III-VI, or IV-VI materials [11, 12 and 13]. As light absorbers QDs have drawn great interest as sensitizers in quantum dot sensitized solar cells (QDSSCs).

QDs possess versatile optical and electrical properties including: 1) a tuneable band gap depending on QD size [34], 2) a larger extinction coefficient, 3) higher stability towards natural elements such as water and oxygen, and 4) multiple exciton generation (MEG) with single-photon absorption. Another important aspect of QDs is based on their molecular-like electronic levels. QDs could make it possible to slow down the thermalisation of excitons via phonon emission when energetic photons are absorbed by the QDs. This would allow implementation of the processes such as hot carrier extraction and multiple excitons generation and splitting [8].

As the field of QDSSCs is relatively new, there is a limited amount of research gathered at this point. Because of this insufficiency, there are still many issues with QDSSCs that must be

addressed through further research. Issues such as those faced by the Schottky device are already beginning to be solved; however, there are many more ahead. The ACS Nano article states, “the optimal QDSSCs configuration has not been obtained yet, and issues as the optical absorption, charge recombination, hole scavenging, electrolyte, recombination, and series resistance (counter electrode effect) need to be improved”. Because these areas still must be improved, QDSSCs haven’t yet reached their theoretical efficiency. Additionally, researching QDSSCs is logical because their development can positively impact society as a whole. If the energy of the sun can be harnessed efficiently and cost effectively, the issues of greenhouse gas emission, limited natural resources, and dangerous mining conditions can be significantly alleviated. This project therefore has the potential to enhance quality of life by providing electricity to an otherwise impoverished community.

1.4 Quantum Dots Sensitised solar cells (QDSSCs)

The working principle of a typical QDSSC is similar to that of a DSSC. Figure 1.3 shows the schematic diagram of a typical QDSSC solar cells. QDs are deposited onto a wide bandgap metal oxide semiconducting electrode like TiO_2 and permeated by a liquid redox couple [35]. In a typical cycle, the QD is first excited by absorption of a photon from HOMO to the LUMO. In favourable conditions, the QD injects a photo-excited electron to the conduction band of TiO_2 resulting in the QD becoming oxidized. The injected electron is transported within TiO_2 and then extracted through the external load to the counter electrode to reduce the redox mediator. The QD is regenerated by electron donation from the electrolyte, usually an organic solvent containing a redox system, such as the iodide/ triiodide couple. The iodide is regenerated, in turn, by the reduction of triiodide at the counter electrode, with the circuit being completed via electron

migration through the external load [27, 28]. Overall, the device generates electric power from light without suffering any permanent chemical transformation [27].

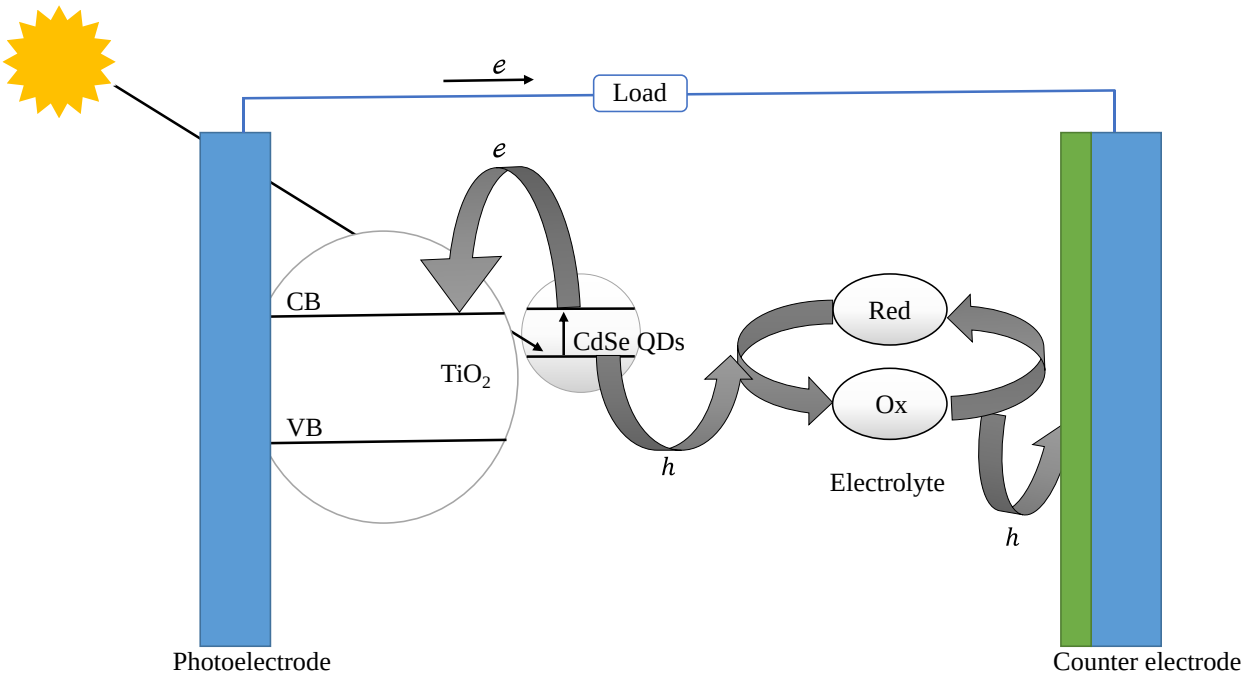

Figure 1.3: *An illustration of the working principle of a QDSSC.*

Moreover, it has been suggested that QDSSCs might offer favourable features compared to their DSSC counterparts based on the simple synthesis and processing of QDs and the abundance and variety of different materials which can be used [36]. In principle, it is believed that the size-dependant bandgap tuneability of QDs permits the harvesting of photons over the optimum spectral range and the design of multijunction cycle solar cells [33, 29]. Obviously, there are some areas that need to be improved in the field of QDSSCs, but the diversity of different possible device architectures such as liquid or solid state QDSSCs, extremely thin absorber (ETA) cells, Schottky-junction cells, fully inorganic/organic depleted or bulk heterojunction cells makes them very attractive for a wide range of applications.

1.5 Problem Statement

The use of solar cells has attracted world-wide attention. Although the monocrystalline Silicon solar cell has achieved the highest photon conversion efficiency, their relatively high manufacturing cost has inhibited their commercialization [14]. Several new photovoltaic systems have been presented including dye-sensitized solar cells (which was invented by Michael Gratzel and Brian O'Regan in 1991 [25]), multi-junction solar cells and organic solar cells. As a promising alternative to Si-based solar cells, DSSCs have played a promising role in the development of renewable energy. DSSCs are made from low-cost materials and do not require any elaborate or complicated machinery to operate. Also, they can be engineered into flexible sheets and are resilient.

This project aims to address the inherent problem with the dye molecular sensitizer used in DSSCs, which is extremely inefficient at converting absorbed photons into free electrons in the TiO_2 layer and at the same time the molecular dyes available to date absorbs a small section of the solar spectrum.

DSSCs are limited by how many photons the dye can absorb. The photons that do not get absorbed are the ones that produce energy. The rate at which the photons are absorbed depends on the overlap between the absorption spectrum of the TiO_2 and the entire flux spectrum. Additionally, the major problems associated with using expensive dyes to sensitise solar cells is still not worthwhile. Therefore, this study aims to replace these expensive molecular dyes by synthesizing CdSe QDs of various sizes to broaden the spectral response of QDSSC devices. The use of nano-sized narrow band gap semiconductor QDS as sensitizers instead of molecular dyes is preferred as an effective and favourable alternative due to a number of factors presented above.

1.6 Motivation of the Study

The motivation behind this project stands on the fact that there is a constant rise in the prices of conventional energy resources (fossil fuels) and their associated negative environmental impact. Countries like South Africa are forced to look into alternative renewable energy solutions. As such, South Africa has unambiguously acknowledged the potential of solar energy that has gone unnoticed for so long. If, however, South Africa, with almost double the annual solar resource as Europe, wants to be a meaningful global role player in solar energy in general and photovoltaics in particular, it must dramatically improve its knowledge base in this field. In this regard, the South African government's primary objective of The Ten-Year Plan for Science and Technology, is to ensure that government investment in scientific research not only strengthens the effectiveness of our National System of Innovation, but also yields tangible socio-economic benefits and human capital development for our country. The plan necessitates funding of well-structured and coordinated programmes.

The PV Spoke is well aligned and situated to contribute significantly in achieving this objective. Furthermore, the main motivation behind solar energy lies in the sole purpose of this Ten-Year Innovation Plan that is to help drive South Africa's transformation towards a knowledge-based economy, in which the production and dissemination of knowledge leads to economic benefits and enriches all fields of human endeavour. The plan proceeds from government's broad socioeconomic mandate – particularly the need to accelerate and sustain economic growth – and is built on the foundation of the national system of innovation (NSI). It recognises that while the country's science and technology system has taken important strides forward, there is a tremendous gap between South Africa and those countries identified as knowledge-driven economies. To close this gap, the NSI must become more focused on long range objectives,

including urgently confronting South Africa's failure to adequately provide in both a qualitative and quantitative sense of knowledgeable human capital capable of building a globally competitive economy. Also the main motivation behind the study is therefore to address the grand challenges in Energy to provide safe, clean, affordable and reliable energy supply and South Africa must meet its medium-term energy supply requirements while innovating for the long term in renewable energy.

The rationale behind the study is that renewables are well suited for meeting decentralized Southern Africa rural energy demand and create new jobs, increase access to clean energy and lower greenhouse emissions. Silicon solar cells have achieved significant electricity conversion efficiencies [17] However, the high fabrication cost and the usage of toxic chemicals in producing highly purified silicon during the manufacturing process has motivated this work to search for an environmentally friendly, low-cost solar cell QDSSC a derivative of the DSSC. DSSCs have received considerable attention since O'Regan and Grätzel reported a remarkably high conversion efficiency of nearly 13 % using nanocrystalline mesoporous TiO_2 film. Also a further motivation of this work is that the manufacturing cost of DSSCs, which are 3^{rd}-generation solar cells, is approximately 1/3 to 1/5 times that of silicon solar cells [18]. However, the development of a single-molecule panchromatic sensitizer still remains a molecular engineering challenge in efforts to improve the overall power conversion efficiency of DSSC device beyond 13 %. In this regard the main motivation behind the study is that new initiatives are needed to harvest photons employing nano-structured semiconductor QDs and molecular assemblies. Narrow band gap semiconductors quantum dots such as CdSe, PbS, Bi_2S_3, CdS and lnP can serves as sensitizers because they can transfer electrons to large band gap semiconductors such as TiO_2 [19] . These semiconductor quantum dots have tuneable band gap edge and can offer new opportunities to harvest light in the useful section of the solar spectrum. These narrow band gap semiconductor

nano-structures can harvest visible light if assembled on an electrode in an orderly fashion. The motivation of this study is to also address the shortcomings of the Grätzel type solar cell by synthesising and characterizing CdSe quantum dots for solar cell application. Quantum dots have a great potential to become efficient energy generators. The energy band gap of these semiconductor quantum dots can be adjusted by size to match the entire solar spectrum. Small band gap semiconductors like CdSe can act as a sensitizer because they can transfer electrons to large band gap semiconductors when illuminated in sunlight.

1.7 Aims and Objectives

Aims

[1] Synthesize CdSe Quantum dots using the hot injection method.

[2] Characterize the as synthesized CdSe QDs using FTIR, XRD, HRTEM, RS and UV-Vis spectroscopy.

Objectives

[1] To synthesize of CdSe QDs at different temperature using the hot injection

[2] To investigate the effect of synthesis temperature on the Morphological, Structural and Optical properties of CdSe QDs synthesized by the hot injection method

[3] To evaluate the structural properties of CdSe QDs using FTIR.

[4] To determine the crystal structure of CdSe QDs by using XRD.

[5] To evaluate the morphological evaluation of the CdSe QDs using HRTEM

[6] To investigate the Raman modes of CdSe QDs synthesised by hot injection method using RS.

[7] To evaluate the optical properties and particle sizes of CdSe QDs using UV-Vis spectroscopy.

1.8 Research Questions

[1] Is it possible to synthesise high quality CdSe QDs with different particle sizes using the hot injection method?

[2] Which way can precursor solutions of CdSe QDs be synthesized using the hot injection method?

[3] What is the effect of varying synthesis temperature on the morphological, structural and optical properties of CdSe QDs synthesised by the hot injection method?

[4] What is the effect of capping CdSe QDs on its crystal structure?

1.9 Limitations and Delimitations of the study

[1] This dissertation focuses on Fabrication and Characterization of CdSe QDs using the hot injection method. The application of the Fabricated CdSe QDs in QDSSC at this stage is beyond the scope of this MSc work.

[2] This dissertation focuses on evaluating the structural, morphological and optical properties of the fabricated CdSe QDs. Evaluation of the electronic properties of the CdSe QDs at this stage is beyond the scope of this dissertation.

[3] The characterization of a QDSSC is beyond the scope of this research at this level.

This dissertation is divided into five chapters. **Chapter 1** provides an overview of the work done. **Chapter 2** provides a detailed literature review on the synthesis methods available for preparing quantum dots. **Chapter 2**, also provide a review on the applications of QDs ranging from biological imaging, light emitting diodes (LEDs), to photovoltaic applications. **Chapter 3** presents experimental set up and research methodologies employed in the synthesis of CdSe QDs.

Chapter 3 also presents the detailed experimental procedures used in the morphological, structural and optical characterization of the CdSe QDs. **Chapter 4** presents the major research findings from this work. **Chapter 4** presents and discusses in detail effect of synthesis temperature on the morphological, structural and optical properties of CdSe QDs. This work signs off by presenting the concluding remarks and future recommendations in **Chapter 5**.

1.10 References

[1] D. M. Chapin; C. S. Fuller & G. L. Pearson. *A New Silicon p-n Junction Photocell for Converting Solar Radiation into Electrical Power*. Journal of Applied Physics. 25 **(1954)** 676–677

[2] M.A. Green, A. Ho- Baillie. *Forty-three per cent composite split-spectrum concentrator solar cell efficiency*. Progress in Photovoltaics.18 **(2010)** 42-47.

[3] P. Wolfgang. *Power for the World-The Emergence of Electricity from the Sun*. World Council for Renewable Energy, Belgium. Pan Stanford Publishing. **(2010)** 6

[4] D.L. Pulfrey. *Photovoltaic power generation*. Van Nostrand Reinhold, New York. **(1978)** 230

[5] H. Gerischer. *Photovoltaic and photoelectrochemical energy conversion*. In F. Cardon, W.P. Gomez, W. Dekeyser (Eds). NATO ASI summer school. vol. B69. Plenum Press, New York. **(1981)** 129-262

[6] S. Wieder. *An introduction to solar energy for scientists and engineers*. Krier Publisher, Florida, USA. 5 **(1992)**

[7] www.nrel.gov

[8] K. Kalyanasundaram. Dye-Sensitized Solar Cells, CRC Press, Boca Raton. **(2010)**

[9] W.A. Badawy, S.A. Elmeniawy, A.N. Hafez. *Improvement of the power of industrially fabricated solar cells by etching of the Si surface and the use of surface analytical technique.* Egypt Journal of Analytical Chemistry. 22 **(2013)** 97-113

[10] P. Palinginis. *Nonlinear Optical Spectroscopy or Dipole and electron spin Coherences in Semiconductor Nanostructure*. A Ph.D. Dissertation. (**2004**).4

[11] A.P. Alivisatos. *Perspectives on the Physical Chemistry of Semiconductor Nanocrystals*. Journal Physical Chemistry. 100 (31) **(1996)** 13226–13239

[12] A.J. Sutherland. *Quantum dots as luminescent probes in biological systems*. Current Opinion in Solid State and Material Science. 6 (4) **(2002)** 365–370

[13] A.M. Smith and S. Nie. *Chemical analysis and cellular imaging with quantum dots.* Analyst. 129 **(2004)** 672.

[14] A. Ambrosi and M. Pumera. *Electrochemistry at CVD Grown Multilayer Graphene Transferred onto Flexible Substrates.* Journal of Physical Chemistry C.117 (5) **(2013)** 2053–2058

[15] M. Simon, Y. Aswani, Peng Gao, R. Humphry-Baker, B. Curchod, N. Ashari-Astani, I. Tavernelli, U. Rothlisberger, M. Rothlisberger, M Nazeeruddin, M. Gratzel. *Dye-sensitized solar cells with 13% efficiency achieved through the molecular engineering of porphyrin sensitizers.* Nature Chemistry. 6 **(2014),** 242-247

[16] T. Swethaa, S. Nivedithaa, K. Bhanuprakasha, Surya Prakash Singha. *Panchromatic Ru(II) Dipyrrins as NCS Free Sensitizers Showing Highest Efficiency for DSSCs*. Electrochimica Acta. 153 **(2015)** 343–351

[17] M. Grätzel. *The Advent of Mesoscopic Injection Solar Cells.* Progress in Photovoltaics. 14 **(2006)** 429

[18] F.Gao. *A New Heteroleptic Ruthenium Sensitizer Enhances the Absorptivity of Mesoporous Titania Film for a High Efficiency Dye-Sensitized Solar Cell*. Chemical Communications. (23) (**2008**) 2635

[19] A. Kongkanand, K. Tvrdy, K. Takechi, M. Kuno, and P. V. Kamat. *Quantum dot solar cells. Tuning photoresponse through size and shape control of CdSe-TiO2 architecture.* Journal of the American Chemical Society. 130 (12) (**2008**) 4007–4015

[20] H.H. Afify, R.M. Momtaz, W.A. Badawy, S.A. Nasser. *Some physical properties of fluorine doped SnO2 films prepared by spray pyrolysis*. Journal of Material Sciences. (**1991**) 40

[21] L. W. Creator. Application of nanotechnology in energy sector. *Aktionslinie Hessen-Nanotec* of the Hessian Ministry of Economy, Transport, Urban and Regional Development. 9 **(2008)** 36.

[22] W.A. Badawy. *Preparation and characterization of TiO2/Sb thin films for solar energy applications.* Solar Energy Materials and Solar Cells, 28 (**1993**) 293

[23] W. Shockley and H. J. Queisser. *Detailed Balance Limit of Efficiency of p-n Junction Solar Cells*. Journal of Applied Physics. 32 **(1961)** 510-519

[24] H. Queisser. Computer History Museum. Retrieved January 17 (**2017**)

[25] B. O'Regan and M. Grätzel. *A Low-Cost, High-Efficiency Solar Cell Based on Dye-Sensitized Colloidal TiO2 Films.* Nature. 353 **(1991)** 737-740

[26] G. Chen, J. Seo, C. Yang and P. N. Prasad. *Nanochemistry and nanomaterials for photovoltaics*. Chemical Society Reviews. 42 **(2013)** 8304-8338.

[27] L. EL Chaara, L. Lamonta and N. EL Zeinb. *Review of photovoltaic technologies*. Renewable and Sustainable Energy Reviews.15 (5) (**2011**) 2165-2175

[28] A. Yella, H.-W. Lee , H. N. Tsao, V. Yi, K. A. Chandiran, M. K. Nazeeddin, E. W.-G. Diau, C. Y. Yeh, S. M. Zakeeruddin and M. Gratzel. *Cobalts, Porphyrin-Sensitized Solar Cells with Cobalt II/III- Based Redox Electrolyte Exceed 12 % efficiency*," Science,4 (334) (**2011**) 629-634

[29] S. D. Sung, I. Lim, P. Kang, C. Lee and W. I. Lee. *Design and development of highly efficient PbS quantum dot-sensitized solar cells working in an aqueous polysulfide electrolyte* Chemical Communications. 49 **(2013)** 6054-6056

[30] S. Mathew, A. Yella, P. Gao, R. Humphry-Baker, F. E. CurchodBasile, N. AshariAstani, I. Tavernelli, U. Rothlisberger, K. NazeeruddinMd and M. Grätzel. *Dye-sensitized solar cells with 13% efficiency achieved through the molecular engineering of porphyrin sensitizers*. Nature Chemistry. 6 **(2014)** 242-247.

[31] J. Burschka, A. Dualeh, F. Kessler, E. Baranoff, N.-L. Cevey-Ha, C. Yi, M. K. Nazeeruddin and M. Grätzel. *Tris(2-(1H-pyrazol-1-yl)pyridine)cobalt(III) as p-Type Dopant for Organic Semiconductors and Its Application in Highly Efficient Solid-State Dye-Sensitized Solar Cells.* Journal of the American Chemical Society. 133 **(2011)** 18042-18045.

[32] L. M. Peter. *Towards sustainable photovoltaics: the search for new materials.* Philosophical Transactions of the Royal Society A: Mathematical, Physical and Engineering Sciences. 369 **(2011)** 1840-1856.

[33] Z. Ning, D. Zhitomirsky, V. Adinolfi, B. Sutherland, J. Xu, O. Voznyy, P. Maraghechi, X. Lan, S. Hoogland, Y. Ren and E. H. Sargent. *Graded doping for enhanced colloidal quantum dot photovoltaics*. Advanced Materials. 25 **(2013)** 1719-1723

[34] P. V. Kamat. *Boosting the Efficiency of Quantum Dot Sensitized Solar Cells through Modulation of Interfacial Charge Transfer*. Accounts of Chemical Research. 45 **(2012)** 1906-1915.

[35] Z. Yang, C.-Y. Chen, P. Roy and H.-T. Chang, *Quantum dot-sensitized solar cells incorporating nanomaterials. Chemical* Communications. 47 **(2011)** 9561-9571.

[36] C. Wadia, A. P. Alivisatos and D. M. Kammen. *Materials Availability Expands the Opportunity for Large-Scale Photovoltaics Deployment*. Environmental Science & Technology. 43 **(2009)** 2072-2077.

Chapter 2
Literature Review

2.1 Overview

Chapter 2 provides a detailed literature review of quantum dots. This chapter commences by providing a brief explanation about nanostructured materials, history of quantum dots and their properties. Moreover, chapter 2 talks about the current methods available for synthesising CdSe QDs specifically top down methods and bottom up approaches. Lastly, Chapter 2, also presents possible applications of QDs.

2.2 Nanostructured Materials

The discipline of nanotechnology is built around the exploitation of materials, which show unique physical properties at nanometer size scales. By definition, nanostructured materials are materials with at least one dimension in the size range from approximately 1-100 nanometers [1], they can exist as individual particles or clusters of nanoparticles of various shapes and sizes [2]. In nanotechnology, a particle is defined as a small object that behaves as a whole unit with respect to its transport and properties [3]. Nanoparticles can be made from a wide variety of materials, including metals, semiconductors, organic materials or biomaterials. All these materials can be incorporated into nanomaterials. As previously defined, a nanomaterial is a material with at least one external dimension in the nanoscale (1–100 nm); whereas a nanoparticle is defined as a material with all three external dimensions in the nanoscale [4]. Research has revealed that nanostructured materials mostly exhibit geometries that reflect the atomistic bonding analogous to the bulk structure. The nanomaterials are of interest due to their ability to bridge the gap between the bulk and molecular levels and lead to entirely novel avenues for application. Nanostructured materials exhibit a high surface-to-volume ratio compared to their bulk counterparts. In this

regard, a large fraction of atoms is present on the surface, which makes them possess different thermodynamic properties. During the past two decades, huge attention has been focused on the optoelectronic properties of nanostructured semiconductors with an emphasis on fabrication of the smallest possible particles. Investigations have revealed that many fundamental properties are size-dependent in the nanometer range. For instance, the density of states (DOS), that is the number of quantum states per energy for periodic materials with three, two or one dimension, is shown in Fig. 2.1 [4]. If the extent of the material is on the order of one to ten nanometers in all three directions, the material is said to be a quantum dot (QD). A QD is zero-dimensional comparative to the bulk, and the DOS depends upon whether or not the QD have aggregated. The DOS for a molecule and an atom are also shown in Fig. 2.1. The electron density in a three-dimensional bulk crystal is so great that the energy of the quantum states becomes nearly continuous. However, the limited number of electrons results in discrete quantized energies in the DOS for two, one and zero dimensional structures. The presence of one electronic charge in the QDs repels the addition of another charge and leads to a staircase-like I-V curve and DOS. The step size of the staircase is relative to the reciprocal of the radius of the QDs. The restrictions as to when a material has the properties of bulk, QD or atoms, are dependent on the composition and crystal structure of the compound or elemental solid. When a solid exhibits a distinct variation of optical and electronic properties with a variation of size, it can be called a nanostructure. And nanostructures are characterised as two-dimensional, e.g. thin films or quantum wells, one-dimensional, e.g. quantum wires; or zero-dimensional, e.g. QDs.

Even though each of these categories shows interesting optical properties, our discussion will be focused solely on QDs.

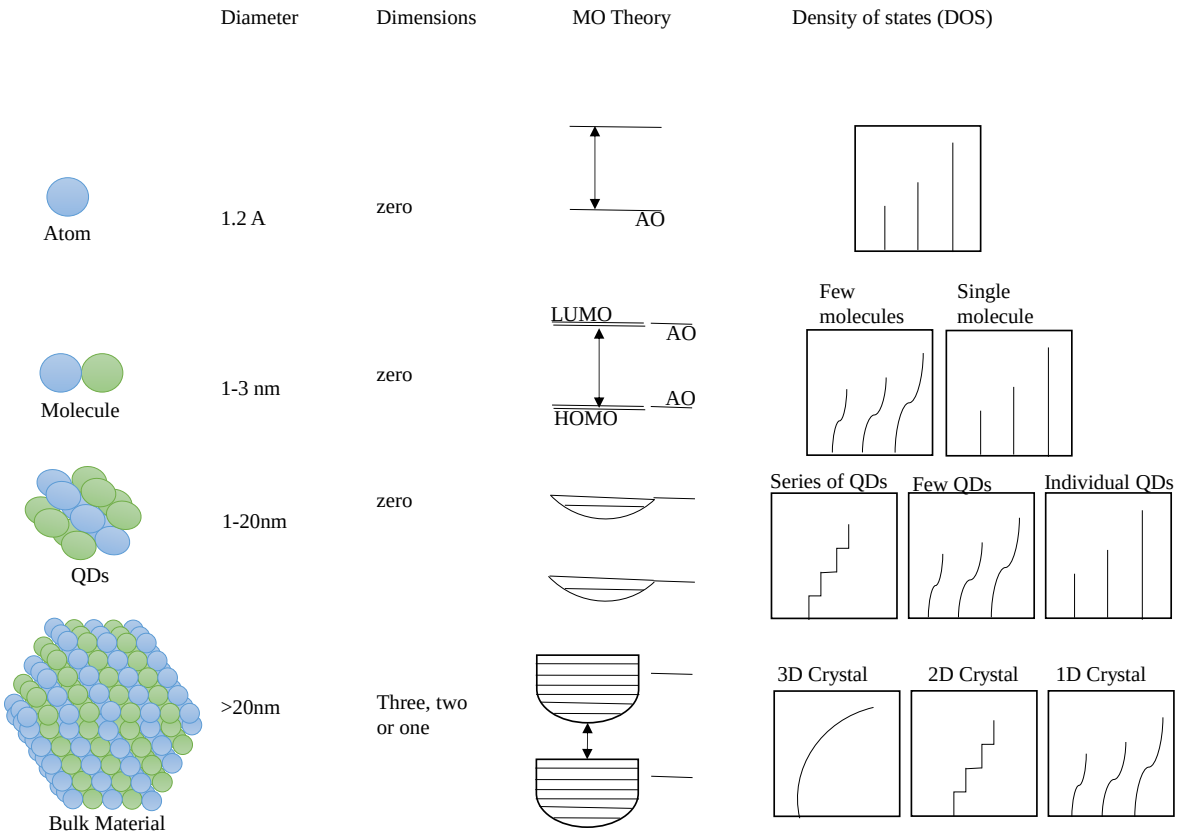

Figure 2.1: *Schematic illustration of the changes of the density of quantum states (DOS) with changes in the number of atoms in materials.* [4]

2.3 Quantum dots

2.3.1. History of Quantum dots

Ever since the early days of the 1960s, the concept of semiconductor crystallites has been suggested as a new structure of a semiconductor material. Ekimov and Brus developed the conceptual idea of QDs in solid and liquid state respectively [5], but the term "QDs" was created by Mark Reed and after then it became one of the most fascinating area of research [6]. Currently, QDs are known as the new generation of materials and technically defined as “small crystals containing a variable number of electrons that occupy well-defined, discrete quantum states and have electronic properties intermediate between bulk and discrete fundamental particle.

Moreover, a procedure for synthesizing PbS QDs was first proposed more than two centuries ago using low-cost natural materials such as PbO, $Ca(OH)_2$ and H_2O [7]. Greeks and Romans used these materials as cosmetics to dye their hair. Recently it was discovered that controlling the size of QDs in silicate glasses is one of the oldest and most regularly used techniques to change the colour of glass. In the early twentieth century, CdS and CdSe were combined to obtain red-yellow colours into silicate glasses. In 1932, Rocksby [8] used X-ray diffraction to determine the precipitates of CdS and CdSe in generating colours. Semiconductor doped glasses were used as filters in optics. Ekinov and Onushchenko [9] reported a blue shift of the optical spectrum for nanometre sized CuCl in silicate glass. In 1982, Efros and Efros [10] advanced that quantum size effects (the change of optical and optoelectronic properties with size) could be used to control the colour of glass by either varying the size or stoichiometry of CdS_xSe_{1-x}. In 1991, Rosetti et al. [11] discussed the change in colour of colloidal solutions of semiconductor. Over the last two decades, experimental and theoretical research on nanoparticles has significantly increased.

Quantum dots are very small crystals of semiconductor materials. Their size ranges from about a hundred to a few thousand atoms. The diameter of a quantum dot is approximately between one and ten nanometres, which puts them in a special size range that retains some properties of bulk materials, as well as some properties of individual atoms and molecules. As semiconductors, quantum dots have certain associated electronic and optical properties [12]. Their high fluorescence and narrow spectrum shape makes them an excellent tagging alternative to conventional fluorescent dyes.

During the past three decades, extensive research has been performed on the properties and uses of quantum dots. For bulk semiconductors, the band gap of the material is a set energy barrier between the valence and conduction bands, dictated by the composition of the material [13]. Unlike bulk semiconductors, the bandgap of a quantum dot is also influenced by its size. Small QDs produce light with short wavelength and large QDs produce light of longer wavelength. When interpreted in terms of the colour in the visible spectrum, this implies that small QDs emit blue light and larger ones, red light which makes the wavelength of light emitted by the particles tunable (Fig. 2.2).

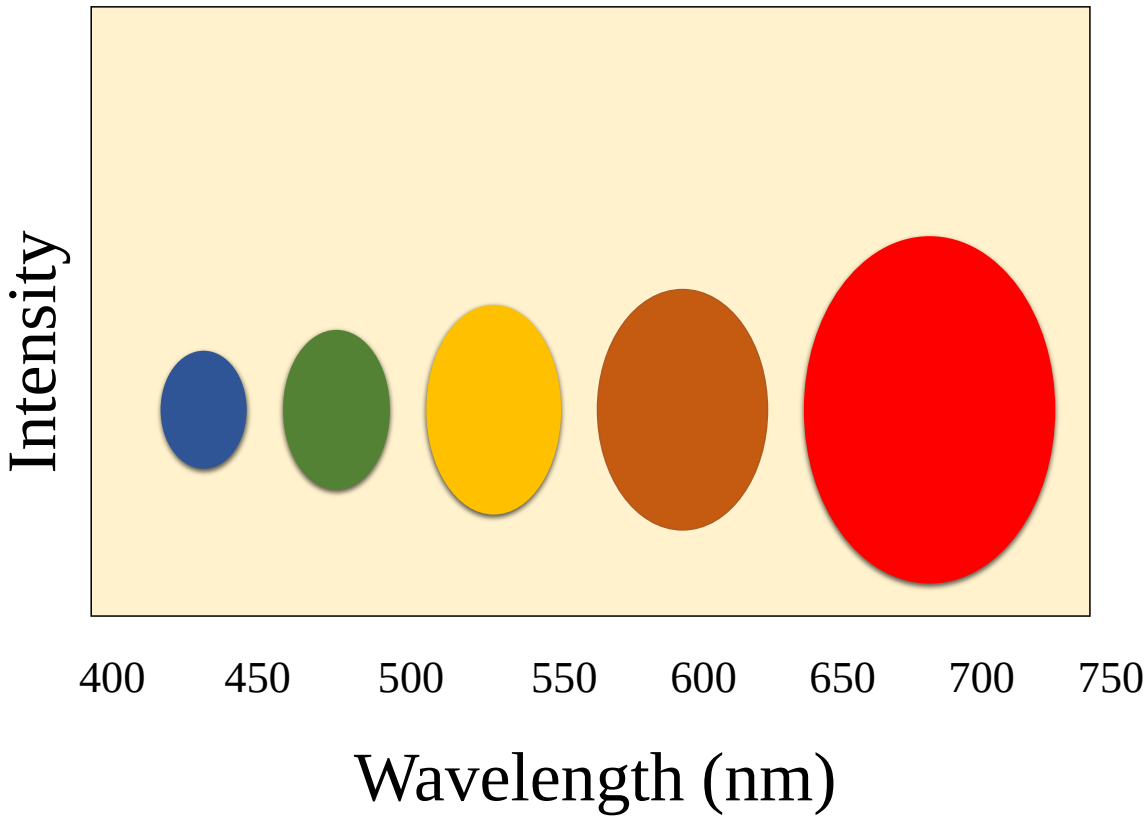

Figure 2.2: *Energy and size correlation in a QD confined system*

There are many advantages of using QDs. It has already been mentioned that they are notable for their high fluorescent intensity. The fluorescent spectrums of quantum dots have a narrower full width half maximum (FWHM, the width of the spectrum at half of the peak intensity) than fluorescent dyes, this makes the dots more precise. Quantum dots have a much longer shelf life when compared to organic fluorescent dyes. They can be stored for months with no deterioration of their fluorescent properties. [16]. Quantum dots have also proved to be stable semiconductors [15]. Due to their properties, different sizes of QDs can be used at once with the same excitation wavelength and can clearly be distinguished from each other, to both the naked eye and using spectrometers [14].

Additionally, QDs exhibit solid-solid phase transition like bulk semiconductors, and these transitions have a substantial influence on the optical properties of QDs. Phase transitions in bulk

materials can be induced by varying pressure, temperature and composition [17,18]. Bulk CdSe may exhibit either a hexagonal wurtzite or a rock salt cubic structure with a direct or indirect band-gap, respectively. Above a certain pressure, bulk CdSe QD can be converted reversibly from low pressure wurtzite to the high pressure rock salt structures [19]. The low intensity optical emission from the rock salt form of CdSe is in the near infrared (NIR) spectral region at 0.67 eV (1.8 μm). Using high pressure XRD and optical absorption, Alivisatos and co-workers showed that the wurtzite to rock salt structural transformation also occurred in CdSe QDs [17, 18]. The ratio of oscillator strength between direct and indirect structures did not vary with size of QDs.

2.3.2. Properties of Quantum dots

The most significant property that makes QDs applicable to solar cell and other applications comes from a property known as quantum confinement, which arises due to change in density of states and was first reported by Ekimov and Onushchenko [9]. Since then, a lot of research has been conducted in the field of quantum confinement effect in semiconductors and in low dimensional nanostructures [21, 22]. The quantum confinement effect is the widening of the band-gap (gap between the valence and conduction band) with a reduction in the size of the quantum dot. It is because of this effect that the quantum dots prepared using the same material but with different sizes display several colours (Fig.2.2) [26]. QDs exhibit exclusive electronic and optical properties due to this effect.

Moreover, CdSe QDs have received extensive attention owing to their unusual electronic and optical properties and are of great use in various applications. These properties can be transformed by simply manipulating the number of atoms in the QDs while maintaining the same chemical composition. The optical and electronic properties of semiconductor nanoclusters come up from interactions between electrons, holes, and their local environments [23]. QDs undergo

photoexcitation on absorption of photons when the excitation energy exceeds their band gap and electrons get promoted from the valence band to the conduction band.

The electron in an excited state is a high energy electron. The excited electron and hole form an exciton. The electron and hole may recombine and relax to a lower energy state, ultimately reaching the ground state. The excess energy resulting from recombination and relaxation may be either radiative (emits photon) or nonradiative (emits phonons). The luminescence of QDs is due to radiative relaxation. Measurements of UV-visible spectra show a great number of energy states in QDs. A remarkable peak is observed as the first observable peak from the lowest excited energy state. Excitations at shorter wavelengths are also likely due to multiple electronic states present at higher energy levels. The size of CdSe QDs is used to tune the optical gap across a major portion of the visible spectrum [24, 27]. In the case of CdSe QDs, the optical gap can be tuned by reducing the QD size from red (approximately 1.7 eV) to green (approximately 2.4 eV). Therefore, tuning their size allows for modification of their optical properties [25].

2.4. Synthesis Methods

High quality QDs have been synthesised either on a substrate or dispersed in an organic/inorganic solution. Several techniques have been employed in the synthesis of CdSe QDs. These techniques are categorised as either top-down (carving large piece of a material to the desired nanostructures) or bottom-up (assembling atoms to form the desired nanostructures) methods. Generally, some of these techniques are practical in solar cells applications. Below both approaches are discussed briefly.

2.4.1. Top-Down Approach

In the top-down approaches, a bulk semiconductor is thinned to form the QDs. Electron beam lithography, reactive-ion etching and/or wet chemical etching are examples of top down techniques. Electron beam lithography has been widely used to synthesise QDs by the combination of high resolution electron beam lithography and subsequent etching. However, it was found the spatial resolution required for acquiring the best size regime, where significant quantization effects can be expected tends to be larger than the desirable level. Moreover, lithographic processes and subsequent processing often produce contamination, formation of defects, size non-uniformity, poor interface quality, and even damage to the bulk of the crystal itself [28]. Lastly, it was found that traditional top–down patterning methods like photolithography and beam lithography are time-consuming and expensive processes [29].

Alternatively, focused ion or laser beams have also been used to fabricate QDs. The shortfalls of this process include incorporation of impurities into the QDs and structural imperfections by patterning. Etching, known for more than 20 years, plays a very important role in these nanofabrication processes. In dry etching, a reactive gas species is inserted into an etching chamber and a radio frequency voltage is applied to create a plasma which breaks down the gas molecules to more reactive fragments. These high kinetic energy species strike the surface and form a volatile reaction product to etch a patterned sample. When the energetic species are ions, this etching process is called reactive ion etching (RIE). With a masking pattern, selective etching of the substrate is achieved. Fabrication of GaAs/AlGaAs quantum structures as small as 40 nm has been reported using RIE with a mixture of boron trichloride and argon [30]. This RIE process has been used to produce close-packed arrays for testing of lasing in QD semiconductors. Close packed arrays of ZnTe QDs with interdot distance of 180 nm to 360 nm were produced by RIE using CH_4 and H_2 [31].

Focused ion beam (FIB) techniques also offer the possibility of fabricating QDs with extremely high lateral precision. Highly focused beams from a molten metal source (e.g., Ga, Au/Si, Au/Si/Be, or Pd/As/B) may be used directly to sputter the surface of the semiconductor substrate. The shape, size and inter-particle distance of the QDs depend on the size of the ion beam but a minimum beam diameter of 8–20 nm has been reported for both lab and commercial systems, allowing etching of QDs to dimensions of <100 nm. The FIB technique can also be used to selectively deposit material from a precursor gas with a resolution of ~100 nm. Scanning ion beam images (analogous to scanning electron microscope images) can be developed by ion beam nanofabrication at the desired, predetermined locations with high resolution [32]. However, this is a slow, low throughput process which requires the use of expensive equipment that leaves residual surface damage, therefore there is a demand for new more sophisticated techniques for the fabrication of QDs.

2.4.2. Bottom- up Approach

In the bottom up method, QDs are assembled from basic building blocks such as molecules or nanoclusters. Unlike the top down methods, whereby high power techniques are used to physically decrease the size of the particle, the bottom up approach employs a much gentler approach. Bottom up approaches are subdivided into two categories, wet chemical methods and vapour phase methods.

Vapour phase methods

In vapour-phase methods layers of quantum dots are grown in an atom-by-atom process without any patterning instead by hetero-epitaxial growth of highly strained material. Vapour phase methods are widely used with optoelectronics such as lasers, infrared photodetectors and

nanotechnologies. Vapour phase methods can be classified according to their reaction types. They are classified into physical vapour deposition (PVD) and chemical vapour deposition (CVD).

Physical Vapour Deposition

PVD refers to a variety of thin film deposition techniques where solid metal is vaporized in a high vacuum environment and deposited on electrically conductive materials as a pure metal or alloy coating. Layer growth by physical vapour deposition (PVD) results from condensation of a solid from vapours produced by thermal evaporation or by sputtering [33]. As a process that transfers the coating material on a single atom or molecule level, it can provide extremely pure and high performance coatings which for many applications are much preferable to electroplating. PVD coating processes are environmentally friendly processes that can greatly reduce the amount of toxic substances that must be disposed of with more conventional types of coating that involve fluid precursors and chemical reactions. Different techniques have been used to cause evaporation, such as electron beam heating, resistive or Joule heating, arc-discharge and pulsed laser ablation. In any case, strain and surface energies control the formation of QDs from the deposited thin films.

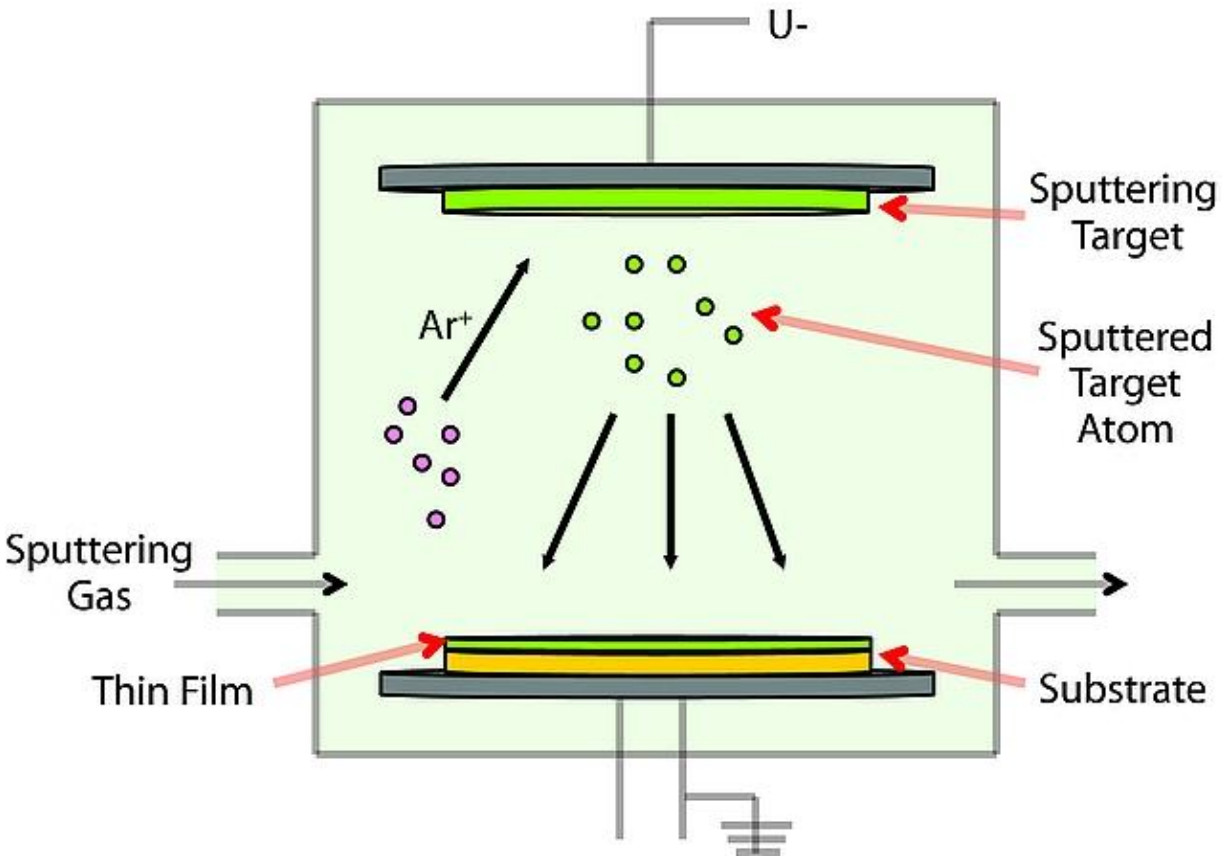

Figure 2.3*: Diagram showing an example of PVD technique, sputtering*

Chemical vapour deposition

CVD is the formation of non-volatile solid film on a substrate by the reaction of vapour phase chemicals (reactants) that contain the required constituents. In CVD, precursors are introduced in a chamber at a particular pressure and temperature and they diffuse to the heated substrate, react to form a film, followed by gas-phase by-products desorbing from the substrate and being removed from the chamber [34]. The substrate temperature is critical and can influence what reactions will take place. The problem with both PVD and CVD is that they are line of sight techniques meaning that it is extremely difficult to coat undercuts and similar surface features. Both techniques require high capital costs, some processes operate at high vacuums and

temperatures requiring skilled operators. Processes that require large amounts of heat also require an appropriate cooling systems, which is costly. And lastly, the rate of coating deposition is usually quite slow.

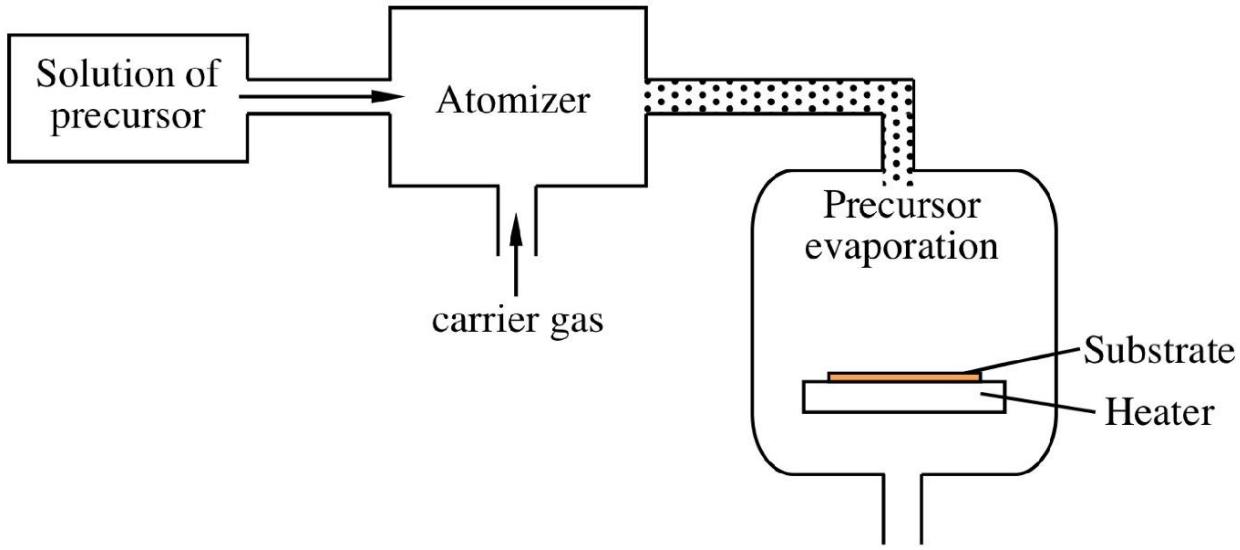

Figure 2.4: *Schematic diagram showing an example of a CVD technique*

Wet chemical methods

Wet-chemical methods mainly follow the conventional precipitation methods with careful control of parameters for a single solution or mixture of solutions. The precipitation process invariably involves both nucleation and limited growth of nanoparticles. Nucleation may be categorized as homogeneous, heterogeneous or secondary nucleation [33]. Homogeneous nucleation occurs when solute atoms or molecules combine and reach a critical size without the assistance of a pre-existing solid interface. By varying factors, such as temperature, electrostatic double layer thickness, stabilizers or micelle formation, concentrations of precursors, ratios of anionic to

cationic species and solvent, QDs of the desired size, shape and composition can be achieved. Some of the common synthesis processes are briefly discussed below.

Sol-gel method

The sol-gel technique has been used for many years to synthesize nanoparticles including II-VI & IV-VI QDs like CdS [35] and PbS [36]. The three significant steps in this process are hydrolysis, condensation (sol formation) and growth (gel formation). In a typical technique, an inorganic network of colloidal suspension (sol) is formed, followed by the gelation of the sol solution to form a continuous liquid phase (gel). The formed gel can be used to fabricate different nanomaterials and nanostructures such as powders, aerogels, xerogels, etc. [37]. There are number of precursors that can serve as sol forming constituents such as, metal alkoxides, metal organic compounds, salts of inorganic acids, salts of organic acids, etc. However, the most commonly used precursors are metal alkoxides; these are compounds in which a metal is bonded to one or more alkyl groups through an intermediate oxygen atom.

In a typical process, precursor solution is dissolved in a solvent or a mixture of organic solvents. An acid or base catalyst may be added to increase the rate of the reaction. Inspite of the range of the precursors that can serve the function of precursor materials, they will undergo hydrolysis of and polycondensation processes to form M-O-M bonds. In the hydrolysis process, precursor will hydrolyse in the medium and gets a hydroxyl group typically through the reaction with water. Polycondensation is the process in which the hydrolysed species combines to make an inorganic polymer like chains through elimination of a water molecule. Depending on the process conditions and the chemical constituents in the sol-gel bath, sol properties can be tuned. Typically, the process conditions are designed in such a way as to obtain short or long polymeric

chains or colloidal particles. These differences in sol properties can be advantageous for specific applications such as thin film coating, powder preparation and spray pyrolysis. The sol can be transformed in to a gel state through continuous polycondensation and solvent evaporation. The resulting gel is a system consisting of a solid and three dimensional network of sol and the solvent. The gel can be further processed to remove the solvent residue and other chemical traces. Once the residue is removed, the sol system collapses in to an amorphous solid structure, which is known as xerogel [38]. This material can be sintered in a furnace to transform the xerogel to a solid crystalline material.

Additionally, the sol gel process can be of help in obtaining materials with a wide range of oxygen and some metallic compositions. The main shortfalls of the sol gel technique include a broad size distribution and a high concentration of defects [36].

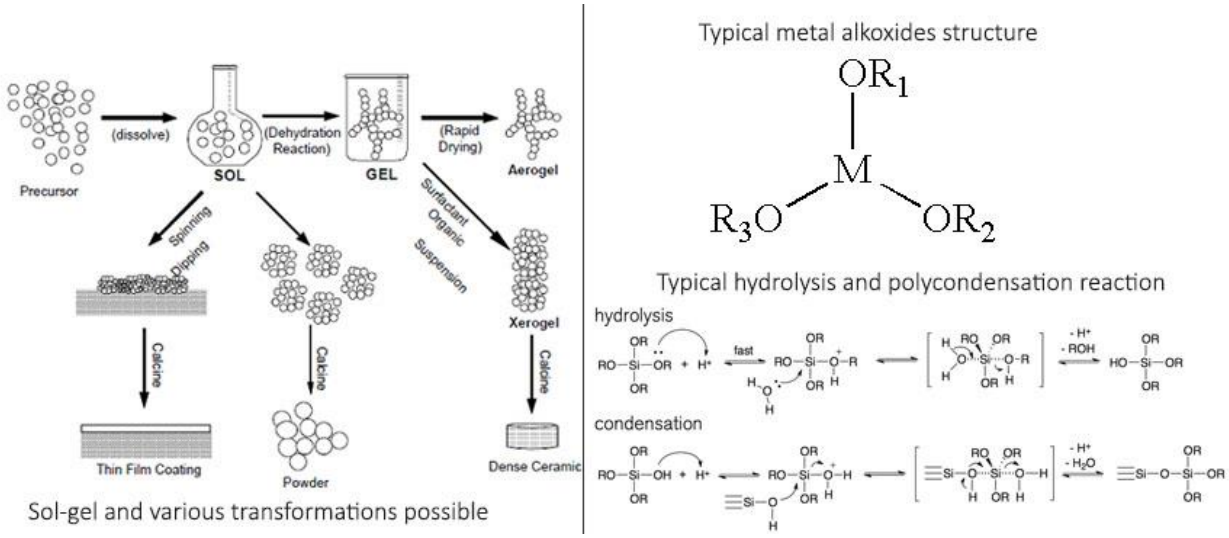

Figure 2.5: *Schematic diagram showing the process of the sol gel technique.* [77]

Hot Injection Method

The decomposition of molecular precursors at high temperatures in a coordinating solvent is one of the most successful and popular routes to prepare high-quality QDs [69] This approach was first developed by Bawendi et al. in 1993 [70]. In a typical synthesis process, they prepared CdE QDs (E = Se, S, and Te) through distinct, rapid injections of a solution of cadmium dimethyl ($CdMe_2$) and selenium powder (Se) dissolved in trioctylphosphine (TOP) and Trioctylphosphine oxide (TOPO) and heated up to high temperatures in an oxygen free environment [70]. CdSe nanocrystallites immediately begin to nucleate and grow. The desired size of CdSe quantum dots can be achieved by adjusting the amount of injected precursors and the reaction time. The capping agent allowed particle stability in organic solvents, prevented particle aggregation, and electronically passivated the semiconductor surface. Although this method has been successful at producing high-quality QDs, it is hindered by the toxicity of the starting materials. Particularly, the alkyl metal ($CdMe_2$) is pyrophoric, explosive at high temperatures, and emits highly toxic gases of metal oxide. It was later discovered that cadmium oxide (CdO) and cadmium salts such as cadmium acetate ($Cd(Ac)_2$) and cadmium carbonate ($CdCO_3$), proved to be adequate substitutes of cadmium dimethyl ($CdMe_2$). Compared to the highly unstable $CdMe_2$, the cadmium salt substitutes offer several advantages which include: [1] the injection temperature can be much lower (220 °C to 300 °C), [2] both nucleation and growth are almost independent of injection therefore ensuring great reproducibility, and [3] the slow nucleation suggests that the injection can be complete within a longer time, therefore allowing large amounts of stock solutions to be added to the reaction vessel, making the process more feasible for scale-up productions.[69] Today, a typical reaction involves the dissolution of the cadmium salt in a mixture of a coordinating and non-coordinating solvents at 300°C or below, followed by the addition of a solution of the chalcogenide (Se, S, or Te) in a cation precursor [69,72]. The chalcogenide and

cadmium precursor combine to form stable nuclei that subsequently grow as the reaction proceeds [72]. At the growth temperature, surfactant molecules adsorb and desorb rapidly from the QD surface, enabling the addition (as well as removal) of atoms from the nanocrystal, while aggregation is suppressed by the presence of one monolayer of surfactant at the nanocrystal surface [73] The QDs resulting from this method are typically monodisperse, with sizes ranging from 1 nm to 10 nm [69]. The hot injection synthesis method was developed to produce superior crystallinity and to provide better size control and surface passivation than other synthesis methods [74, 75]. At these higher temperatures, there is more thermal energy to assist each added-atom find more energetically favourable bonding positions in the crystal lattice, therefore reducing defects by annealing during growth, leading to increased overall quantum efficiency [77]. Another advantage associated with the hot injection synthesis method is that a narrower size distribution of QDs may be attained compared to other synthesis techniques because effective separation of the two synthesis stages (nucleation and growth) is achieved by the 'hot injection technique. It is estimated that the fluorescence peak of CdSe QDs immediately after nucleation is around 500. The subsequent growth of the QD, however, results in the red shift of the fluorescence peak to green, yellow, and red as the size of the QD continues to increase [76]. The 'hot injection technique' was utilized in this thesis.

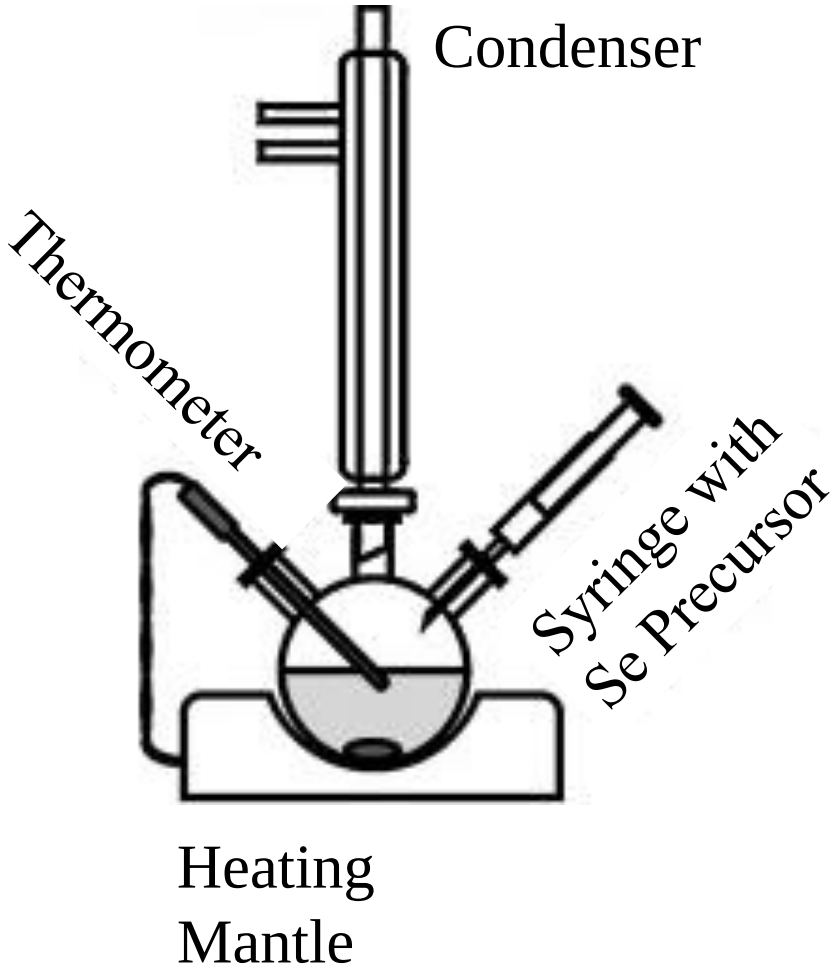

Figure 2.6: *A schematic diagram of the hot injection synthesis method*

2.5. Surface Passivation

Capping or passivation of the surface of the QDs is very crucial for their development. High performing QDs rely on the presence of surfactants for the passivation and stabilisation of QDs upon synthesis. The word *passivation* literally means to make a material less attractive to its surroundings. The surfaces of nanoparticles can be very unstable due to strains, uncontrolled reconstruction, or unbalanced charges. These unstable sites are ready to bond with pretty much anything so as to relax to a lower surface energy state. The most common contaminants are oxides coming from oxygen or moisture in air. These species have the potential to be detrimental on the

properties of the particles by adding new surface states to the overall crystal energy structure. Surface passivation involves introducing ligand molecules to coordinate with unstable sites by inducing minimum change in the energy state distribution, while preventing other opportunistic contaminants from being adsorbed [39]. In this regard, surface passivation of QDs is very crucial in the development of photostable QDs and is generally carried out by depositing an organic or inorganic capping layer on the QDs surface [40].

Usually, CdSe QDs have a diameter between 1 nm to 10 nm, with roughly 100 to 1600 CdSe ion pairs, and approximately 40 to 250 capping agents on the QDs surface [49]. Ligands play at least four different roles in the overall electronic function of the QDs. First, they are present during the nucleation process and determine the reactivity and availability of the crystal precursors and ligands [50]. Secondly, they control the growth rate and size distribution of the QDs [50] by keeping the particles sequestered and facilitating homogenous growth during synthesis [41]. Thirdly, capping agents provide colloidal stability, which helps in the prevention of aggregation and growth [42, 50, and 43]. Finally, surfactants interact electronically with surface sites and may passivate defects on the surface of QDs [41] Defects exist on the surface of QDs due to the large surface-to-volume ratio of QDs [45,44,46] which results in the formation of dangling bonds from some of the surface atoms [16]. Capping agents serve to donate electrons to, or accept electrons from, these dangling bonds of incompletely coordinated metal ions (Cd^{2+} sites are electron acceptors, and Se^{2-} are electron donors) in order to preserve the original structure of the QD [46,47]. Surface defects usually act as nonradiative recombination sites for electron-hole pairs produced by incident excitation light, thereby reducing the quantum efficiency of the QDs [51, 48]. In CdSe QDs, these nonradiative traps are located above the valence band [45]. Capping agents then passivate different amounts of these surface defects to influence the quantum efficiency of the QDs. If the capping agent provides good passivation of surface defects, high

quantum efficiency is expected. The nature and density of the surface trapping sites depends strongly on the surface structure and shape of the QD, along with the nature of the defect sites on the QD surface [51, 42].

Because ligands play such a pivotal role on the overall quality of QDs, many efforts have been made to synthesise high quality QDs using different capping agents. Recently, several workers reported that replacing oleate molecules with short ionic dithiol ligands such as 1.2 ethanedithiol (EDT) revealed promising results for PbS QD films [52]. Other groups reported that EDT showed a poor resistance to ambient atmospheric conditions [53], while 3-Mercaptopropionic acid (MPA) resulted in better stable conditions and improved mobility [54]. Furthermore, Jeong *et al* [55] proposed that the great chemical diversity of MPA (thiol and carboxylic group) in comparison to EDT could passivate a broader distribution of surface states.

Even though, there are several different types of capping agents, we have chosen to use 2-mercaptoethanol (βME) as a capping agent for this work simply because it is an environmentally friendly, cheap, and safer capping agent. Additionally, research has shown that βME can yield much more stable QDs than other capping agents.

2.6. Applications

The ability to tune the size of quantum dots allows for their potential application in a number of photonic devices [56], laser technology [57], life sciences [58] and photovoltaics [59]. Because of their small size and photostability, QDs can be used in cells for longer times than organic dyes and can enter into live cells to interact with DNA and proteins. There has been interest in detection of cancer cells by means of QDs binding to altered DNA sequences or proteins that are present in certain types of cancer. Moreover, QDs have found application in multiple-colour imaging of live cells without any effect on normal growth and development due to the narrow and tunable emission spectra.

QDs show exceptional optoelectronic properties that have found application in solar cells, while the narrow emission spectra have given rise to the idea that quantum dots can be made into light emitting diodes (LEDs), with the colour of the LEDs being tuneable through controlling the QD size. Lately, there has been interest in the development of white light emitting diodes made of semiconductor nanocrystals which has the probability to replace conventional lighting. At the early stages of LED technology development, LEDs were used in illuminated signs or traffic lights and they are now widely used in television backlight units. The major challenge for the energy saving devices is the high cost of fabrication. This could be improved by designing LED structures that are less complex and by improving the emitting materials. Compared with phosphor-converting LEDs based on GaN, one of the earlier LED technologies, organic light emitting devices (OLEDs) can be flexible and fabricated into large areas with low-cost fabrication techniques such as evaporation and spin-casting due to the solution-based emitting materials [68]. Colloidal CdSe/ZnS core-shell QDs have been the most widely investigated materials for these applications due to their high quantum yield and high photostability at room temperature.

Advances in nanomaterial synthesis have led to the development of solar cells that can potentially combine high efficiency with lower production costs than conventional cells. Quantum dot sensitized solar cells (QDSSCs) are a modified version of a DSSCs design with more efficiency in which QDs replace the organic dye [60]. The main property that makes QDs better photoabsorbers is their band gap that can be size-tuned to optimize exploitation of the entire solar spectrum. They exhibit multiple exciton generation with high photostability and highly absorbing nature [61]. QDs can also be used to replace the electrolyte as the hole-transporting medium [62]. A wide variety of QDs have been investigated as sensitizers for QDSSCs, because of their tunable band gap energy, high extinction coefficients and large dipole moment. The most commonly used are CdSe, PbS and CdTe. Usually these materials are coupled with metal oxide entities to improve the efficiency of the solar cells [63]. Reports have suggested that coupled QDSSCs systems are advantageous over single QDs-sensitized cells due to their enhanced photocurrent generation [64].

Many scientists and engineers are now focusing on co-sensitized solar cells with CdS/CdSe QDs due to their strong visible light harvesting ability and high carrier migrating speed [65]. CdSe QDs have wider absorption scope (approximately 730 nm) [66], and CdS QDs are stronger oxidizers to gain electrons from the electrolyte. Combined together, theory predicts that CdS/CdSe QDs can ensure high photoelectric conversion efficiency at full visible light spectrum [67].

2.7. References

[1] H. Gleiter. *Nanostructured materials: basic concepts and microstructure*. Acta Materialia. 48 (1) (**2000**) 1-49

[2] P. Moriarty. *Nanostructured Materials*. Reports on Progress in Physics. 64 (3) (**2001**) 297

[3] S.V.N.T. Kuchibhatla, A.S. Karakoti, D. Bera and S.Seal. *One dimensional nanostructured materials*. Progress in Material Science. 52 (5) (**2007**) 699-913

[4] D. Bera, S.C. Kuiry and S. Seal. *Synthesis of nanostructured materials using template assisted electrodeposition*. The Journal of Minerals, Metals & Materials Society. 56 (1**)** (**2004**) 49–53.

[5] A. I. Ekimov and A. A. Onushchenko. *Quantum size effect in three-dimensional microscopic semiconductor crystals*. JETP Letters. 34 (6) (**1981**) 345

[6] M.A Reed., J. N. Randall, R. J. Aggarwal, R. J. Matyi, T. M. Moore, and A. E. Wetse. *Observation of Discrete Electronic States in a Zero-dimensional Semiconductor Nanostructures*. Physics Review Letters. 60 (6) (**1998**) 535-537

[7] P. Walter, et al. *Early use of PbS Nanotechnology for an Ancient Hair Dyeing Formula*. Nano Letters. 6 (10) (**2006**) 2215–2219.

[8] H.P Rocksby. Journal: Society of Glass Technology. 16 (**1932**) 171.

[9] Ekimov, A.I. and Onushchenko, A.A. (1981) 'Quantum Size Effect in 3-Dimensional Microscopic Semiconductor Crystals'. *Jetp Lett.* **34(6)**: p. 345–9.

[10] A.L Efros and A.L Efros. *Interband Absorption of Light in a Semiconductor Sphere*. Soviet Physics Semiconductors-Ussr. 16 (7) (**1982**) 772–5.

[11] R. Rossetti, J. L. Ellison, J. M. Gibson, and L. E. Brus. *Size effects in the excited electronic states of small colloidal CdS crystallites.* Journal of Chemical Physics. 80 (9) (**1984**) 4464

[12] B.O. Dabbousi, et al. *(CdSe)ZnS Core-Shell Quantum Dots: Synthesis and Characterization of a Size Series of Highly Luminescent Nanocrystallites*. The Journal of Physical Chemistry B. 101(46) (**1997**) 9463-9475.

[13] R. Koole, E. Groeneveld, D. Vanmaekelbergh, A. Meijerink and C. Donegá. *Size Effects on Semiconductor Nanoparticles.* Nanoparticles. (**2014**)

[14] B. Marcel, M. Moronne, P. Gin, S. Weiss, A. P. Alivisatos. *Semiconductor Nanocrystals as Fluorescent Biological Labels*. Science. 281 (5385) (**1998**) 2013-2016

[15] W. Chan and S. Nie. *Quantum Dot Bioconjugates for Ultrasensitive Nonisotopic Detection*. Science.281 (5385) (**1998**) 2016-2018

[16] L. Qu and X. Peng. *Control of Photoluminescence Properties of CdSe Nanocrystals in Growth.* Journal of the American Chemical Society. 124 (9) (**2002**) 2049-2055

[17] S.H. Tolbert; A.B. Herhold, C.S. Johnson, A.P and A.P. Alivisatos. *Comparison of quantum confinement effects on the electronic absorption-spectra of direct and indirect gap semiconductor nanocrystals*. Physical Review Letters. 73 *(***1994)** 3266–3269.

[18] S.H. Tolbert, A.P. Alivisatos. *The wurtzite to rock-salt structural transformation in CdSe nanocrystals under high-pressure*. Journal of Chemical Physics. 10 (**1995**) 4642–4656.

[19] U. Woggon. *Optical Properties of Semiconductor Quantum Dots*. Springer. 136 (**1997**)

[20] P.V. Radovanovic and D.R. Gamelin. *Electronic absorption spectroscopy of cobalt ions in diluted magnetic semiconductor quantum dots: Demonstration of an isocrystalline core/shell synthetic method*. Journal of American Chemical Society. 123 (**2001)** 12207–12214.

[21] S.L. Hou, X.G. Zhang, H.B. Mao, J.Q. Wang, Z.Q. Zhu, W.P. Jing. *Photoluminescence and XPS investigations of Cu2+-doped ZnS quantum dots capped with polyvinylpyrrolidone*. Physical Status Solidi B. 246 (**2009)** 2333–2336.

[22] J.U. Kim, Y.K. Kim and H. Yang. *Reverse micelle-derived Cu-doped Zn1-xCdxS quantum dots and their core/shell structure*. Journal of Colloid and Interface Science. 341 (**2010)** 59–63.

[23] M. Fujii, Y. Yamaguchi, Y, Takase, K. Ninomiya and S. Hayashi. *Photoluminescence from impurity codoped and compensated Si nanocrystals*. Applied Physical Letters. 87 (**2005**) 1–3.

[24] S.B. Orlinskii, J. Schmidt, P.G. Baranov, D.M. Hofmann, C.D. Donega and A. Meijerink. *Probing the wave function of shallow Li and Na donors in ZnO nanoparticles*. Physical Review Letters. 92 (**2004**) 1–4.

[25] H.S. Yang, S. Santra and P.H. Holloway. *Syntheses and applications of Mn-doped II-VI semiconductor nanocrystals*. Journal of Nanoscience and Nanotechnology. 5 (**2005**) 1364–1375.

[26] A.P. Alivisatos. *Semiconductor clusters, nanocrystals, and quantum dots*. Science. 271 (**1996**) 933–937.

[27] V.I. Klimov, A.A. Mikhailovsky, S. Xu, et al. *Optical gain and stimulated emission in nanocrystal quantum dots*. Science. 290 (**2000**) 314–317.

[28] M. Henini. *Properties and applications of quantum dot heterostructures grown by molecular beam epitaxy*. Nanoscale Research Letters. 1 (**2006**)32-45.

[29] C.A Dai, Y.L. Wu, Y.H. Lee, C.J. Chang, W.F. Su. *Fabrication of 2D ordered structure of self-assembled block copolymers containing gold nanoparticles*. Journal of Crystal Growth, 288 (**2006**) 128-136

[30] A. Scherer, H.G. Craighead and E.D. Beebe. *Gallium-arsenide and aluminum gallium-arsenide reactive ion etching in boron-trichloride argon mixtures*. Journal of Vacuum Science and Technology B. 5 (**1987**) 1599–1605.

[31] K. Tsutsui, E.L. Hu and C.D.W. Wilkinson. *Reactive ion etched II-VI quantum dots–dependence of etched profile on pattern geometry*. Japanese Journal of. Applied Physics. Part 1. 32 (**1993**) 6233–6236

[32] E. Chason, S.T. Picraux, et al. *Ion beams in silicon processing and characterization*. Journal of Applied Physics. 81 (**1997**) 6513–6561

[33] C. Burda, X.B. Chen, R. Narayanan and M.A. El-Sayed. *Chemistry and properties of nanocrystals of different shapes*. Chemical Reviews. 105 (**2005**) 1025–1102.

[34] C. Lobo and R. Leon. *InGaAs island shapes and adatom migration behavior on (100), (110), (111), and (311) GaAs surfaces*. Journal of Applied Physics. 83 (**1998**) 4168–4172

[35] L. Spanhel, M. Haase, H. Weller and A. Henglein. *Photochemistry of colloidal semiconductors.20. Surface modification and stability of strong luminescing CdS particles*. Journal of American Chemical Society. 109 (**1987**) 5649–5655

[36] A. Sashchiuk, et al. *Optical and conductivity properties of PbS nanocrystals in amorphous zirconia sol-gel films*. Journal of Sol-Gel Science and Technology. 24 (**2002**) 31–38

[37] D. Bera, L. Qian, S. Sabui, S. Santra and P.H. Holloway. *Photoluminescence of ZnO quantum dots produced by a sol-gel process.* Optical Materials. 30. (**2008**) 1233–1239

[38] L. Spanhel and M.A. Anderson. *Semiconductor clusters in the sol-gel process quantized aggregation, gelation, and crystal-growth in concentrated ZnO colloids*. Journal of American Chemical Society. 113 (**1991**) 2826–2833

[39] V. Malgras. *Lead sulfide colloidal quantum dots passivation and optoelectronic characterisation for photovoltaic device application*. University of Wollong Thesis Collection. (**2014**)

[40] D. Bera, L. Qian, T. Tseng and P. H. Holloway. *Quantum Dots and Their Multimodal Applications: A Review.* Materials. (**2010**) 2271

[41] B.D. Dickerson. *Organometallic Synthesis Kinetics of CdSe Quantum Dots*. Virginia Polytechnic Institute and State University, Blacksburg, Virginia. (**2005**)

[42] R.A. Sperling. *Surface Modification and Functionalization of Colloidal Nanoparticles*, Fachbereich Physik, Universität Marburg. (**2008**)

[43] I. Liu, H. Lo, et al. *Enhancing photoluminescence quenching and photoelectric properties of CdSe quantum dots with hole accepting ligands.* Journal of Materials Chemistry. 18 (**2008**) 675-682

[44] O. Micic, H. Cheong, H Fu, A. Zunger, J Sprague, A. Mascarenhas, A.J. Nozik. *Size-Dependent Spectroscopy of InP Quantum Dots*. The Journal of Physical Chemistry B. 101 (**1997**) 4904-4912

[45] D.V. Talapin, S. Haubold, A.L. Rogach, A. Kornowski, M. Haase and H.J. Weller. *A Novel Organometallic Synthesis of Highly Luminescent CdTe Nanocrystals*. The Journal of Physical Chemistry B. 105 (12) (**2001**) 2260-2263.

[46] X.Wang, L. Qu, J. Zhang, X. Peng and M Xiao. Nano Letters. *Surface-Related Emission in Highly Luminescent CdSe Quantum Dots*. 3 (8) (**2003**) 1103-1106

[47] K.E. Knowles, D.B. Tice, E.A. McArthur, G.C. Solomon and E.A. Weiss. *Chemical Control of the Photoluminescence of CdSe Quantum Dot−Organic Complexes with a Series of Para-Substituted Aniline Ligands.* Journal of American Chemical Society. 132 (**2009)** 1041-1050.

[48] G.W. Bryant and W.J. Jaskolski. *Large Resonant Stokes Shift in CdS Nanocrystals*. The Journal of Physical Chemistry B. 107 (24) (**2005**) 5670–5674.

[49] P. Schapotschnikow, B. Hommersom and T.H.J. Vlugt. *Adsorption and Binding of Ligands to CdSe Nanocrystals.* The Journal of Physical Chemistry C. 113 (**2009**) 12690-12698.

[50] C. Bullen, C and P Mulvaney. *The Effects of Chemisorption on the Luminescence of CdSe Quantum Dots*. Langmuir. 22 (7) (**2006**) 3007-3013

[51] D. Godovsky. *Biopolymers·PVA Hydrogels. Anionic Polymerisation Nanocomposites* Advances in Polymer Science. (**2000)** 163-205.

[52] J.M. Luther et al. *Structural, optical and electronic properties of self-assembled films of PbSe nanocrystals treated with 1, 2-ethanedithiol.* ACS Nano. 2 (2) (**2008**) 271

[53] E.J. Klem, et al. *Impact of dithiol treatment and air annealing on the conductivity, mobility and hole density in PbS colloidal quantum dot solids*. Applied Physics Letters. 93 (21) (**2008**) 212105

[54] O. Voznyy et al. *A charge-orbital balance picture of doping in colloidal quantum dot solids*. ACS Nano. 6 (9) (**2012**) 8448

[55] K.S. Jeong et al. *Enhanced mobility-Lifetime Products in PbS Colloidal Quantum Dot Photovoltaics*. ACS Nano. 6 (10) (2012) 89

[56] P.D. Persans, A. Tu, Y.J. Wu and M. Levis. *Size-distribution-dependent optical properties of semiconductor microparticle composites.* Journal of the Optical Society of America B. 6 (**1989**) 818

[57] V. Jungnickel and F. Henneberger. *Luminescence related processes in semiconductor nanocrystals —The strong confinement regime*. J. Lumin. 70 (**1996**) 238

[58] T. Arai, K. Matsuishi, J. Lumin. *Electronic state of Cd-chalcogenide microcrystals embedded in GeO_2 glass studied by means of spectroscopy*. 70 (**1996**) 281

[59] Z. Yang, C.Y. Chen, P. Roy and H.-T. Chang. *Quantum dot-sensitized solar cells incorporating materials.* Chemical Communications. 47 (**2011**) 9561-9571.

[60] A. H. Ip, S.M Thon, S Hoogland, O. Voznyy, D. Zhitomirsky, R. Debnath, L. Levina, L.R. Rollny, G.H. Carey, A. Fischer, K.W. Kemp, I.J. Kramer, Z. Ning, A.J Labelle, K.W. Chou, A. Amassian and E.H. Sargent. *Hybrid passivated colloidal quantum dot solids*. Nature Nanotechnology. 7 (**2012**) 577-582

[61] R.J. Ellingson, M.C. Beard, J.C. Johnson, P. Yu, O.I. Micic, A.J. Nozik, A. Shabaev and A.L. Efros. *Highly efficient multiple exciton generation in colloidal PbSe and PbS quantum dots*. Nano Letters. 5(5) (**2005**) 865-871

[62] N. McElroy, et al. *Comparison of solar cells sensitised by CdTe/CdSe and CdSe/CdTecore/shell colloidal quantum dots with and without a CdS outer layer*. Thin Solid Films.560 (**2014**) 65–70

[63] K.S. Pralay and V.K. Prashant. *Mn-Doped quantum dot sensitized solar cells: A strategy to boost efficiency over 5%*. Journal of American Chemical Society. 134 (**2012**) 2508–2511

[64] K. Cheng, et al. *Plasmon-enhanced photocurrent generation in quantum dots-sensitized solar cells by coupling of gold nanocrystals*. Science Bulletin. 60(5) (**2015**) 541-548

[65] Q. Zhang, G Chen, Y Yang, X. Shen, Y. Zhang, C. Li, R Yu, Y Luo, D. Li and Q. Meng. *Toward highly efficient CdS/CdSe quantum dots-sensitized solar cells incorporating ordered photoanodes on transparent conductive substrates*. Physical Chemistry, Chemical Physic.14 (**2012**) 6479–6486

[66] H.K. Jun, M.A. Careem and A.K. Arof. *Quantum dot-sensitized solar cells—perspective and recent developments: A review of Cd chalcogenide quantum dots as sensitizers*. Renewable and Sustainable Energy Reviews. 22 (**2013**) 148–167

[67] H.M. Cheng, et al. *High-efficiency cascade CdS/CdSe quantum dot-sensitized solar cells based on hierarchical tetrapod-like ZnO nanoparticles*. Physical Chemistry, Chemical Physic. 14 (**2012**) 13539-13548

[68] M. Kneissl, et al. *Advances in group III-nitride-based deep UV light-emitting diode technology*. Semiconductor Science and Technology. 26 (**2011**) 014036

[69] O. Masala and R. Seshadri. *Synthesis routes for large volumes of nanoparticles*. Materials Research. 34 (**2004**) 41-81

[70] M. G. Bawendi, C. B. Murray and D. J. Norris. *Synthesis and characterization of nearly monodisperse CdE (E = sulphur, selenium, tellurium) semiconductor nanocrystallites.* Journal of American Chemical Society. 115 (19) (**1993**) 8706–8715

[71] B.D. Dickerson. *Organometallic Synthesis Kinetics of CdSe Quantum Dots*. VirginiaPolytechnic Institute and State University, Blacksburg, Virginia. (**2005**)

[72] K.H. Lee et al. *Quantitative Molecular Profiling of Biomarkers for Pancreatic Cancer with Functionalized Quantum Dots.* Nanomedicine. 8 (7) (**2012**) 1043-1051

[73] X. Peng, L Manna, W Yang, J Wickham, E Scher, A. Kadavanich and A. Alivisatos. *Shape control of CdSe nanocrystals*. Nature.404 (**2000)** 59-61

[74] D.V. Talapin, S. Haubold, A.L. Rogach, A. Kornowski, M. Haase and H. Weller. *A Novel Organometallic Synthesis of Highly Luminescent CdTe Nanocrystals.* Journal of Physical Chemistry B. 105 (**2001**) 2260-2263.

[75] D.V. Talapin, A.L. Rogach, I. Mekis, S. Haubold, A. Kornowski, M. Haase and H. Weller. *Synthesis and surface modification of amino-stabilized CdSe, CdTe and InP nanocrystals*. Colloids and Surfaces A: Physicochemical and Engineering Aspects. 202 (**2002**) 145-154.

[76] L. Liu, Q. Peng and Y Li. *An Effective Oxidation Route to Blue Emission CdSe Quantum Dots.* Inorganic Chemistry. 47 *(***2008)** 3182-3187.

[77] A. Kolodziejczak-Radzimska and T. Jesionowski. *Zinc Oxide-from Synthesis to Application: A review*." Materials. 7(4) (**2014**) 2833-2881.

Chapter 3
Methodology

3.1. Overview

Chapter 3 presents, the detailed experimental procedures used in the synthesis of CdSe QDs by the hot injection method as a method of choice. Here we report on an easy and low cost method to synthesise high quality CdSe QDs. The chapter starts off by providing the reagents and material used for the preparation of CdSe QDs. Moreover, this chapter presents the experimental set up of the system used in fabrication of CdSe quantum dots using the hot injection method. Chapter 3 closes off by presenting the detailed experimental procedures used in the morphological, structural and optical characterization of CdSe QDs synthesized by the hot injection method.

3.2. Hot Injection Method

The hot-injection method is arguably the most versatile and well-studied approach. The hot injection method was first reported in the early 90s by Murray and his co-workers [1]. In a typical synthesis procedure, trioctylphosphine oxide (TOPO), which is a coordinating solvent, was degassed in a three-neck round bottomed round flask. Afterwards, a mixture of methyl-Cd and tri-n-octyl-phosphine (TOP) selenide prepared separately was injected with vigorous stirring into the flask at a certain temperature. Simultaneous injection of precursors solutions into the flask, along with TOPO, results in homogeneous nucleation and formation of the desired quantum dots. This method has been extensively used over the years to synthesize II-VI and III-V quantum dots [2]. The hot injection method has been widely adopted as a method of choice for fabricating II-VI and III-V quantum dots mainly due to the numerous advantages it presents as compared to other methods discussed in Chapter 2. The hot injection method has been adopted due to the fact that it provides sufficient thermal energy to facilitate fast controlled growth of quantum dots which are defect free and monodispersed as compared to other methods presented in Chapter 2. Moreover,

the ability to fabricate QDs with tuneable dimensions and shapes translates into direct experimental control over the energy gap of the QD. Size-tuneable energy band gaps are arguably the most attractive features of semiconductor QDs and have been demonstrated in a broad range of material systems. Owing to the advantages indicated above, the hot injection method was adopted to fabricate CdSe QDs in this work. Fig. 3.1 presents a flow chart diagram that shows the main stages of involved in the synthesis of CdSe QDs by the hot injection method.

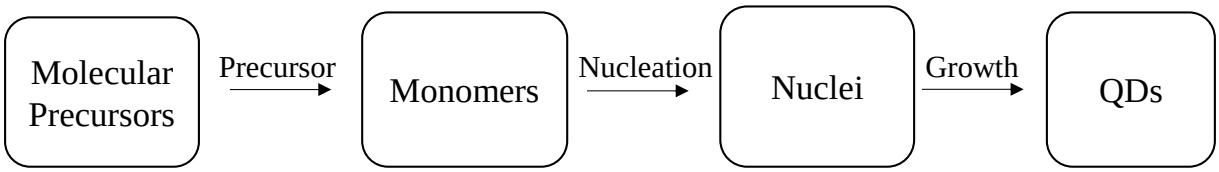

Figure 3.1: *Flow chart illustrating the main stages of QD synthesis by the hot injection method.*

3.2.1. Reagents and Raw Materials

The materials considered in this work are of the high quality and used as received.

[1] Cadmium acetate dihydrate [$Cd(CH_3COO)_2 \cdot 2H_2O$] (99%) from Merck

[2] Selenium powder -100 mesh,99%,Sigma-Aldrich

[3] 2-mercaptoethanol($HS(CH_2)2OH$),99.0%,Sigma-Aldrich

[4] Dimethyl formamide(DMF) of analytical grade, 99%, Merck

[5] Octadecene (ODE), (99%) from Merck

[6] Ethanol, Sigma Aldrich, 99.5%

[7] Toluene, CP, Merck

3.2.2. Experimental Setup

Fig. 3.2 presents the actual photograph of the hot injection method system used in preparation of CdSe QDs in this work.

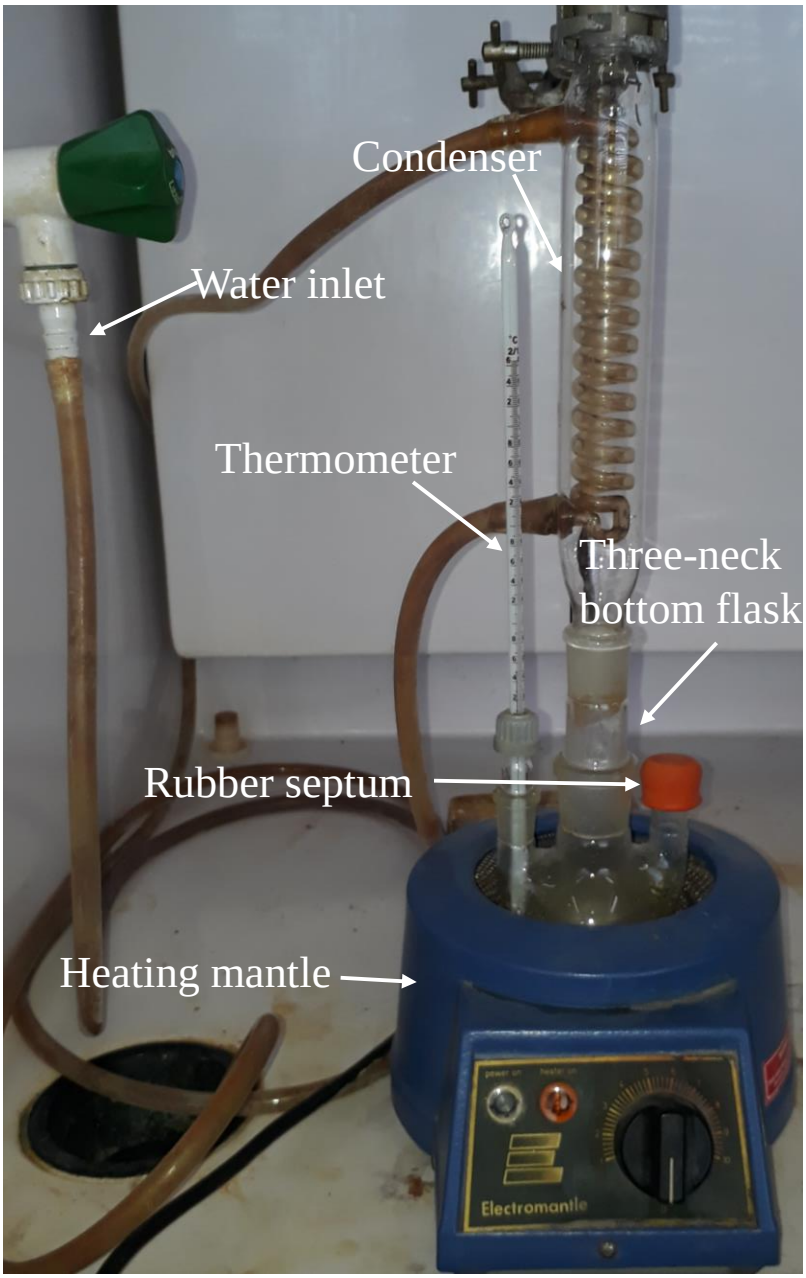

Figure 3.2*: Image of the experimental setup of the hot injection method used in this study in a fume cupboard.*

3.2.3. Heating mantle

An Electromantle Heating Mantle (Model EM 0250) was the heat source of choice for this study. EM 0250 are designed with flexibility and ease of use in mind, the EM heating mantle is a reliable workhorse for heating applications in the laboratory. The EM heating mantle has the following features: [1] They have a chemically resistant polypropylene outer casing, [2] Use with round bottom flasks from 50ml to 5 litres, [3] unique ventilation system which allows outer casing to remain safe to touch, [4] Maximum element temperature 450°C, [5] Built-in energy regulator and [6] Indicator lamps for power and heater operation, just to name a few. The significance of this instrument in this study was to provide maximum mixing of the quantum dots and to achieve the desired quantum dots at different temperatures.

3.2.4. Thermometer

In this study, an economy Glass thermometer with a glass ring top was used. The thermometer was used to monitor the temperature changes during the synthesis of CdSe QDs.

3.2.5. Glass Syringe

A 51 mm gas and liquid tight Hamilton syringe (Model 1005 RN Syr) was used for this work. Its main purpose was to inject the precursor solution into the reaction flask. It was also used to extract aliquots of the CdSe QDs from the reaction flask into the collection glass bottles.

3.3. Synthesis procedures

3.3.1. Synthesis of CdSe QDs

In a typical synthesis, selenium solution was prepared by reacting Se powder (0.036 g) and Octadecene (10 ml) in a two neck round bottom flask. The prepared selenium solution was subsequently heated at 150℃ until the colour of the solution changed from black to bright yellow. The solution was then cooled down and stored at room temperature for future use. In a 250 ml three neck bottom flask, a cadmium solution was prepared by dissolving 1.62 g of cadmium acetate dihydrate ($[Cd(CH_3)COO_2] \cdot 2H_2O$) into a solution containing 20 ml of Dimethylformadide (DMF) and 0.54 ml 2-mercaptoethanol.

Afterwards, the Cd precursor solution was then heated to 150℃ for 30 minutes and subsequently degassed with nitrogen to flush out any oxygen in the reaction flask. For the synthesis of CdSe QDs, the bright yellow selenium solution was then injected to the 250 ml three-neck round bottom flask containing Cd solution. After the injection of the Se precursor, aliquots of CdSe QDs were withdrawn at different temperatures of 150℃, 175℃, 200℃, 225℃, 250℃, 275℃ and 300℃. Moreover, the colour of the solution changed almost immediately indicating fast nucleation and growth. The prepared CdSe QDs were then suspended in toluene to prevent any further reactions.

Prior sample analysis, the prepared and suspended CdSe QDs were separated from the toluene solution by centrifugation. The collected centrifuged CdSe QDs samples were further centrifuged in ethanol at 5560 rpm for about 10 minutes. Using multiple washing steps enabled the removal of any starting materials that may be bound to the CdSe QDs surface, so we could achieve highly stable solutions of CdSe QDs. Fig. 3.3 presents the schematic diagram illustrating the sequence of events taken during the synthesis of CdSe QDs.

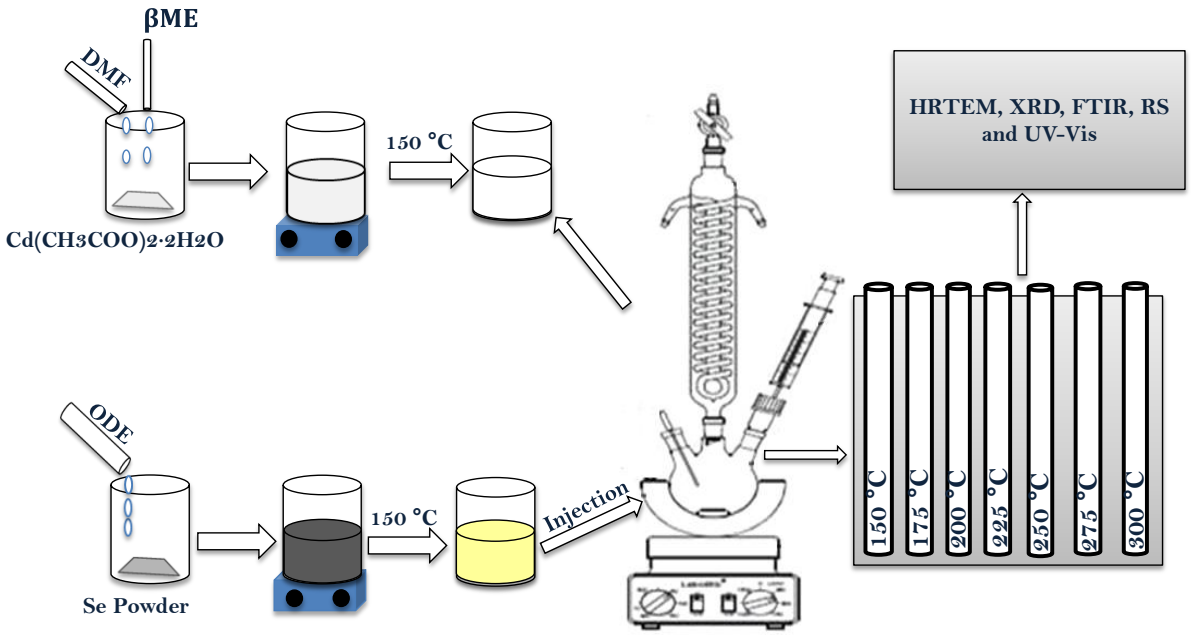

Figure 3.3: *A schematic diagram of the fabrication of CdSe QDs with different particle sizes using the hot injection method.*

3.4. Characterizations

Characterisation of nanocrystals is a fundamental process whereby a material's structure and properties are investigated and measured. It is a process in the field of science, without which no scientific understanding of engineering materials could be ascertained. Various properties of nanocrystals such as morphological, optical, and structural properties depend on the size and shape of the fabricated materials [4]. The size and crystal nature of CdSe QDs are their most important properties. In this study, a variety of techniques were used to evaluate the structural, morphological and optical properties of CdSe QDs. Thus, this section of Chapter 3 gives a more detailed report on the characterisation techniques that were used to characterise CdSe QDs.

3.4.1 Fourier Transform Infrared Spectroscopy

Fourier Transform-Infrared Spectroscopy (FTIR) is a non-destructive technique that provides a precise measurement method that requires no external calibration [5]. It is an analytical technique used to identify vibrational properties of organic and inorganic materials. FTIR measures the absorption of infrared radiation by the sample material versus wavelength. The infrared absorption bands identify molecular components and structures.

When a material is irradiated with infrared radiation, absorbed IR radiation usually excites molecules into a higher vibrational state. The wavelength of light absorbed by a particular molecule is a function of the energy difference between the at-rest and excited vibrational states. The wavelengths that are absorbed by the sample are characteristic of its molecular structure [6]. The efficacy of infrared spectroscopy arises when different chemical structures (molecules) produce a molecular fingerprint of the sample. Like a fingerprint, no two unique molecular structures produce the same infrared spectrum. This makes it useful for several types of analysis [7].

The FTIR spectrometer uses an interferometer to control the wavelength from a broadband infrared source. A detector measures the intensity of transmitted or reflected light as a function of its wavelength. The signal attained from the detector is an interferogram, which must be analysed with a computer using Fourier transforms in order to obtain a single-beam infrared spectrum. The FTIR spectra are usually presented as plots of intensity versus wavenumber (in cm-1). Wavenumber is the reciprocal of the wavelength. The intensity can be plotted as the percentage of light transmittance or absorbance at each wavenumber [6]. Figure 3.4 shows the spectrum two FTIR spectrometer used in this study from Perkin Elmer. The spectrometer is a compact instrument equipped with a standard high-performance, room temperature $LiTaO_5$ (Lithium

tantalite), mid-infrared (MIR) detector for enhanced signal-to-noise detection and a temperature stabilized detector [8]. FTIR spectrum of CdSe QDs is considerably different from that of the bulk. This is mostly due to changes in surface area, quantum confinement, particle size decrease, etc. [9]. In this regard, FTIR was employed to identify the bond between two or more atoms and identify functional groups of the synthesized CdSe QDs samples. The spectrum two FTIR spectrometer used in this study did not require any sample preparation.

In this study, FTIR spectra was obtained by placing crystalline samples on a flat top plate sample holder equipped with a 25 reflection, 45°, 50 mm ZnSe crystal, with a single reflection diamond that uses a pressure arm for contact between the sample and diamond. CdSe QDs were scanned in wavenumber range of 4000-350 cm^{-1}.

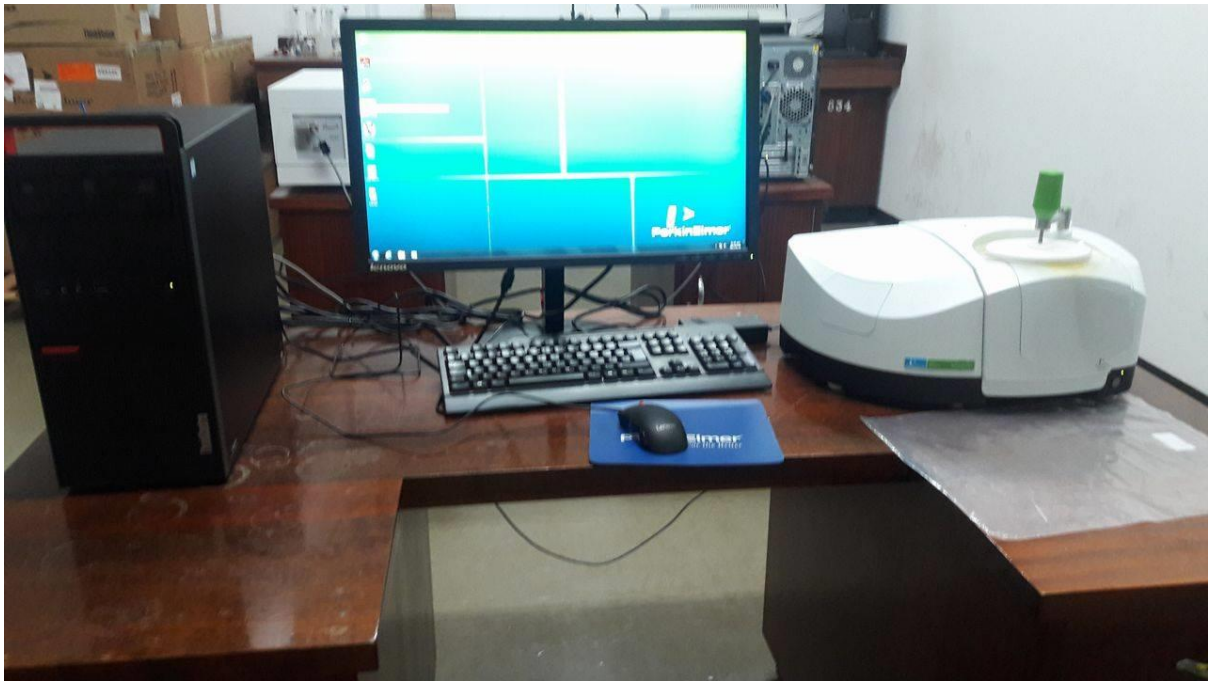

Figure 3.4: *Spectrum two FTIR (Perkin-Elmer)*

3.4.2. X-Ray Diffraction (XRD)

X-ray powder diffraction is a rapid analytical technique primarily used for phase identification of a crystalline material and can provide information on unit cell dimensions. The material being analysed is finely ground, homogenized, and average bulk composition is determined.

This technique was discovered by Max von Laue, in 1912 [10], and he found that crystalline substances act as three-dimensional diffraction gratings for X-ray wavelengths similar to the spacing of planes in a crystal lattice. X-ray diffraction is now the most used technique for the study of crystal structures and atomic spacing.

Moreover, X-ray diffraction is based on constructive interference of monochromatic X-rays and a crystalline sample. These X-rays are created by a cathode ray tube, filtered to produce monochromatic radiation, collimated to concentrate, and directed toward the sample. The interaction of the incident rays with the sample yields constructive interference (and a diffracted ray) when conditions satisfy Bragg's Law ($n\lambda=2d \sin \theta$) [11]. This law relates the wavelength of electromagnetic radiation to the diffraction angle and the lattice spacing in a crystalline sample. These diffracted X-rays are then detected, processed and counted. In this regard, by scanning the sample through a range of 2θ angles, all possible diffraction directions of the lattice should be achieved due to the random orientation of the powdered material. Conversion of the diffraction peaks to d-spacings allows identification of the material because each material has a set of unique d-spacings. Typically, this is achieved by comparison of d-spacings with standard reference patterns.

In conventional XRD, only crystalline materials can be visualized, as it is necessary to have a periodicity in the structure in the long-range, which nanomaterials lack (owing to their size). The method can be used to image powders in the dry state or suspended in a medium. The method can

also be used to measure the nanoparticle size. Moreover, the degree of atomic order can be studied using XRD.

In this work, X-ray measurements were carried out using the Bruker D8 Advance X-Ray diffractometer (XRD) with Cu anode generating Kα radiation of wavelength 1.544 Å and operating at 40 kV and 40 mA. For each measurement, a complete scan was made at (2θ) range of 10°-70° with scan rate of 3°/216s. The samples for the XRD measurements were prepared by casting the CdSe QDs dissolved in toluene on a glass substrate and subsequent drying under ambient conditions. The crystallite size d (nm) can be estimated using Debye Scherer's equation:

$$d = {k\lambda}/{\beta cos\theta} \qquad [3.1]$$

where d is the crystallite size, λ is the wavelength of the X-ray ($Cu_{k\alpha} = 0.154\, nm$), θ is the diffraction angle of the dominant peak, β is the full width at half maximum (FWHM) in radians, and k is the shape factor with a value of 0.89. Fig. 3.5 shows an image of a XRD instrument

Figure 3.5: *Image of an XRD instrument- A Bruker D8 Advanced diffractometer*

3.4.3. High Resolution Transmission Electron Microscopy (HR-TEM)

In order to monitor the size of the as prepared CdSe QDs, HRTEM was employed. High-resolution transmission electron microscopy (HRTEM) is an imaging mode of the transmission electron microscope (TEM) that allows for direct imaging of the atomic structure of the sample [12, 13]. The image is then magnified and focused onto an imaging device, such as a fluorescent screen, on a layer of photographic film, where the final image is formed [14]. In conventional HRTEM, image interpretation is performed by comparing numerically simulated images with images acquired at the electron microscope. The computer-simulated images are based on atomic model structures, including all imaging parameters that need to be known as precisely as possible. The resolution limit of the structure analysis is determined by the point resolution of the microscope which is the optical resolution of the objective lens.

For a few years HRTEM structure analysis has now been performed more reliably and with better resolution by object wave reconstruction. There are different methods to retrieve the object wave, and we use the reconstruction from focus series [15, 16, and 17]. A series of 10 to 30 images with defined focus increment is acquired from the region of interest. On the basis of the recorded image intensities, a first approximation of the exit wave is calculated by the so-called paraboloid method [18]. The object wave is then refined with a maximum-likelihood approach [19], and for that iterative procedure the comparison is made at the level of experimentally observed and calculated image intensities. In that method the imaging process in the electron microscope is virtually inverted. The final result is the retrieved object or exit wave. The exit wave can be reconstructed from the focus series and, compared to single exposures, be interpreted up to a higher resolution that corresponds to the so-called information limit (CM3000FEG: approx. 0.12 nm). The big advantage of the object wave is that the imaging procedure in the electron microscope with its entire imperfect imaging properties is eliminated, and thereby highly resolved

information directly from the electron exit surface of the specimen is recovered. Furthermore, HRTEM information is obtained in the form of two images, the phase and the amplitude contrast, and these contain much less noise than the original images of the electron microscope [20]. HRTEM has been extensively and successfully used for analysing crystal structures and lattice imperfections in various kinds of advanced materials on an atomic resolution scale. It can be used for the characterization of point defects, stacking faults, dislocations, precipitates grain boundaries, and surface structures [21] HRTEM yields information about particle size, size distribution and morphology of the QDs. This technique can also be used to find whether particles are uniformly dispersed and whether agglomeration is present in the sample.

In this study, the High resolution Transmission Electron Microscopy (HRTEM) coupled with FFT and SAED of CdSe QDs were performed on JEOL- JEM 2100 HRTEM. The HRTEM samples were prepared by dispersing purified CdSe QDs in toluene, followed by placing a small portion of the solution onto a carbon coated copper grid. The grids were then dried in a desiccator before images were taken. Fig. 3.6 shows a diagram of an HRTEM system.

Figure 3.6: *Image showing the HRTEM used in this study.*

3.4.4. Raman Spectroscopy

Raman spectroscopy is a technique that is useful in observing rotational, vibrational and other frequency modes in a system [27]. It is mostly used in chemistry to provide a structural fingerprint by which molecules can be identified. Raman spectroscopy represents a powerful non-destructive characterization technique to study structural properties of complex materials at a local level. The effect of Raman is based on inelastic scattering of laser light [23, 24], mostly in the visible range, by dynamic inhomogeneity of the system, e.g. phonons. In actual fact, Raman scattering by phonons is largely determined by electrons that mediate the scattering event. Scattering occurs when a monochromatic light beam passes through a crystal, involving Rayleigh scattering and Raman scattering. If there is an elastic collision between the incidents photons with the phonons in the material, a light with the same vibration frequency will be generated and noticed by Rayleigh scattering. However, if there is an inelastic collision between the incident photons with the phonons of the material, Raman scattering will be generated [23]. Therefore, Raman spectra contain information not only related to phonons, but also to electrons and electron-phonon interactions. Generally, all materials produce Raman spectra, with the exception of pure metals. Photons with smaller energy (or frequency) are perceived if compared to the incoming photon. This perceived energy is denoted as a Raman wavenumber if the reference energy (or frequency) is set as that of the incident radiation [25]. The Raman wavenumber is strongly influenced by impurities, microscopic structural changes and residual strains. These characteristics of materials cause changes on the phonon vibration. Due to this, one can observe the Raman peaks broadening and correlate with the breakdown of Raman selection rules [26]. There are three possible mechanisms for the phonon peak shifts in Raman spectra of nanostructures. The first one is spatial confinement within the quantum dot nanocrystal boundaries. The second one is related to the phonon localization by defects. Nanocrystals or quantum dots, produced by chemical methods or by the molecular-beam epitaxy, normally have

more defects than corresponding bulk crystals. The spatial confinement of optical phonons was studied by Richter et al. [27] who showed that the Raman spectra of nanocrystalline semiconductors are red-shifted and broadened due to the relaxation of the q-vector selection rule in the finite size nanocrystals. Optical-phonon confinement in wurtzite nanocrystals leads to somewhat different changes in Raman spectra due to the optical anisotropy of wurtzite lattice. Recently, Fonoberov and Balandin [28, 29] derived analytically an expression for the interface and confined polar optical phonon modes in spheroidal QDs with wurtzite crystal structure. Confined optical phonons in wurtzite nanocrystals were shown to have a discrete spectrum of frequencies different from those of bulk phonons.

We use Raman Spectroscopy in this study to examine the vibrations in Raman active vibrational modes of CdSe QDs. This was carried out by using Confocal Raman Imaging System (WITec) alpha 300RS. A fibre coupled DPSS laser 532 nm with 74 maximum output power after single mode fibre coupling of 44 mW was used as the excitation source. Data was then collected using a multimode fibre into a high throughput lens based spectrograph (UHTS 300) with 300 mm focal length and two gratings 600 g/mm & 1800 g/mm, both blazed at 550 nm. The UHTS 300 spectrograph was connected to a peltier cooled back illuminated CCD camera with better than 90% QE in the visible excitation. Each spectrum was acquired at an integration time of 1.09667s and about 200 accumulations were collected per each spectrum in the scan range 200-2400 cm^{-1}. Fig. 3.7 shows a Raman spectrometer used in this study.

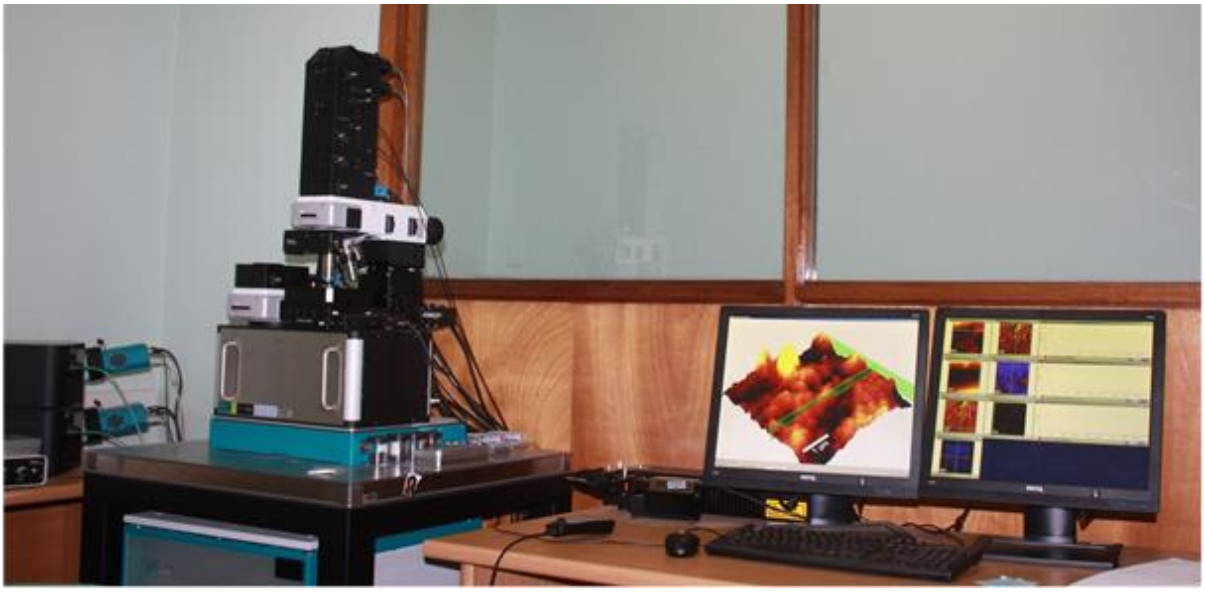

Figure 3.7: *Shows the picture of alpha300 Raman Confocal Microscope used in this study*

3.4.5. UV-Visible Spectroscopy

Ultraviolet and Visible absorption spectroscopy is the measurement of the attenuation of a beam of light after it passes through a sample or after it passes through a sample's surface. Absorption measurements can be at a single wavelength or even an extended spectrum.

It can also be described as an analytical technique that is widely employed for the quantitative analysis of a variety of analytes. Analysis using spectroscopic methods are commonly done with liquid samples, however solids and gases can also be analysed using this technique. Common analysed samples include transition metal ions, highly conjugated organic compounds and biological macromolecules. A UV-Vis spectrophotometer measures transmittance (%T) which is the ratio of the intensity of light that passes through a sample (I) and the intensity of the light before it passes through a sample (Io) at a given wavelength. Since absorbance is based on

transmittance, the Beer-Lambert law can be applied to determine concentration of species in solution:

$$A = Log10\,(Io/I) = c.L \qquad [3.2]$$

where A is the measured absorbance, $\%T = (Io/I)$, L is the path length through the sample, and c is the concentration of the absorbing species. And ε is the molar absorptivity constant which differs from one element to the next. In this study, analysis of optical properties of CdSe QDs were carried out at room temperature using the Perkin Elmer Lambda 365 Spectrometer and 10 mm quartz cuvettes in wavelength range of 400 - 750 nm. Fig. 3.8 (a and b) shows the schematic diagram of a double beam UV-Vis Spectrometer and image of a 365 Perkin Elmar Lambda 365 Spectrometer used in this study.

a) b)

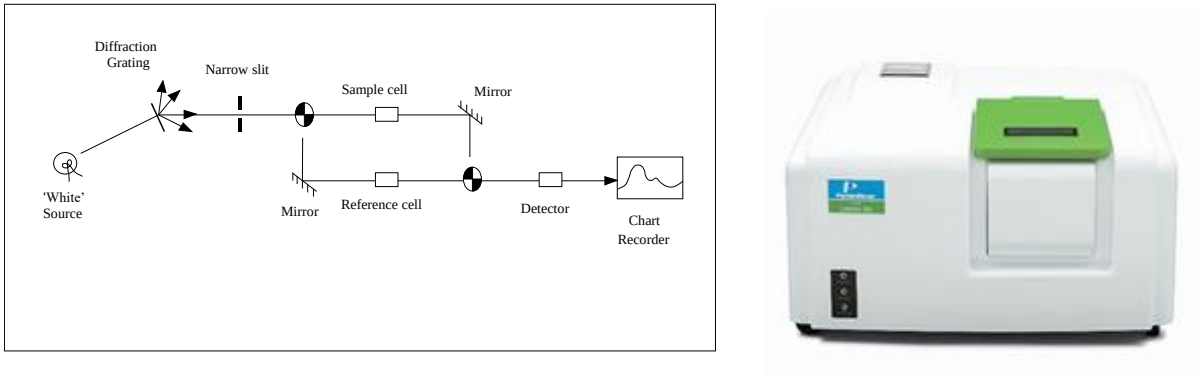

Figure 3.8: *(a) Shows schematic of a UV-Vis Spectrometer and (b) image of UV-Vis spec used in this study - Perkin Elmar Lambda 365 Spectrometer*

3.5. Conclusions

In conclusion, chapter 3 has presented a detailed experimental procedures used in the fabrication of CdSe QDs using the hot injection method. In a typical synthesis procedure, a selenium precursor solution was prepared and injected into the cadmium precursor containing reaction flask, nucleation occurred and CdSe QDs were formed. Additionally, Chapter 3, has presented actual photograph of the experimental set up of the system used in synthesis of CdSe Quantum dots. Additionally, Chapter 3 has presented the theoretical framework and the detailed experimental techniques used in the morphological, structural and optical characterization of CdSe quantum dots.

3.6. References

[1] C.B. Murray, D.J. Norris & M.G. Bawendi. *Synthesis and Characterization of Nearly Monodisperse CdE (E = Sulphur, Selenium, Tellurium) Semiconductor Nanocrystallites*. Journal of the American Chemical Society. 115(19) (**1993**) 8706-8715.

[2] D. Battaglia and X. Peng. *Formation of High Quality InP and InAs Nanocrystals in a Noncoordinating Solvent*. Nano Letters. 2 (9) (**2002**) 1027-1030

[3] J.D Bryan and D.R. Gamelin. *Doped semiconductor nanocrystals: Synthesis, characterization, physical properties, and applications.* Progress in Inorganic Chemistry. 54 (**2005**) 47–126.

[4] M. Op de Beeck, D. Van Dyck and W.M.J. Coene: *Wave function reconstruction in HRTEM: the parabola method.* Ultramicroscopy. 64 (**1996**) 167

[5] B. Stuart. *Infrared Spectroscopy: Fundamentals and Applications*. (**2004**)

[6] http://www.mee-inc.com/hamm/fourier-transform-infrared-spectroscopy-ftir/

[7] M.J. Baker, J. Trevisan, etal. *Using Fourier transform IR spectroscopy to analyze biological materials.* Nature Protocols. 9 (**2014**) 1771–1791

[8] Spectrum Two users Guide Perkin Elmer. (**2016**)

[9] J. A. Eastman, L. J. Thompson and B. J. Kestel, *Narrowing of the palladium-hydrogen miscibility gap in nanocrystalline palladium*. Physical Review B. 48 (1) (**1993**) 84-92

[10] P.P. Ewald. (ed.) *50 Years of X-Ray Diffraction* (Reprinted in pdf format for the IUCr XVIII Congress, Glasgow, Scotland, International Union of Crystallography). 4 (**1999**) 37–42

[11] N. Kumar and S. Kumbhat, Essentials in Nanoscience & Nanotechnology, Hoboken: John Wiley & Sons. (**2016**)

[12] J.C.H. Spence. *Experimental high-resolution electron microscopy*. New York: Oxford U. Press. (**1988**)

[13] J. C. H. Spence. *Imaging dislocation cores - the way forward*. Philosophical Magazine. 86 (**2006**) 4781–4796

[14] Z.L. Wang, Y. Liu, Z. Zhang. *Handbook of nanophase and nanostructured materials*.4th edition, New York. (**2003**)

[15] W.O. Saxton. *Object reconstruction, In Computer Techniques for Image Processing in Electron Microscopy* (Ed. L. Marton), Academic Press, New York. (**1978**) 236.

[16] D. Van Dyck, W.M.J. Coene: *A new procedure for wave reconstruction in high resolution electron microscopy*. Optik 77 (**1987**) 125.

[17] D Van Dyck, M. Op de Beeck, W.M.J. Coene: *A new approach to object wave reconstruction in electron microscopy*. Optik 93 (**1993**) 103.

[18] M. Op de Beeck, D. Van Dyck, W.M.J. Coene. *Wave function reconstruction in HRTEM: the parabola method*. Ultramicroscopy 64 (**1996**) 167.

[19] W.M.J. Coene, A. Thust, M. Op de Beeck. *Maximum-likelihood method for focus variation image reconstruction in high resolution transmission electron microscopy*. Ultramicroscopy 64 (**1996**) 109.

[20] https://www.researchgate.net/post/What_is_the_difference_between_TEM_and_HRTEM [accessed Aug 10, 2017]

[21] https://www.researchgate.net/post/What_is_the_difference_between_TEM_and_HRTEM [accessed Aug 10, 2017]

[22] D.J. Gardiner. *Practical Raman spectroscopy*. Springer-Verlag. 94 (9) (**1989**) 1047

[23] J. Yan., T. Asami, T. Kuriyagawa. *Nondestructive measurement of machining-induced amorphous layers in single-crystal silicon by laser micro-Raman spectroscopy*. Precision Engineering 32 (**2008**) 186-195.

[24] D.C. Harris, M.D. Bertolucci. *Symmerty and Spectroscopy: an Introduction to Vibrational and Electronic Spectroscopy*. Dover Publications (**1989**)

[25] C. Smit, R.A C.M.M. Swaai, H. Donker, A.M.H.N. Petit, W.M.M. Kessels, M.C.M. Sanden. *Determining the material structure of microcrystalline silicon from Raman spectra*. Journal of Applied Physics. 94 (**2003**) 3582-3588.

[26] J. A. Eastman, L. J. Thompson and B. J. Kestel. *Narrowing of the palladium-hydrogen miscibility gap in nanocrystalline palladium*. Physical Review B. 48 (1) (**1993**)

[27] H. Richter, Z. P. Wang, and L. Ley. *The one phonon Raman spectrum in microcrystalline silicon.* Solid State Communications. 39 (**1981**) 625-629

[28] V. A. Fonoberov and A. A. Balandin. *Interface and confined optical phonons in wurtzite nanocrystals*. Physical Review B. 70 (**2004**) 233205

[29] V. A. Fonoberov and A. A. Balandin. *Interface and confined polar optical phonons in spherical ZnO quantum dots with wurtzite crystal structure*. Physica Status Solidi C. 1 (11) (**2004**) 2650-2653

Chapter 4
Results and Discussion

4.1. Background

Quantum dots (QDs) are currently a subject of intense research activity targeting a wide range of potential applications, including light-emitting diodes (LEDs), fluorescent tags for biological imaging, single-electron transistors, and solar cells. The utility of nanocrystals lies in their unique size-dependent optical, structural, morphological and electronic properties, chiefly a size-tunable optical absorption and emission spectra. Chapter 4 presents and discusses the experimental findings of CdSe QDs synthesised by the hot injection method. It presents the morphological, structural and optical properties of the as synthesised CdSe QDs. Chapter 4 kicks off by presenting the structural properties of CdSe QDs obtained through XRD, FTIR and Raman spectroscopy. The effect of annealing temperature on the Raman vibrational modes of CdSe QDs is also presented and scrutinized here in detail. Lastly the Optical properties of CdSe QDs obtained through UV-Vis spectroscopy, the method devised by Yu et al [28] was adopted to confirm the crystallite size of CdSe synthesized by the hot injection method.

4.2. Structural Characterization

This section of Chapter 4 present the techniques used in this study to structural scrutinize the properties of CdSe QDs.

4.2.1. Fourier Transform Infrared Spectroscopy

Flourier Transform Infrared spectroscopy (FTIR) gives sufficient information about the surface chemical structure of nanomaterials [1]. Transmittance of infrared radiation results in oscillatory change in bond geometry as its dipole moment changes. The bond geometry changes are observed as bond stretching, bending or scissoring movement. [2]. Fig. 4.1 shows FTIR spectra of CdSe QDs synthesized using the hot injection method. In all the FTIR spectra, the QDs show characteristic vibrations at 738-733 cm^{-1} which is associated with Cd-Se bond. This observation confirms that the synthesised QDs consist of Cd~~-~~Se single bond. Moreover, it has been reported that in bulk CdSe, the Cd-Se characteristic vibration is observed at 730 cm^{-1} [3]. Therefore the presence of the peaks at 738, 738, 738, 738, 735, 735 and 733 cm-1 for 150, 175, 200, 225, 250, 275, and 300℃, respectively, further confirms that the fabricated samples in this work are CdSe QDs. This observation is in mutual agreement with literature.

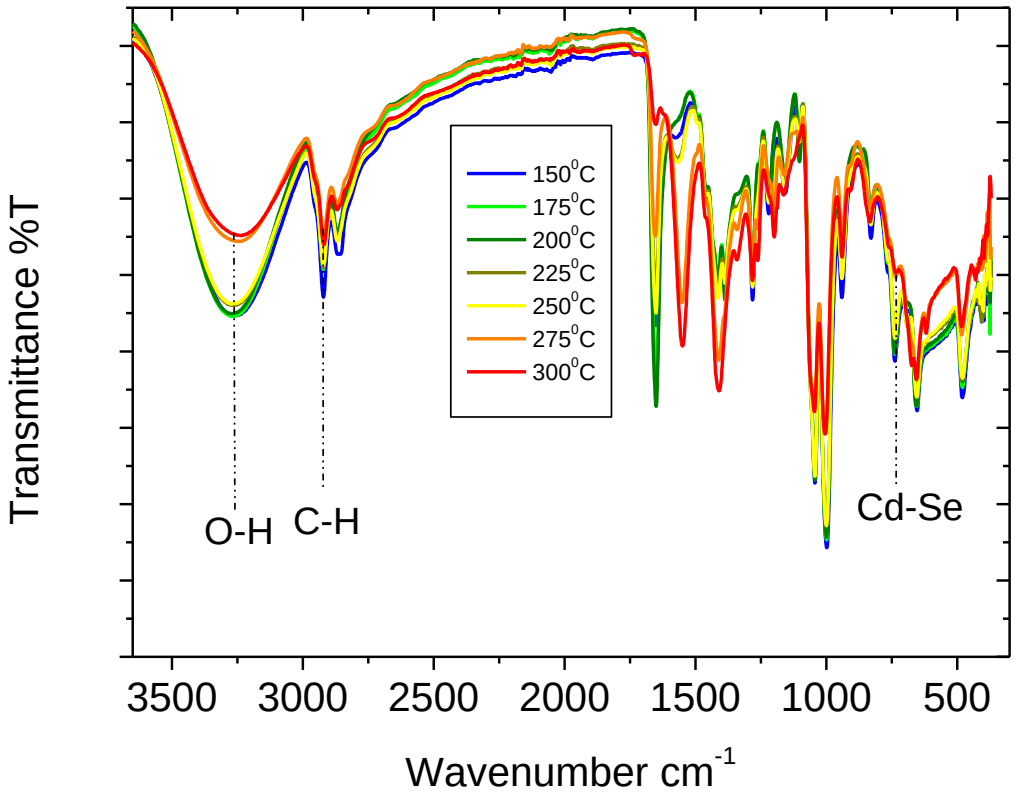

Figure 4.1*: shows FTIR spectra of CdSe–QDs synthesised by the hot-injection method.*

Additionally, the FTIR spectra in Fig 4.1 also reveal peaks at 3279, 3274, 3270, 3270, 3261, 3248 and 3234 cm^{-1} for the CdSe QDs synthesized at 150, 175, 200, 225, 250, 275 and 300℃, respectively. These peaks are due to the O-H stretching from the hydroxyl group stretching originating from absorbed water molecules on the surface of the CdSe QDs. Moreover, the presence of this peak might be due to the OH that is found at the other end of the capping agent, 2-mercaptoethanol. The presence of this peak also confirmed that the QDs are functionalized with hydroxyl group from the capping agent 2-mercaptoethanol.

Furthermore, Fig 4.1 has revealed two sharp peaks observed at around 1648-1404 cm^{-1} due to the stretching vibrations of the thiol capping. This indicates that the capping agent was over coated on the surface of the CdSe. The absence of S-H vibration at 2556-2654 cm^{-1} shows that on the CdSe

QD surface, thiolates are attached to the Cd^{2+} sites via the sulphur atom of the 2-mercaptoethanol to form a Se–Cd–S bonded structure [4]. This means that the capping of 2-mercaptoethanol had taken place through covalent bonding of thiols to the QD surface. Additionally, the peaks which appeared at 2924, 2922, 2921, 2921, 2921, 2920 and 2919 cm^{-1} for 150, 175, 200, 225, 250, 275 and 300℃, respectively were assigned to the overtone band vibrations of C-H from the methyl group coming from the structure of 2-mercaptoethanol.

Moreover, we extend the FTIR spectra in 900-350 cm^{-1} in order to observe the Cd-Se peak which confirms the synthesis of CdSe QDs.

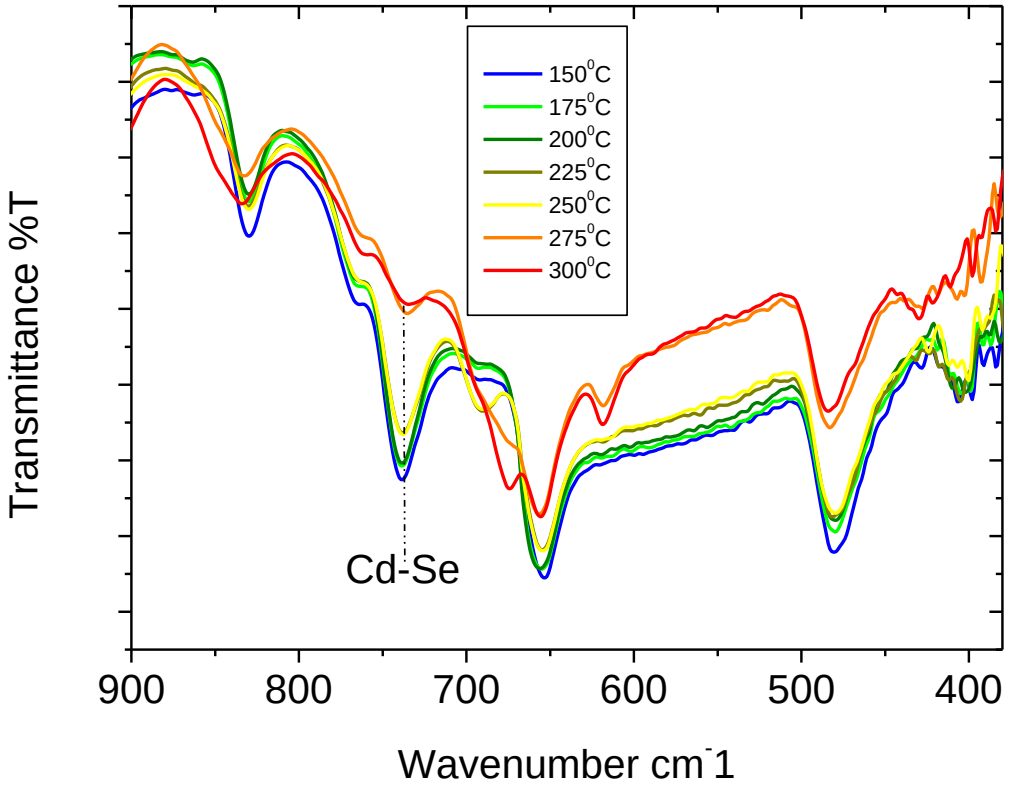

Figure 4.2: *Extended FTIR spectra of CdSe QDs*

Fig. 4.2 represents the extended FTIR spectrum of CdSe QDs. The extended region lies in the range of 900-360 cm^{-1}. The extended spectra of CdSe QDs samples reveal peaks at 738, 738, 738,

738, 735, 735 and 733 cm^{-1} for 150, 175, 200, 225, 250, 275, and 300℃, respectively. The Cd-Se vibration is slightly red shifted to higher wavenumber as temperature was increased. The red shift might be due to change in crystallite size. Furthermore, the intensity of the Cd-Se vibrations increased as the temperature was increased. The change in intensity of Cd-Se vibrations might also be due to change in crystallite size.

Table 4.1: *Summarises the results obtained from FTIR technique. It can be seen that the Cd-Se bonds have shifted to higher wavenumber when compared to the bulk.*

Bond	CdSe Bulk (cm^{-1})	QD1 (cm^{-1})	QD2 (cm^{-1})	QD3 (cm^{-1})	QD4 (cm^{-1})	QD5 (cm^{-1})	QD6 (cm^{-1})	QD7 (cm^{-1})
OH	3600-3200	3279	3274	3270	3270	3261	3248	3234
Cd-Se	730	738	738	738	738	735	735	733
C-H	2950-2750	2924	2922	2921	2921	2921	2920	2919

4.2.2. X-Ray Diffraction

XRD is a primary characteristic tool used for obtaining critical features such as crystal structure and crystallite size [5]. In this study, XRD technique was used to investigate the effect of temperature on the crystalline structure and size of CdSe QDs synthesised using the hot injection method. Figure 4.3 presents the X-ray diffraction pattern of the as synthesised CdSe QDs at 150ºC, 175ºC, 200ºC, 225ºC, 250ºC, 275ºC and 300ºC. The XRD patterns of CdSe QDs were recorded in the 2θ range of 10° – 80° at room temperature. The diffraction patterns were compared with reference to JCPDS database. The XRD diffractograms of CdSe samples exhibited peaks at scattering angles (2θ) of 16.66°, 25.20°, 34.77°, 40.9°, 45.39° and 49.10° for 150°C;

17.40°, 25.22°, 34.85°, 41.7°, 44.45° and 47.5° for 175°C; 17.07°, 25.19°, 34.85°, 41.34°, 44.41° and 48.86° for 200°C; 16.34°, 25.20°, 34.76°, 40.6°, 44.74° and 49.48° for 225°C; 17.44°, 25.17°, 34.19°, 41.70°, 44.45°, 49.24° for 250°C; 16.70°, 25.16°, 34.85°, 40.32°, 45.10° and 49.1°7 for 275°C;and 17.35°, 25.18°, 35.13°, 41.63°, 45.70°, 49.48° for 300°C. According to JCPDS No 08-0456, the XRD peaks correspond to crystal planes of (100), (002), (102), (220), (103) and (112). Earlier studies obtained comparable results as well [7]. All peaks belong to the hexagonal Wurtzite CdSe structure. The presence of these peaks in CdSe QDs samples confirms that the synthesised CdSe QDs have a hexagonal Wurtzite structure.

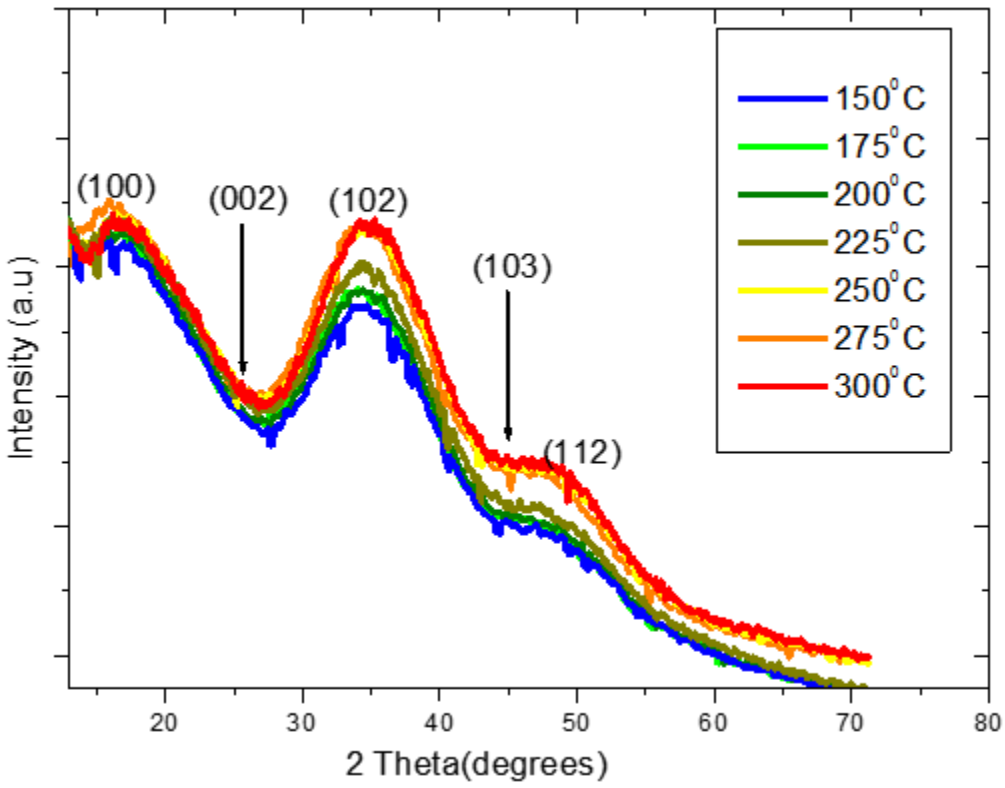

Figure 4.3: *X-Ray diffractogram of CdSe QDs synthesised using the hot injection method.*

Fig 4.3 presents the XRD of the as fabricated CdSe QDs with different growth temperatures.

As already mentioned above, the XRD of CdSe presents peaks at (2θ) angles for crystal planes (100), (002), (102), (220), (103) and (112). The presences of the peaks at crystallographic planes (102) and (103) confirm the Wurtzite crystal structure of CdSe QDs [10, 11], which is good agreement with FTIR results which revealed peaks at 738, 738, 738, 738, 735, 735 and 733 cm^{-1} for 150ºC, 175ºC, 200ºC, 225ºC, 250ºC, 275ºC and 300ºC, respectively, for Cd-Se bond. Moreover, the XRD analysis confirmed peak shift in the (2θ) angles as presented in Fig 4.3. This observation is in close agreement with the calculated crystallite size from equation [1] which show an increase in size as temperature is increased. Furthermore, the increase in temperature highlighted the sharpness and narrowness of the XRD peaks with great intensity. This phenomenon can also be attributed to particle size expansion. The size of CdSe QDs can be estimated by using the peak broadening of the peaks in the XRD pattern. This has been done by employing the Debye-Sherrer method [12], which is considered as a standard method. Equation 3 presents the Debye-Sherrer method and is depicted below as:

$$\tau = {K\lambda}/{\beta cos\theta} \qquad [4.1]$$

where τ is the mean size of the QD, K is a shape factor, λ is the wavelength of the X-rays, β is the full width at half maximum in radians, and θ is the angle between the X-ray source and the detector. The value of K depends on the shape of the particles and here the value 0.94, which is a customary value for spherical QDs has been used [5]. The average particle size calculated from equation [1] was 1.77, 1.82, 1.91, 1.96, 1.97, 3.11 and 3.14 nm at temperatures 150, 175, 200, 225, 250, 275 and 300℃, respectively.

The particle size calculated from the Debye-Scherrer equation according to the full width at half maximum (102) peak is in close agreement with the average sizes estimated from the HRTEM

images. The diffraction patterns of all the samples match with hexagonal Wurtzite phase of CdSe QDs, but the intensities of (002) and (103) are significantly weak when compared to (100), (102) and (112). This might possibly be caused by surface reconstruction occurring during synthesis of the QDs. When compared to bulk CdSe, the central positions of XRD peaks exhibit slight shifts to higher scattering angles. Since it was indicated by the HRTEM images of our QDs that these CdSe QDs are spherical in shape, Murray and his co-workers [1] proposed that the spherical shape can induce some shifts in XRD peaks of CdSe QDs. It is believed that the shifts measured in these samples are not due to the spherical shape, but from the lattice contractions. The lattice contraction effect was first observed in the experiment on CdSe QDs in glass matrices [12, 13]. Since these CdSe QDs are free standing, the presence of the lattice contraction must be induced from surface tension due to surface reconstruction [14].

Additionally, broadening of the XRD peaks was also observed. It is well known that under stress or strain effects, the diffraction peaks get displaced and broadened [8]. Fig. 4.3 has revealed that the diffraction peaks become broader with a decrease in QD size. This means that broadening of the XRD pattern of CdSe QDs is observed due to the small dimensions of CdSe QDs. Broadening and small shifts to higher 2θ angles is the characteristic feature to the formation and growth of CdSe QDs.

Table 4.2 summarises the XRD patterns of the as synthesised CdSe QDs for temperatures 150°C, 175°C, 200°C, 225°C, 250°C, 275°C and 300°C. `

Table 4.2 *Position of the main diffraction peaks from XRD patterns of CdSe QDs*

Temp(°C)	Peak Angles (°) and Crystallographic plane				
	(100)	(002)	(102)	(103)	(311)
150	16.66	25.20	34.77	45.39	49.1
175	17.4	25.22	34.85	44.45	47.5
200	17.07	25.19	34.85	44.41	48.86
225	16.34	25.20	34.76	44.74	49.48
250	17.44	25.17	34.19	44.45	49.24
275	16.70	25.16	34.85	45.1	49.17
300	17.35	25.18	35.13	45.7	49.48

In order to closely monitor the effect of temperature on the XRD pattern of CdSe QDs synthesised by the hot injection method, the dominant peak of CdSe QDs which is at 34.77, 34.85, 34.85, 34.76, 34.19, 34.85 and 35.13 for 150ºC, 175ºC, 200ºC, 225ºC, 250ºC, 275ºC and 300ºC, respectively, belonging to crystal plane (102) was examined. Fig. 4.4 shows the XRD peak shift dependence on temperature. It has been reported elsewhere that an increase in synthesis temperature results in peak shift to higher 2θ values. In CdSe QDs samples, a general increase in 2θ values was observed which indicates the formation and growth of CdSe QDs.

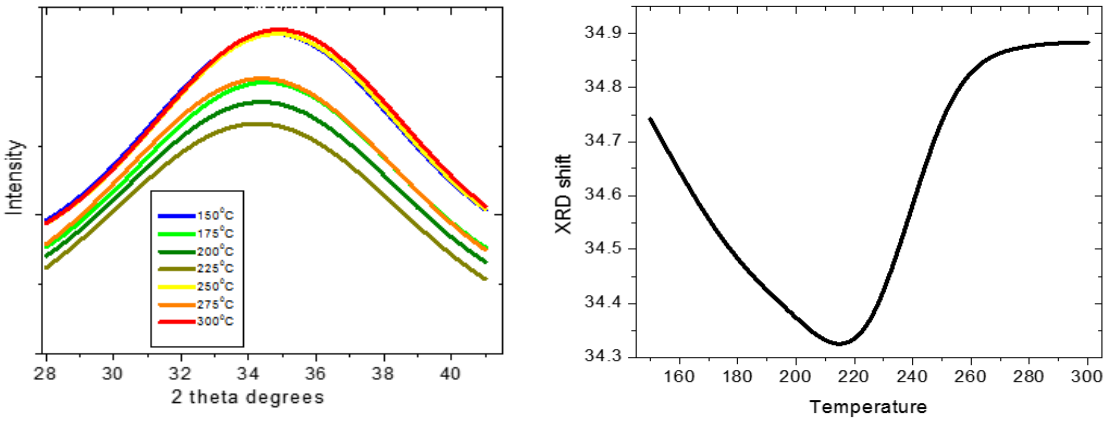

Figure 4.4: *XRD peak shift versus temperature.*

4.2.3. High Resolution Transmission Electron Microscopy

For morphological analysis, HRTEM was used. HRTEM reveals information about the particle size, size distribution and shape of CdSe QDs. Typical HRTEM images of CdSe QDs synthesised using the hot injection method are shown in Fig. 4.5 to 4.11 inclusive. The HRTEM images show that the as synthesised CdSe QDs are spherical in shape and are agglomerated, an observation that is common in QDs synthesized by colloidal routes employing thiols as capping agents [7]. Additionally, Image J was used to estimate the particle sizes of CdSe QDs from their HRTEM images. HRTEM analysis revealed that the modal particle sizes of CdSe QDs synthesised using the hot injection method were 1.79 nm, 1.81 nm, 2.06 nm, 2.08 nm, 2.11 nm, 3.10 nm and 3.12 nm for the QDs synthesized at 150ºC, 175ºC, 200ºC, 225ºC, 250ºC, 275ºC and 300ºC, respectively. The estimated crystallite sizes are in close agreement with the calculated particle sizes from XRD analysis that has revealed QDs sizes of 1.77, 1.82, 1.91, 1.96, 1.97, 3.11 and 3.14 nm at temperatures 150, 175, 200, 225, 250, 275 and 300℃, respectively. This observation is further summarised in Table 4.3.

Table 4.3: *Comparison between the particle sizes estimated from HRTEM and the particle size calculated from XRD.*

QDs sample Temp (℃)	HRTEM QDs size nm	XRD QDs size nm
150	1.79	1.77
175	1.81	1.82
200	2.06	1.91
225	2.08	1.96
250	2.11	1.97
275	3.10	3.11
300	3.12	3.14

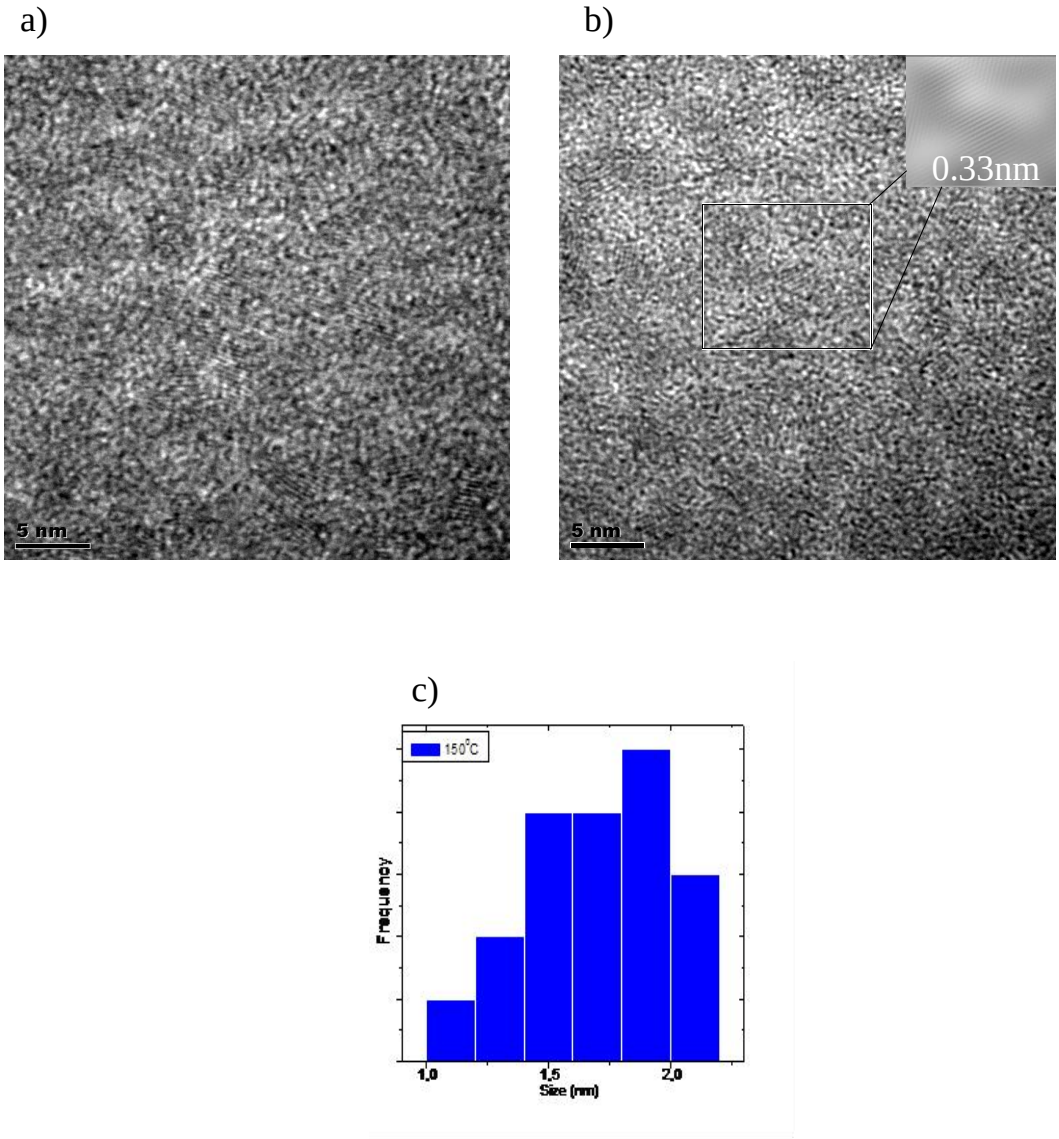

Figure 4.6: a) *HRTEM images with b) IFFT insert and c) histogram of CdSe QDs at 150*℃.

Fig. 4.6 (a) and (b) shows the crystalline structure of CdSe QDs at 150℃ with the spacing between (100) adjacent lattice planes of 0.33 nm. The lattice spacing of 0.33 is in good agreement with the d-spacing of (100) planes of hexagonal Wurtzite CdSe structure. The HRTEM analysis is consistent with the XRD results. The corresponding histogram in Fig 4.6 (c) revealed that CdSe QDs have a uniform size distribution. Among 100 particles measured for CdSe QDs at 150℃ a size of 1.79 nm was the most commonly witnessed.

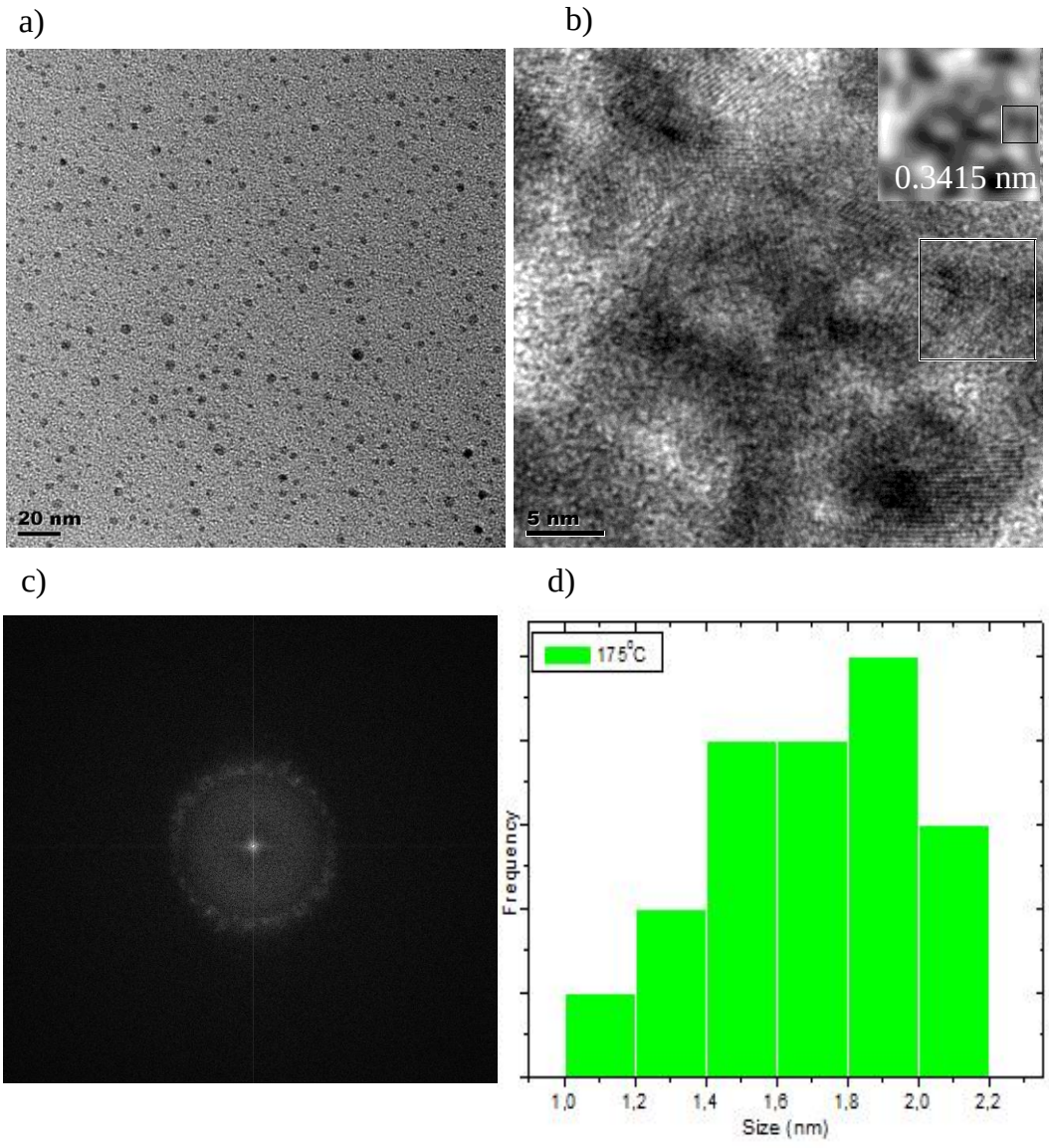

Figure 4.7: a) *HRTEM image with b) IFFT insert, c) SAED image and d) histogram of CdSe QDs at 175℃*

Fig. 4.7 shows the HRTEM image of CdSe QDs synthesized by the hot injection method at 175℃. HRTEM image analysis revealed lattice fringes of 0.345 nm corresponding to lattice plane of (002) of hexagonal Wurtzite CdSe structure. The HRTEM analysis is consistent with the XRD results, which further confirms the crystalline structure of hexagonal Wurtzite CdSe. Moreover, the histogram revealed that CdSe QDs at this temperature has an average particle size of 1.81 nm.

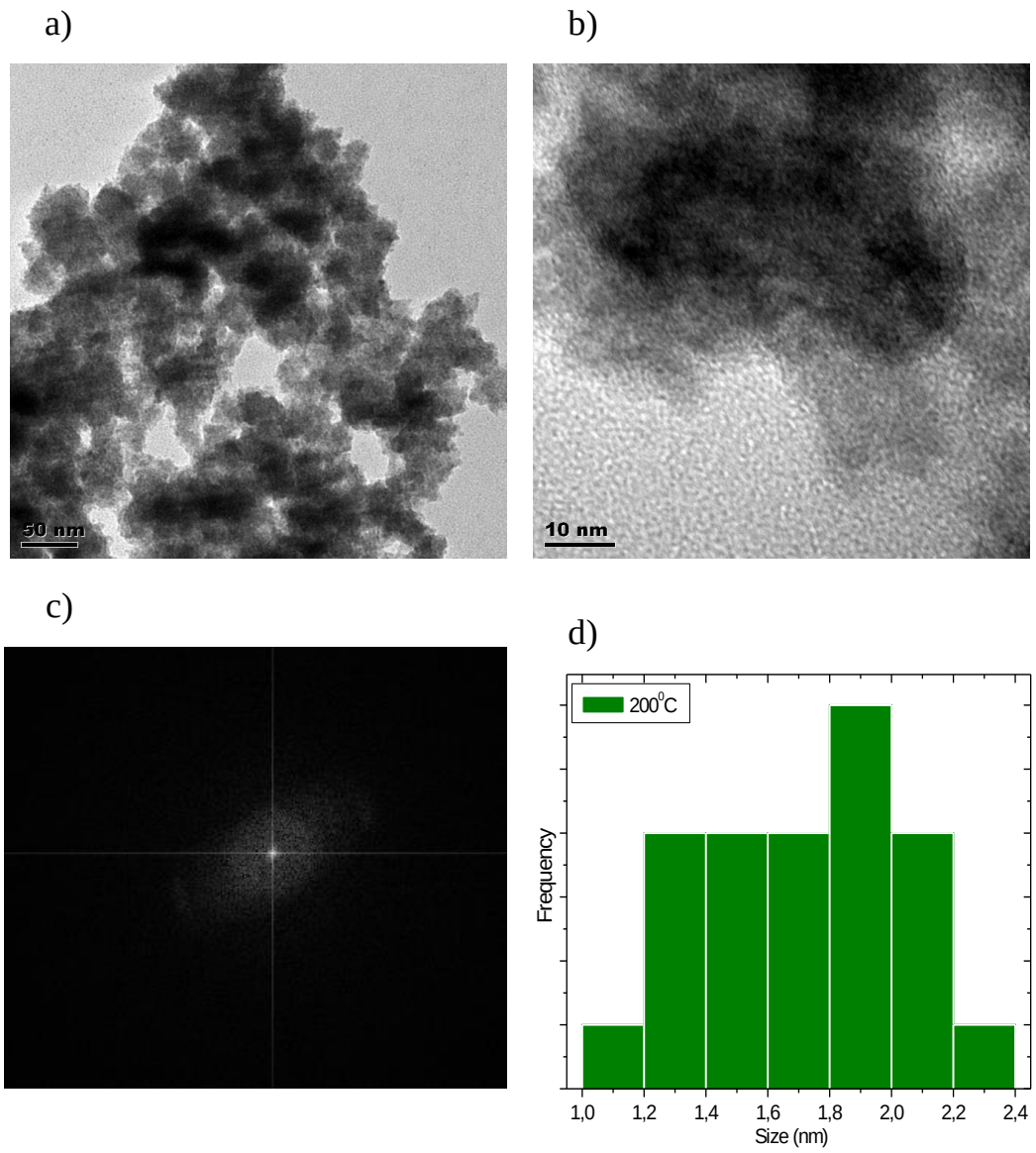

Figure 4.8: a) and b) *HRTEM images, c) SAED image and d) histogram of CdSe QDs at 200℃*

Fig. 4.8 shows the HRTEM images coupled with SAED image and histogram of CdSe QDs synthesised at 200℃ by the hot injection method. The histogram revealed that CdSe QDs at this temperature has an average particle size of 2.06 nm. In addition, the selected area electron diffraction (SAED) showed concentrated electron diffraction rings which confirm that the as synthesised CdSe QDs have a Wurtzite structure.

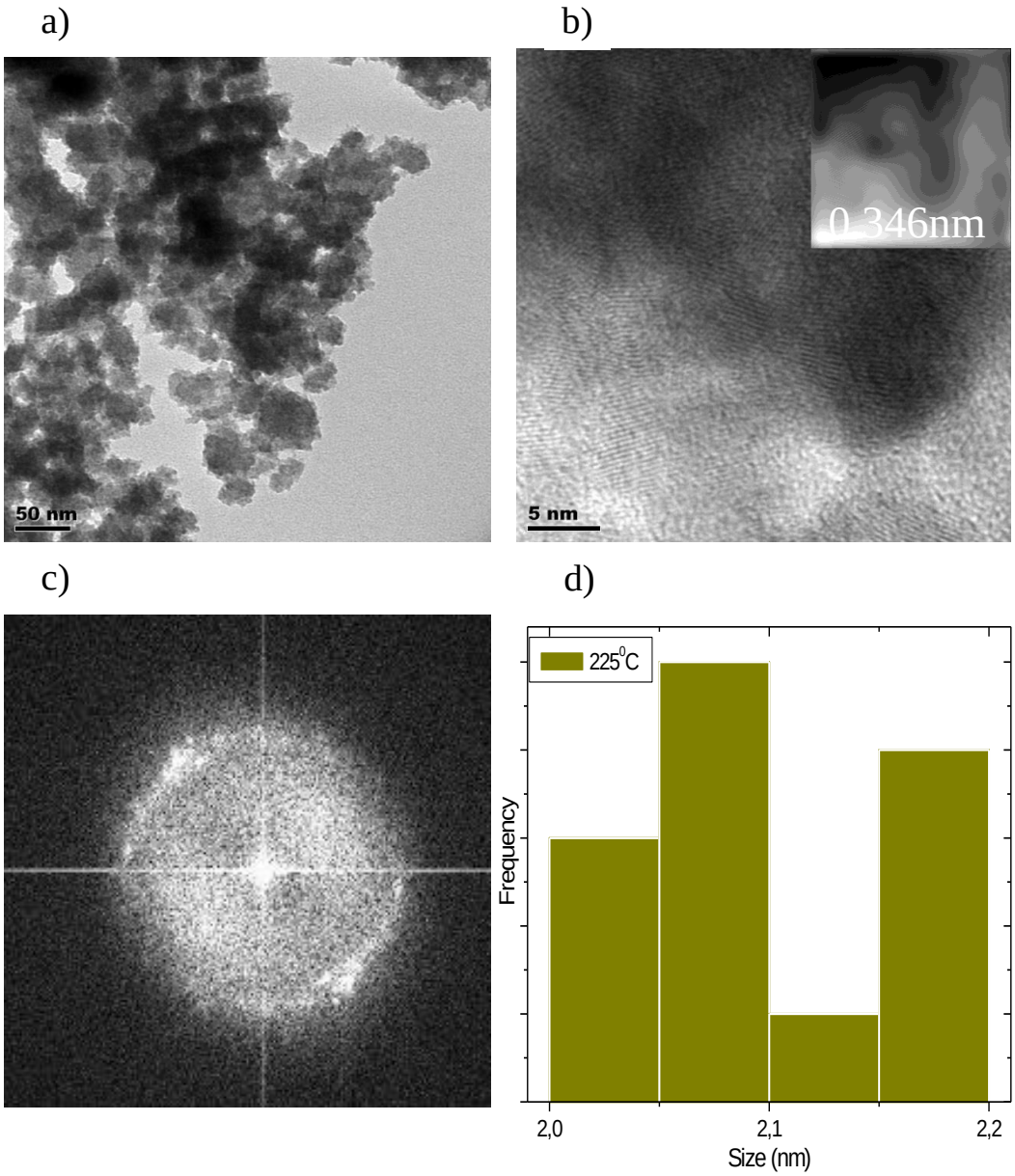

Figure 4.9: a) *HRTEM images with b) IFFT insert, c) SAED image and d) histogram of CdSe QDs at 225 ℃*

Furthermore, the clear lattice fringes in the HRTEM image of fig. 4.9 indicate that CdSe QDs have a high degree of crystallinity. The interplanar distance estimated from the Fast Fourier Transform (FFT) image (insert b) was measured to be approximately 0.3456 nm, which agrees

well with the spacing of the (002) plane of the wurtzite CdSe. These results are in mutual agreement with the XRD results.

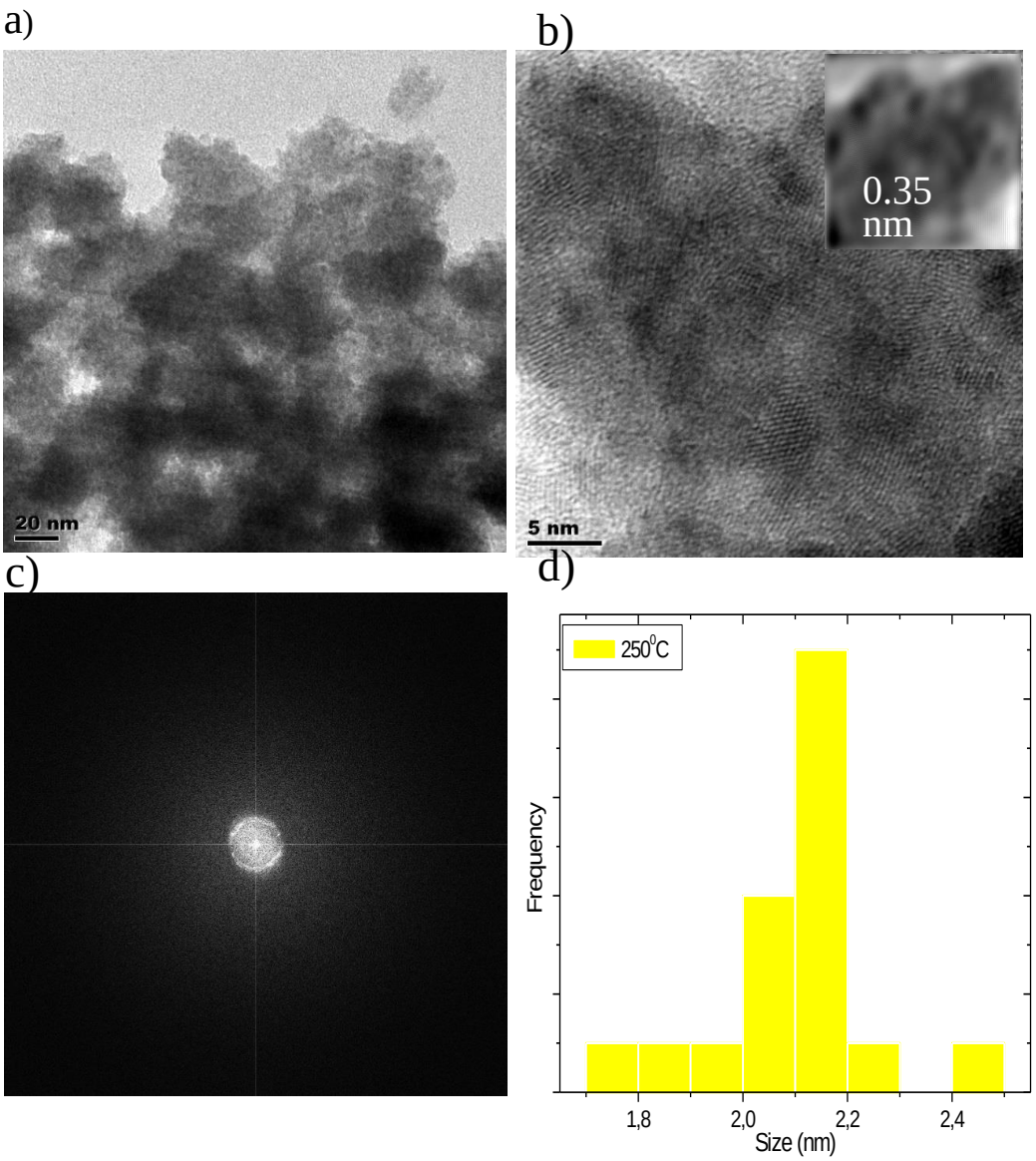

Figure 4.10: a) *HRTEM images with b) IFFT insert, c) SAED image and d) histogram of CdSe QDs at 250℃*

The HRTEM image, lattice fringes (insert b) and histogram of CdSe QDs synthesised at 250℃ are shown in fig. 4.10. The existence of well resolved lattice planes demonstrates the highly crystal structure of CdSe QDs. The HRTEM image shows a detailed view of the HRTEM contrast and the lattice distance was found to be 0.35 nm which is in good agreement with (002) planes of CdSe present in hexagonal phase, which verifies the XRD results. Additionally, the SAED shows bright circular rings which confirm the crystallinity of the as synthesised CdSe QDs.

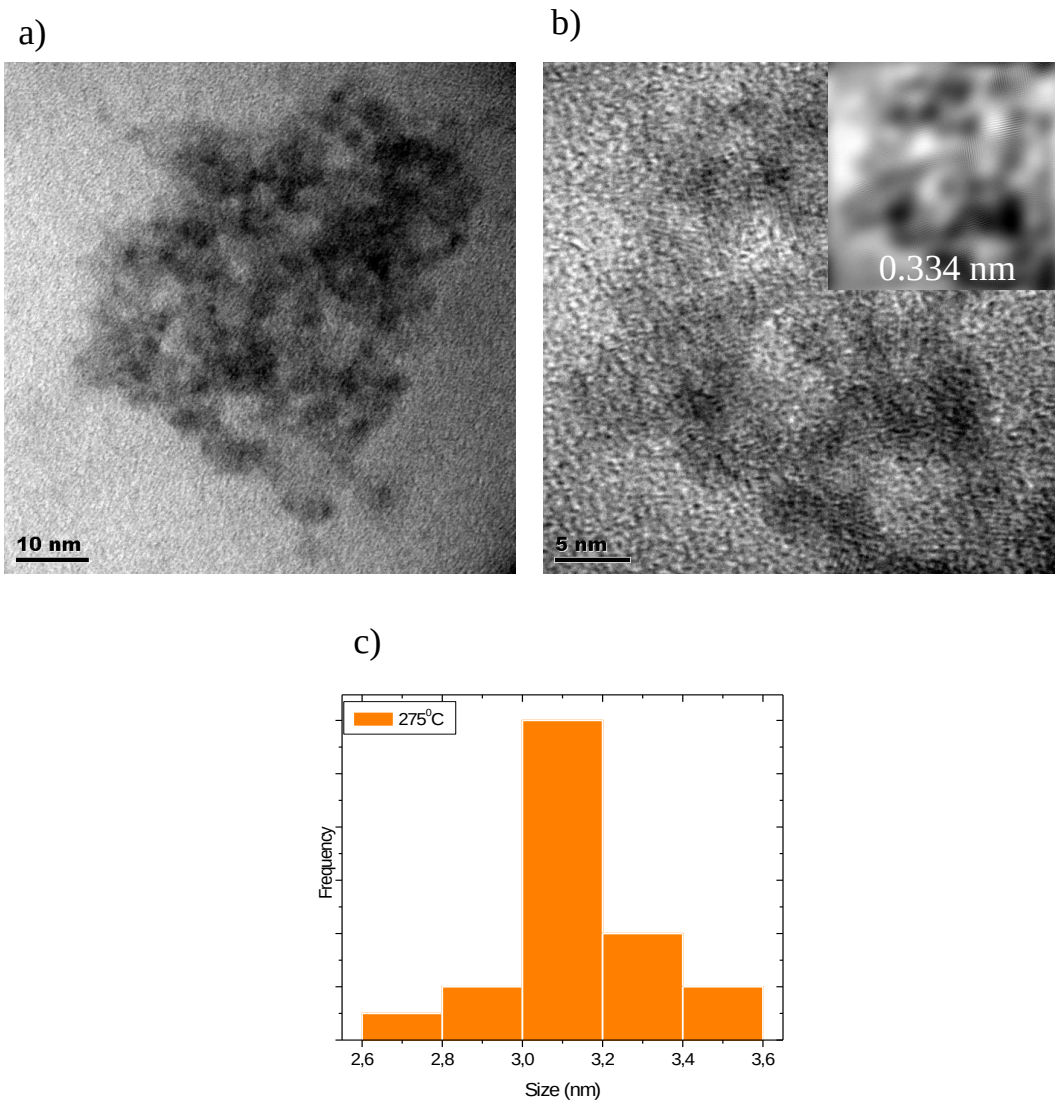

Figure 4.11: a) and b) *HRTEM image with b) IFFT insert and c) histogram of CdSe QDs at 275 ℃*

Moreover, the HRTEM images of CdSe QDs synthesised at 275℃ is shown in fig. 4.11. The images have revealed lattice fringes of 0.334 nm which corresponds to (101) crystal plane for hexagonal wurtzite CdSe. These results are in agreement with XRD. Fig. 4.11 (c) shows the histogram of CdSe QDs fabricated at 275℃. The estimated particle size was found to be 3.10 nm, which agrees with the particle size calculated by the Debye Scherrer method, this means that these results agree with the XRD results.

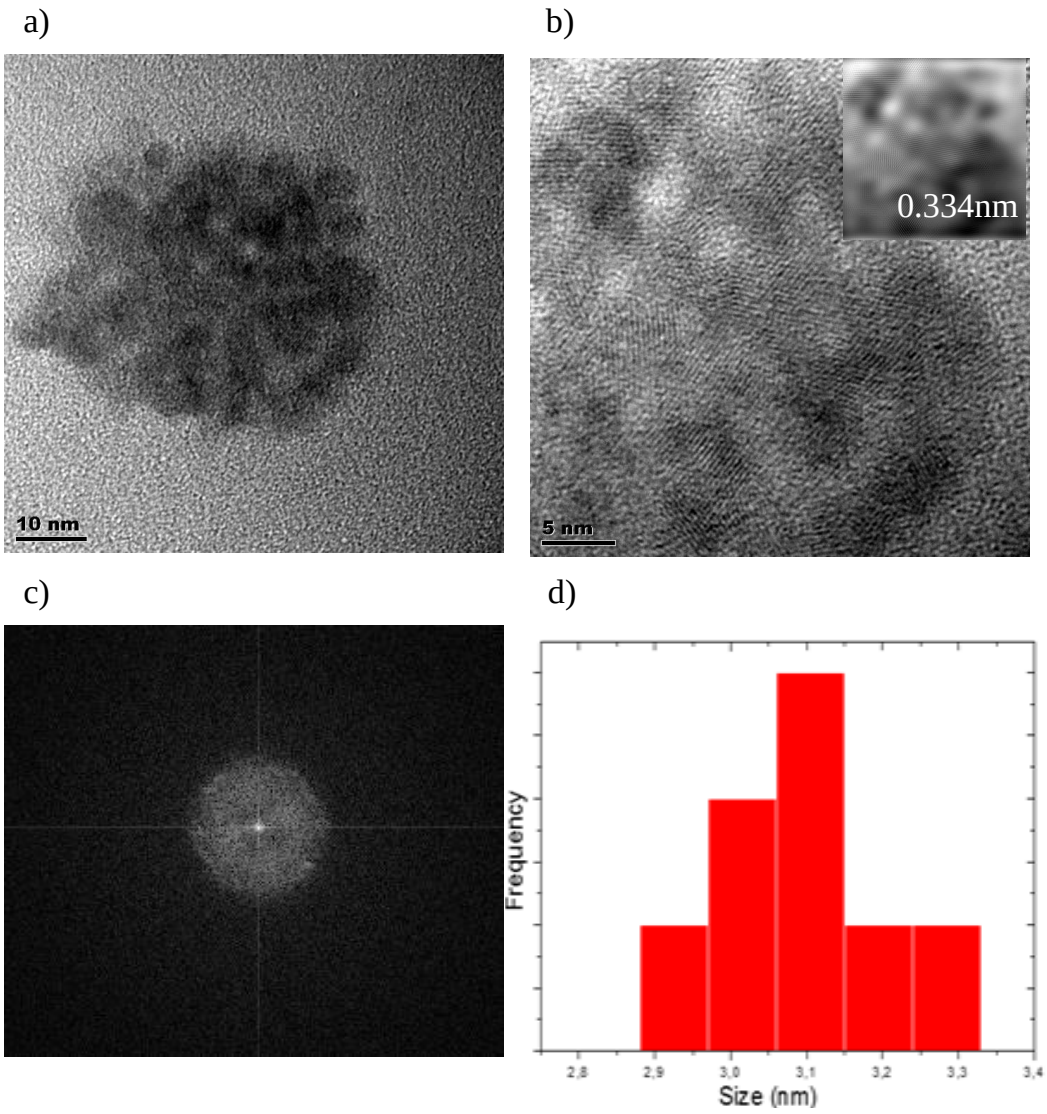

Figure 4.12: a) *HRTEM image with b) IFFT insert, c) SAED image and d) histogram of CdSe QDs at 300℃ synthesised using the hot injection method.*

Fig. 4.12 shows the HRTEM images of CdSe QDs synthesised using the hot injection method at 300℃. The images revealed that the synthesised QDs have lattice fringes of 0.334 nm which corresponds to the (101) planes of wurtzite hexagonal CdSe structure. These results are consistent with the XRD results. Furthermore, the SAED of CdSe at 300℃ disclosed bright circular rings, in actual fact all CdSe QDs samples displayed bright concentrated rings confirming that the as synthesised CdSe QDs are of high crystallinity and have a wurtzite structure.

In addition, it was also observed from the histograms that an increase in temperature equals to an increase in particle size. These findings were in agreement with the XRD observations. In all the HRTEM images it was witnessed that the synthesized CdSe QDs synthesised by the hot injection method have a similar crystal structure which is hexagonal wurtzite but differ in particle sizes. This difference in particles size is due to the fact that the QDs were synthesised at different temperatures.

4.2.4. Raman Spectroscopy

Raman spectroscopy is a non-destructive characterization method of choice for many recent studies of the vibrational properties [15, 16 and 17] of CdSe QDs. In order For us to understand the effect of synthesis temperature variation in the structural properties of CdSe QDs we used Raman spectroscopy to investigate the change in the vibrational modes of CdSe QDs. Several workers have already reported on the sensitivity of the Raman spectroscopy of CdSe QDs, showing shift in the bulk phonon frequencies [18]. It is well recognised experimentally that Raman spectra of low-dimensional crystals of semiconductors (QDs) are modified when compared to the corresponding bulk crystal spectra. One modification is the asymmetric broadening of the Raman peaks, the other is that their positions are shifted. Three possible mechanisms have been reported for the phonon peak shifts in Raman spectra of QDs. The first one is spatial confinement within the QD nanocrystal boundaries. The second one is linked to the phonon localization caused by defects. Furthermore, it has been reported that QDs produced by chemical methods or by the molecular-beam epitaxy, normally exhibit more defects than corresponding bulk crystals. Therefore, Raman spectroscopy was used in order to investigate the vibrational properties [19] of CdSe QDs, .and also to study the effects of changing temperature during the synthesis on the structure, phase and other parameters of CdSe QDs.

CdSe QD is a semiconductor that belongs to the space group $P6_3\,mc$ [21] and crystallizes either in hexagonal wurtzite (WZ) or in cubic zinc blend (ZB) structure [20]. When the temperature used in the synthesis method of CdSe QDs is greater than $95\pm5°C$ it only exists in the wurtzite phase. Moreover, theory also predicts a minor change in the peak positions and broadening of CdSe QDs when the same ensemble of QDs are excited with photons of different energies. Therefore, the asymmetric broadening of the Raman peaks should be strongly increased in very small QDs because of phonon confinement effect [17]. The observable shift in Raman peaks and asymmetric broadening of the Raman peak, confirm phonon confinement effect. Bulk CdSe QDs has two characteristic Raman active modes, longitudinal optical (LO), and its second order (2LO) weaker mode which are located at 212 cm^{-1} and 415 cm^{-1}, respectively. In addition, the LO phonon peak possesses in many cases a notable high frequency shoulder (HFS) which most probably originates from the QD vibrations of selenium on CdSe QDs surface or coupled optical acoustical phonon modes [21].

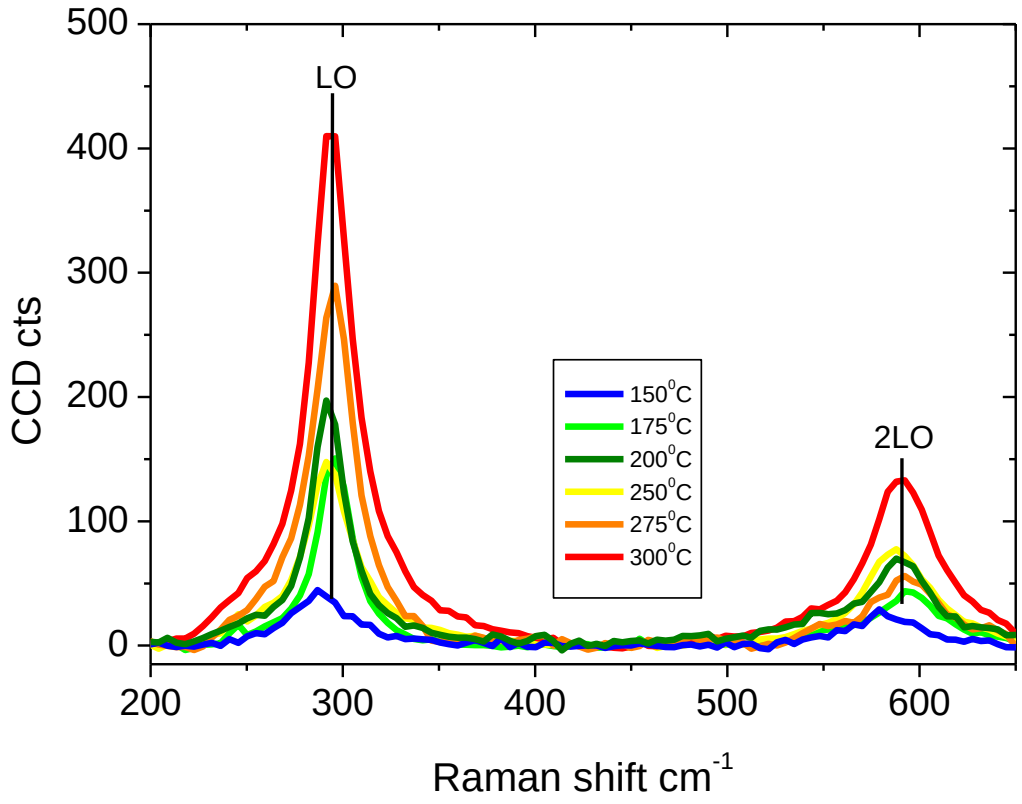

Figure 4.13: *Raman spectra of the phonon mode region of CdSe QDs*

Fig 4.13 presents the Raman spectra of CdSe QDs synthesised by the hot injection method at temperatures 150, 175, 200, 225, 250, 275 and 300℃. The strongest peaks at 287, 295, 290, 290, 293 and 294 cm^{-1} for samples taken at 150, 175, 200, 225, 250, 275 and 300℃, respectively, corresponds to the LO phonons in the CdSe core. The blue shift and broadening of the Raman peaks observed in CdSe QDs from the bulk ($\approx 213\ cm^{-1}$) are attributed to either phonon confinement [22], the size dependant changes that occur in the electronic structure of the QD and the significant amount of compressive strain present in the lattice. The strain and relative frequency shift varies between samples due to a difference in the synthesis temperature and particle size. The LO is characteristically the prominent feature observed in the Raman spectra of II-VI semiconductor nanocrystals. The peaks at 581.36, 588.08, 593.20, 590.65, 588.30, 592.68, and 590.80 cm^{-1} corresponds to the weaker mode of CdSe QDs arising from second order 2LO.

As the QDs decrease in their size more broadening of the peak width is observed in their Raman spectra. The blue shift of the 2LO phonon Raman peak from its position in the bulk CdSe crystal 2LO ($\approx$ 415 cm^{-1}) is related to the phonon confinement effect in small QDs [22]. Such red shift of LO frequency is caused by the negative dispersion curve. The broad weak feature above the LO peaks, denoted as HFS (high-frequency shoulder), was previously reported for spherical QDs and presumably assigned either to the surface-induced phonon density of states or to higher-order scattering process involving optical and acoustical vibrations. Recent studies of CdSe QDs and other spherical nanocrystals (NCs) by means of surface enhanced Raman scattering additionally suggest a contribution of surface Se to this spectral feature.

The data in Fig. 4.13 shows the Raman Spectra of CdSe QDs synthesised at different reaction temperatures using the hot injection method. There is little noticeable shift of the peaks but the broadening is observed between the spectra obtained with different temperatures. It is quite clear that as you increase the synthesis temperature of CdSe QDs, the Raman shift, FWHM, and peak intensity changes. Our Raman spectra showed peaks at 288.16, 292.56, 295, 296.75, 292.35, 294.66 and 294.13 cm-1 for LO and 581.36, 588.08, 593.20, 590.65, 588.30, 592.68, and 590.80 for 2LO for synthesis temperatures 150, 175, 200, 225, 250, 275 and 300℃, respectively. It is evident that particle size influenced the Raman spectra of CdSe QDs as there was more blue shift as the particles increased in size. Furthermore, theory has reported the LO is the characteristic peak for CdSe QDs. We can therefore conclude that the decrease in phonon frequency is caused by a decrease in synthesis temperature. Due to the above observations, we conclude that CdSe QDs of different particle sizes were observed due to the evidence presented by the Raman spectra.

Theoretically, asymmetric broadening of the Raman peak should be strongly increased in very small QDs because phonon confinement. Hence we further extend our Raman Spectroscopy using the Lorentzian symmetry to show broadening between peak samples.

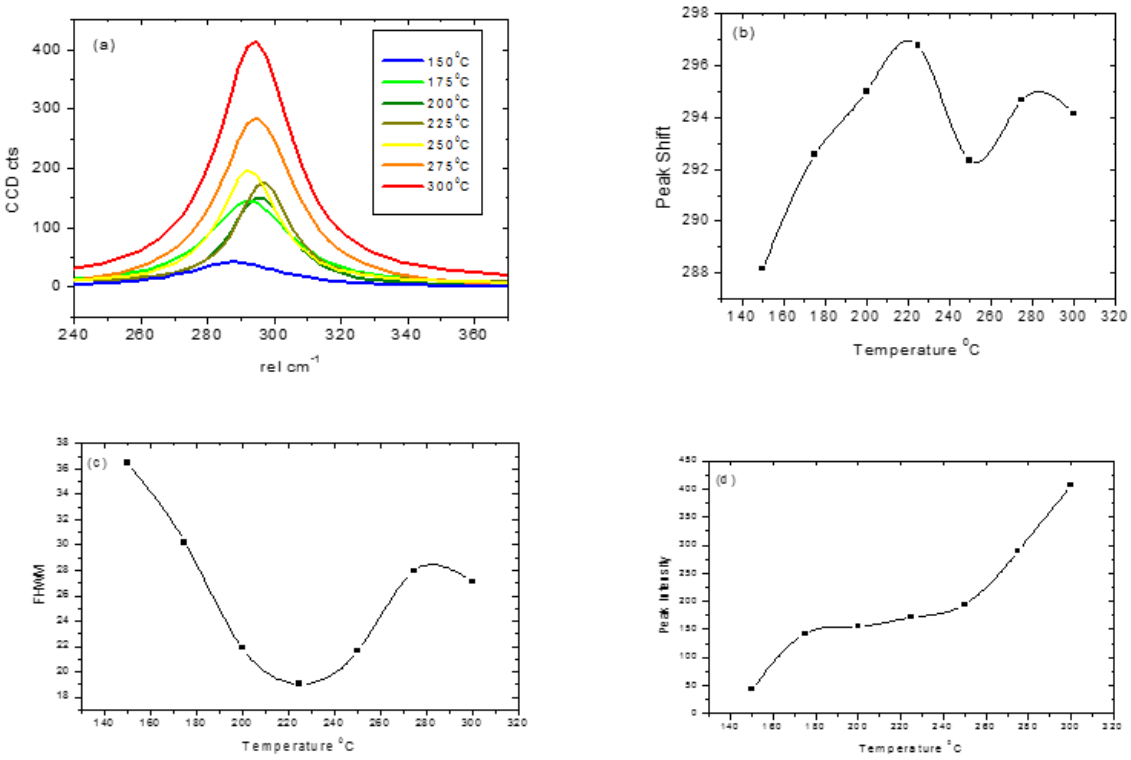

Figure 4.14: *Raman Peak shift of CdSe QDs for (a) Peak of LO phonon (b) Peak Shift of LO phonon (c) Full Width at Half Maximum (FHWM) LO phonon and (d) Peak intensity of LO phonon for CdSe QDs synthesised by the hot injection method*

Fig.4.14 (a) and (b) shows the peak broadening of CdSe QDs synthesised using the hot injection method. Our Raman spectra showed peaks at 288.16, 292.56, 295, 296.75, 292.35, 294.66 and 294.13 cm^{-1} for synthesis temperatures 150°C, 175°C, 200°C, 250°C, 275°C and 300°C. It can be observed that as QDs decrease in their size or for lower synthesis temperatures, more broadening

of the peak width is observed. This is due to the negative dispersion curve [9]. Additionally, Fig. 4.14 also shows the dependence on temperature of the FWHM and peak intensity of the LO phonon mode of CdSe QDs synthesised by the hot injection method. It is quite evident that the vibrational frequencies of these parameters also depend on increasing temperature. In Fig 4.14(c), we observe the effect of variation of temperature on the FWHM. It can be seen that the FWHM decreases with an increase in temperature. It has also been reported by other workers that an increase in FWHM causes weakening of the crystalline structure CdSe structure, which according to our XRD is wurtzite. This therefore implies that a decrease in FWHM with increasing temperature does not weaken or distort CdSe structure. Our Raman analysis which has shown a decrease in the FWHM with increasing temperature did not show any weakening of the CdSe QDs structure. Fig. 4.14 (d) shows that there is an increase in peak intensity with an increase in temperature. Moreover, it has been reported that the observed red shift could be attributed to the intrinsic impurity or defects in the sample. The other reason for causing this red shift is intense heating during synthesis [23].

4.3. Optical Characterization

4.3.1. UV-Vis Spectroscopy

UV-Vis absorption spectroscopy is an analytical technique used to characterise CdSe QDs. Its first exciton peak can yield information about the band gap, particle size and size distribution of CdSe QDs [6].In this work, UV-Visible Spectroscopy is used to explains the formation of different sizes of CdSe QDs according to variation of temperature. UV-Vis was also used in this study to observe the absorbance of CdSe QDs synthesised at different temperatures. Analysis was carried out at the University of Fort Hare, Alice Campus using the Perkin Elmer Lambda 365 Spectrometer and 10 mm quartz cuvettes in wavelength range of 400-750 nm. The optical absorption spectra of CdSe QDs that are in toluene give information on the size of the nanocrystal. The data presented in this table shows that the absorption maximum (peak values) for 7 samples varies from 406 nm to 514 nm

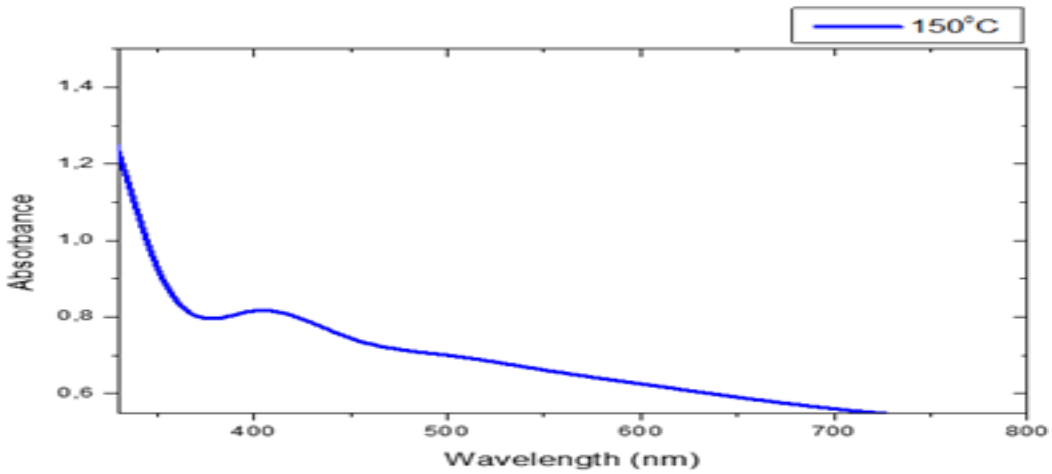

Figure 4.15*: UV-Vis spectra of CdSe QDs at 150^{0}C*

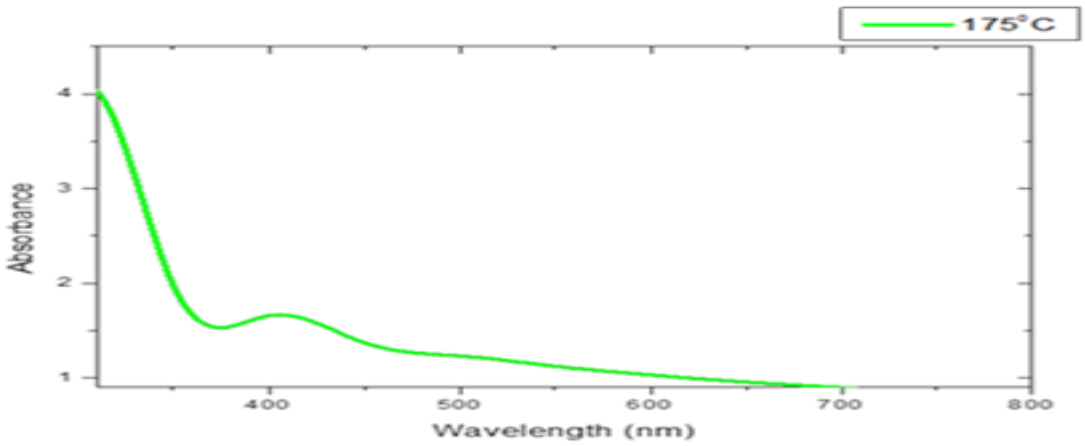

Figure 4.16: *UV-Vis spectra of CdSe QDs at 175^{0}C*

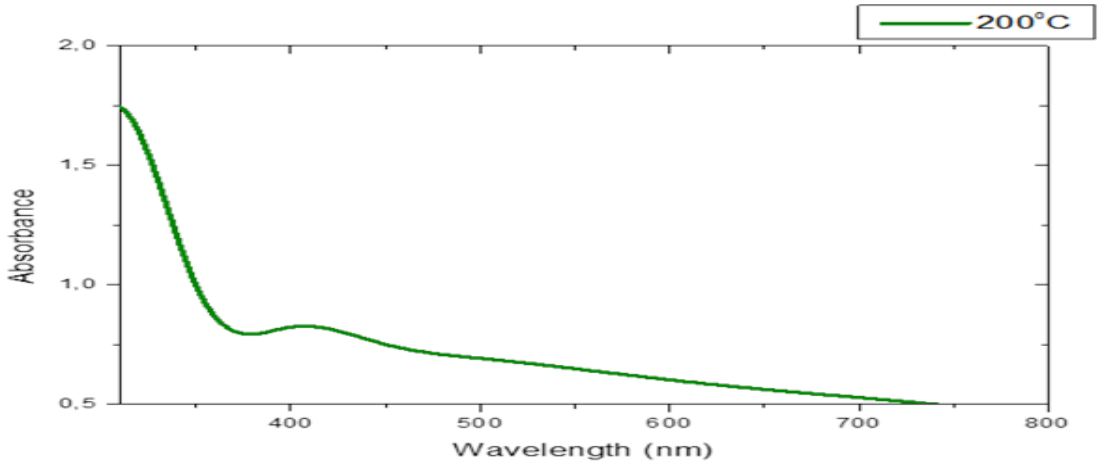

Fig 4.17: *UV-Vis spectra of CdSe QDs at 200^{0}C*

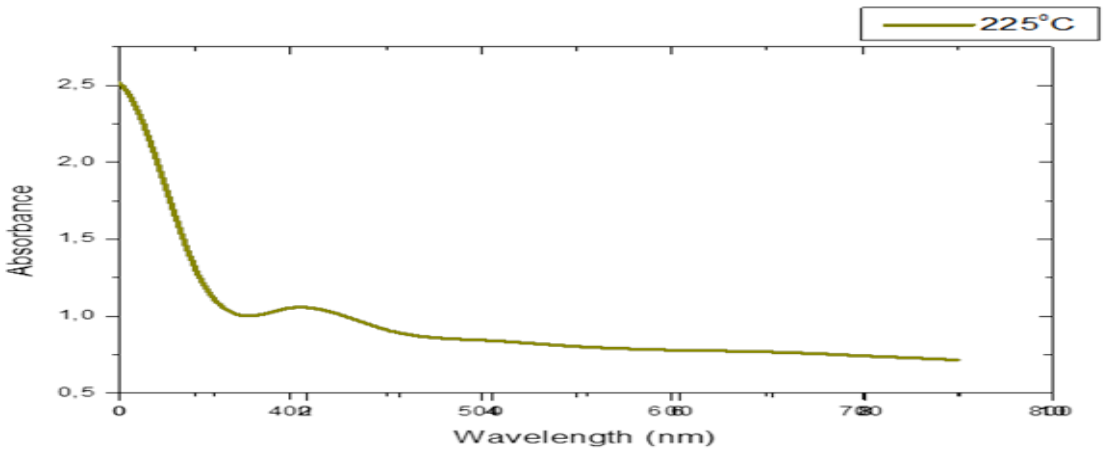

Figure 4.18: *UV-Vis spectra of CdSe QDs at 225^{0}C*

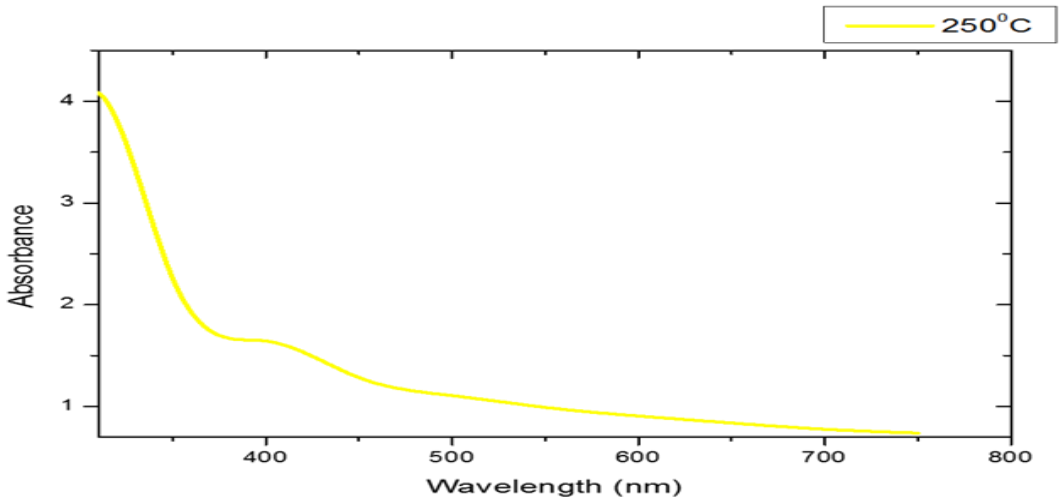

Fig 4.19*: UV-Vis spectra of CdSe QDs at 250^{0}C*

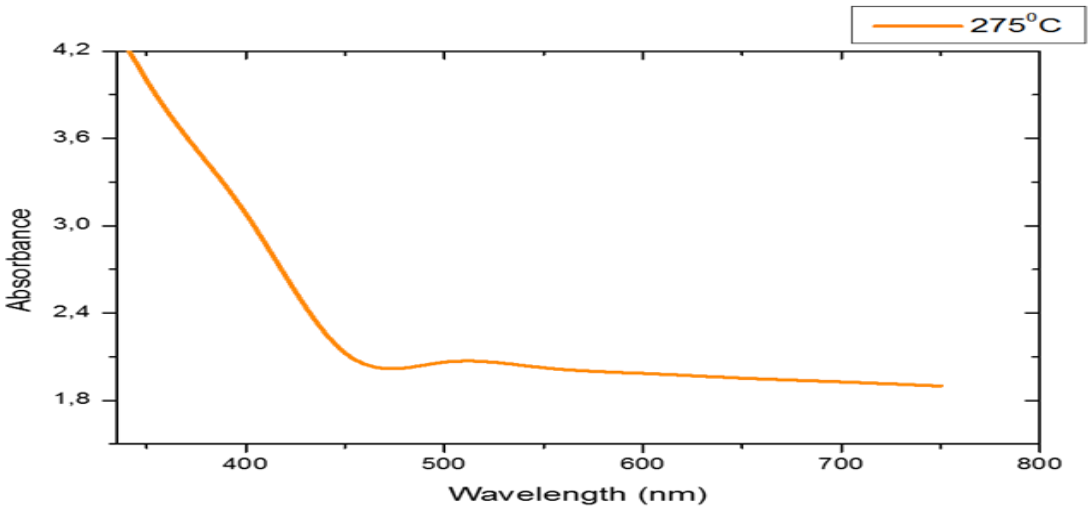

Figure 4.20*: UV-Vis spectra of CdSe QDs at 275^{0}C*

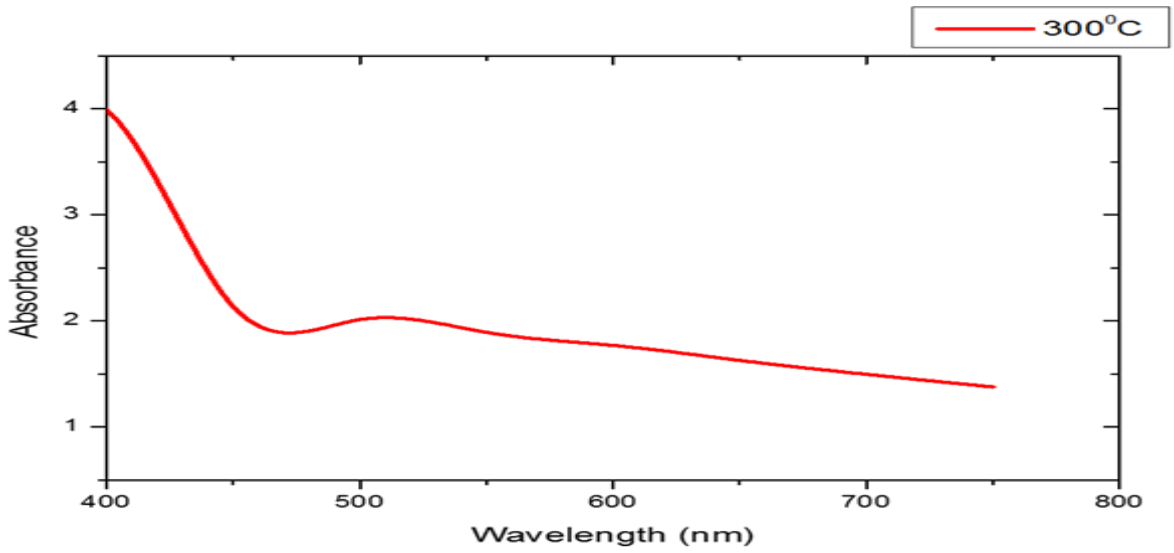

Figure 4.21*: UV-Vis spectra of CdSe QDs at 300^{0}C*

Fig. 4.15, 4.16, 4.17, 4.18, 4.19, 4.20 and 4.21 shows the absorption spectra of CdSe QDs synthesised at temperatures 150ºC, 175ºC, 200ºC, 225ºC, 250ºC, 275ºC and 300ºC. The data was taken for all CdSe samples. These peaks are arising from the absorption of near band excitons. It was found that with an increase in temperature, there's a gradual shift towards the longer wavelength (red-shift), indicating an increase in the particle size. The reason behind the formation of larger CdSe QDs at higher temperatures can be understood by the mechanism of QD formation. The range of absorption edge lies in the region between 514 nm and 406 nm which is a pronounced blue shift from 712 nm of bulk CdSe. The absorption edge is determined as the wavelength with the greatest change in slope, i.e., the wavelength where the absorption curve starts to deviate from the longer wavelength background absorption [24].

Consequently, the samples were administered for further evaluation to obtain the diameter and the band gap energies of the QDs. The wavelengths of each QD were taken from the peak absorbance amplitude and substituted into the band gap and particle size formula to obtain the bandgap energies and the particle sizes of the as synthesised CdSe QDs.

Table 4.4 Extrapolated wavelengths of each CdSe QD at different absorbance peaks.

Sample number	Synthesis Temperature of QDs (℃)	Absorption peak (nm)
1	150	406
2	175	409
3	200	411
4	225	412
5	250	413
6	275	511
7	300	514

Thus, using the energy band gap formula

$$Eg = h\nu = \frac{hc}{\lambda} \qquad [4.2]$$

where the parameter Eg, is the energy band gap of the QD, h is Planck's constant ($6.626070040\times10^{-34}$ J.s), and c is the speed of light (3×10^{8} m.s^{-1}).

The bandgap of each QD as a function of wavelength is shown in Table 4.5 below

Table 4.5: Shows values of the calculated band gap

Sample number	Temperature of QDs (℃)	Absorption peak(nm)	Band gap (eV)
1	150	406	3.11
2	175	409	3.03
3	200	411	3.01
4	225	412	3.01
5	250	413	3.0
6	275	511	2.42
7	300	514	2.41

The stokes of the band edge emission increase with a decrease in particle size due to the larger coupling of the electron and hole pair in the emitting state to phonons LO in the polar CdSe lattice for the smaller QDs.

Additionally, the particle size of CdSe QDs was calculated using the relation given by Yu et al 2003 [28]:

$$D = (1.6122 \times 10^{-9})\lambda^4 - (2.657 \times 10^{-6})\lambda^3 + (1.6242 \times 10^{-3})\lambda^2 - (0.4277)\lambda + (41.577) \quad [4.3]$$

where D is the size of a given sample and λ (nm) is the first exciton peak of CdSe spectrum. The data presented in this table shows that the absorption maximum (peak values) for 7 samples varies from 406 nm to 514 nm.

Table 4.6: Calculated values of the different sizes of CdSe QDs obtained from UV-Vis analysis.

Sample	Synthesis Temperature℃	First peak of Wavelength (nm)	Size of CdSe QDs (nm)	Energy band gap (eV)
1	150	406	1.79	3.11
2	175	409	1.91	3.03
3	200	411	1.93	3.01
4	225	412	1.94	3.01
5	250	413	1.95	3.0
6	275	511	3.13	2.42
7	300	514	3.17	2.41

These results clearly show quantum confinement effect in CdSe QDs. The UV absorbance spectra presented reveal that as the size of the QD increases, the maximum peak shifted to a longer wavelength leading to a corresponding decrease in the confinement energies because the conduction band moves downwards thus shortening the band gap of the semiconductor nanocrystals. The overall effect is that the band gap decreases resulting in a red shift of the band-band excitation energy of the semiconductor.

4.3.2. Effect of temperature on the CdSe QD growth

Since the growth kinetics of CdSe QDs are dependent on temperature, the influence on changes of this condition on the final properties of CdSe QD were investigated. From the findings, it was observed that changing the growth temperature during synthesis has the ability of changing the average particle size. Figure 4.20 shows diameter distribution of QDs grown with different temperatures.

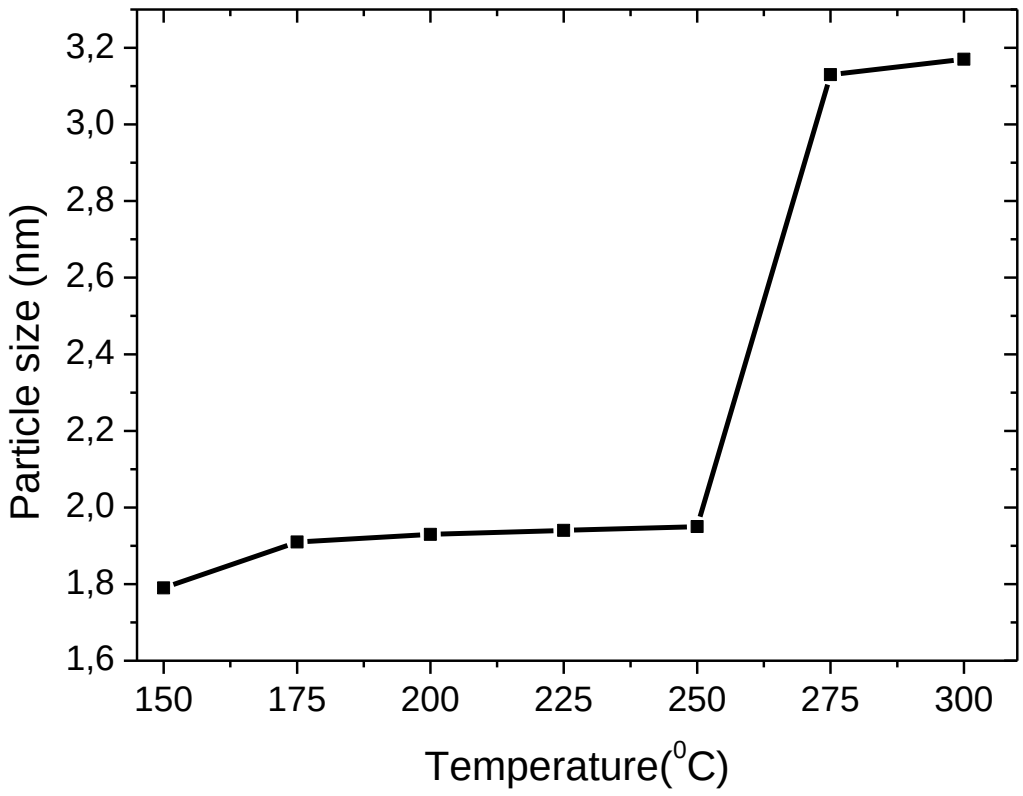

Figure 4.22: Effect of synthesis temperature on size of CdSe QDs

From fig. 4.22, it was observed that as the temperature is increased, the particle size of CdSe QDs also increases. These results are in agreement with the study of Battacharjee et al. [9] because the growth of these QDs is the predominant process over nucleation, which increases the average

particle size under the same experimental conditions. The increase in QD size is also responsible for the red shift in absorption spectra of CdSe QDs.

Additionally, from the results of Table 4.5, a graph of band gap against particle size was plotted for the CdSe QDs.

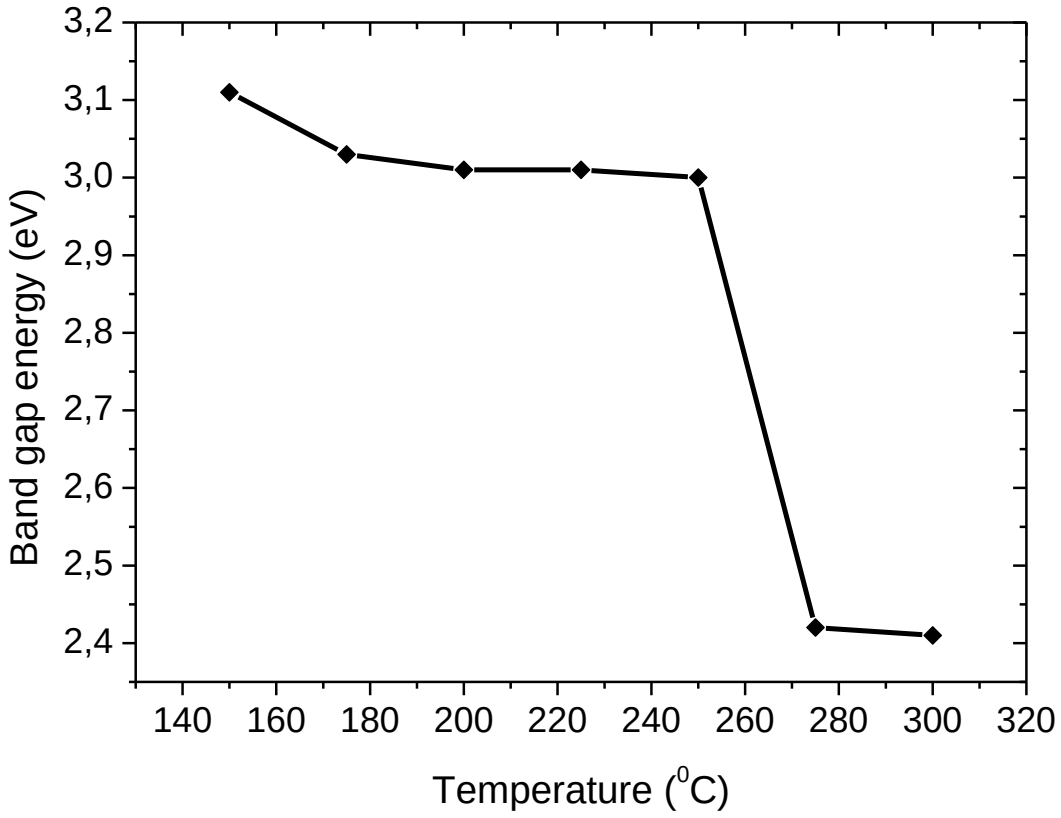

Figure 4.23: Effect of synthesis temperature on band gap energy of CdSe QDs

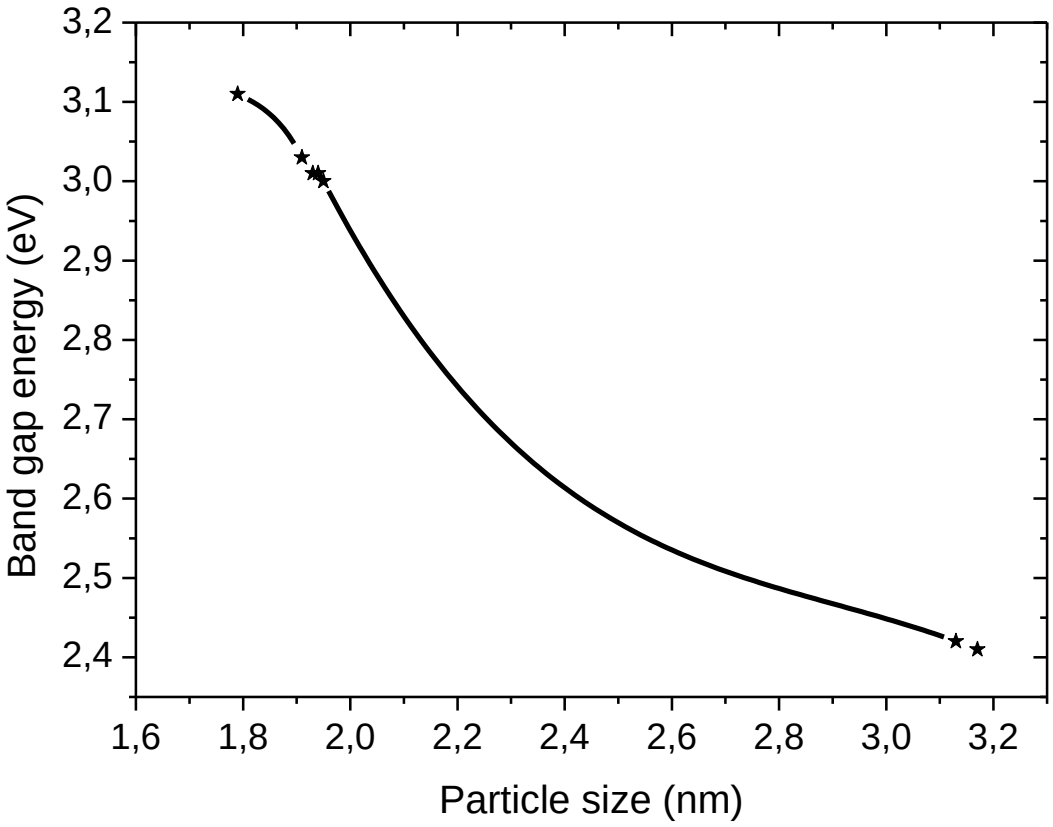

Figure 4.24: shows the effect of particle size on the band gap of CdSe QDs

Fig. 4.22 and 4.23 shows the effect of synthesis temperature on band gap and effect of particle size on the band gap energy of CdSe QDs, respectively. The band gap E_g decreased with increasing synthesis temperature (Fig. 4.24). In summary, these two graphs explain why the band gap reduces with increasing particle size as the synthesis temperature is increased.

4.3.3. Optical Study

An immediate observable optical feature of QDs synthesised is their colour. Even though the CdSe QDs were synthesised using the same materials, their different sizes results into emission of light of different colours. Larger QDs emit red fluorescence, and smaller ones emit blue light [25]. CdSe quantum dots of increasing size from left to right are shown in Fig.4.13.

Figure 4.25: *Images of CdSe QDs, top; under normal light, bottom; under UV light (366 nm)*

Samples were illuminated with UV light and there was an observed fluorescent from the samples. The colour of the samples viewed varied from blue, green, orange and red. Under normal light, the synthesized CdSe QDs appear colourless, to yellow, to reddish orange. The prepared CdSe QDs were irradiated with a short-wavelength ultraviolet lamp; the colourless samples glow blue to green and the colours of the yellow, orange, and red QDs become more pronounced, as shown in fig. 4.25. A very clear distinction is seen between the colours of QDs observed in normal light and under UV light indicating the formation of QDs and their variation in particle size with rise in synthesis temperature. The colours of luminescence change with reaction times. These changes in colour are consistent with observations noted by [26] and [27] they attributed these changes to increasing size of the QDs. In quantitative terms, the band gap energy determines the energy of the light being emitted, which is inversely proportional to the size of the QD. The QD properties intensely change because the quantum size effect arises from the confinement of the electrons and holes in the QD structure. The increased surface area/volume ratio and the increase in oscillator strength as a result of downsizing bulk CdSe to nanometre range is responsible for the unprecedented increase in the band gap of the synthesised CdSe QDs over the bulk CdSe QDs.

4.4. Conclusions

From this study, 2-mercaptoethanol capped CdSe QDs with different particle sizes were synthesised using the hot injection method. FTIR revealed a peaks at 738, 738, 738, 738, 735, 735 and 733 cm-1 for 150, 175, 200, 225, 250, 275, and 300℃, respectively which confirmed the presence of the Cd-Se bond and subsequently confirms the successful fabrication of CdSe QDs. XRD analysis has revealed characteristic peaks of hexagonal wurtzite CdSe QDs at 2θ angles of 34.77 – 35.13° and 45.39 – 45.70° for (102) and (103) crystal planes. HRTEM showed that the as synthesised CdSe QDs have a spherical shape and were agglomerated. Additionally, HRTEM and XRD analysis has revealed that the modal particle size increases with an increase in synthesis temperature. Raman spectroscopy analysis has revealed the presence of peaks corresponding to vibrational modes LO and 2LO, which are characteristic peaks for CdSe QDs. Additionally, RS and XRD, revealed that the as synthesised CdSe QDs have a wurtzite structure. From the absorption spectra, peaks moved towards the longer wavelength with increasing synthesis temperature. This was due to particle size increase. The calculated particle sizes from UV-Vis are in mutual agreement with XRD and HRTEM, thus confirming that controlling reaction temperature has a significant influence on the growth size of CdSe QDs.

4.5. References

[1] C.B. Murray, D.J. Norris & M.G. Bawendi. *Synthesis and Characterization of Nearly Monodisperse CdE (E = Sulphur, Selenium, Tellurium) Semiconductor Nanocrystallites*. Journal of the American Chemical Society. 115 (19) (**1993**) 8706-8715.

[2] S. P. Burrows. *Infrared spectroscopic measurement of titanium dioxide nanoparticle shallow trap state energies*. Virginian Polytechnic Institute and State University, Blacksburg (**2010**)

[3] N.A. Hamizi and M.R Johan. *Optical and FTIR studies of CdSe quantum dots*. Nanoelectronics Conference (INEC) 3rd International Conference (**2010**).

[4] S.Y. Ha, M.S Choo, G.W. Kim, E.S. Lee, et al. *Study on the Physical Properties of CdS Quantum Dots Synthesized by Ligand Exchange in a Cd2+ mercaptopropionic Acid Aqueous Solution at Room Temperature*. Journal of the Korean Physical Society 58 (5) (**2011**) 1274-1278.

[5] H. Kang, M.L Clarke, L.F. Pease, S.H. DePaoliLacaerda, A. Karim, et al. *Analysis of the Optical Properties of Clustered Colloidal Quantum Dots by the Chi-Square Distribution of the Fluorescence Lifetime Curves*. (**2011**)

[6] D.V. Talapin, E.V. Shevchenko, A. Kornowki, N. Gaponik, M. Haase, A.L. Rogach, H.Weller. *Organization of matter on different size scales: Monodisperse Nanostructures and their superstructures.* Advanced Functional Materials. 13 (**2002**) 1868

[7] A.B. Kashyout, M.A. Hesham Soliman, M. Farthy, E.A. Gomaa and A.A. Zidan. *CdSe Quantum Dots for solar cell devices*. International Journal of Photoenergy. 2012 (**2012**)

[8] G. Devi, N. Muthy and G. S. Kumar. *Photocatalytic activity of TiO2 doped with Zn2+ and V5+ transition metal ions: Influence of crystallite size and dopant electronic configuration of photo-activity*. Materials Science and Engineering: B, 166 (1) (**2010**) 1-6

[9] B. Bhattacharjee, C. Hsu, C. Lu and W.H. Chang. *Colloidal CdSe–ZnS Core-Shell Nanoparticles: Dependence of Physical Properties on Initial Cd to Se Concentration*. Physica E: Low-dimensional Systems and Nanostructures. 33 (2) (**2006**) 388-393

[10] D.V. Talapin, E.V. Shevchenko, A. Kornowki, N. Gaponik, M. Haase, A.L. Rogach, H.Weller, Adv. Mater. 13 (**2001**) 1868.

[11] C.B. Murray, C.R. Kagan, M.G. Bawendi. *Self-Organization of CdSe Nanocrystallites into Three-Dimensional Quantum Dot Superlattices*. Science. 270 (**1995**) 1335-1338

[12] G. Scamarcio, M. Lugara, and D. Manno. *Size-dependent lattice contraction in* $CdS_{1-x}Se_x$ *nanocrystals embedded in glass observed by Raman scattering*. Physical Review B. 45 (**1992**) 13792

[13] Y. Hwang, S. Shin, H. Park, S. Park, U. Kim, H. Jeong, E. Shin, and D.Kim. *Effect of lattice contraction on the Raman shifts of CdSe quantum dots in glass matrices.* Physical Review B. 54 (**1996**) 15120

[14] Y. Wang and N. Herron. *Quantum size effects on the exciton energy of CdS clusters* Physical Review B. 42 (**1990**) 7253

[15] K. A. Alim, V. A. Fonoberov, M. Shamsa A. A. Balandin. *Micro-Raman investigation of optical phonons in ZnO nanocrystals*. Journal of Applied Physics 97 (**2005**) 124313

[16] V. A. Fonoberov and A. A. Balandin. *ZnO Quantum Dots: Physical Properties and Optoelectronic Applications*. Nanoelectronics and Optoelectronics. (1) (**2006**) 19-38

[17] H. Kumar Yadav, K. Sreenivas and V.Gupta. *ZnO-Sn Bilayer Ultraviolet (UV) Photon Detector with Improved Responsitivity*. Materials Research Society Symposium Proceedings. 957 (**2007**)

[18] A. G. Rolo and M. I. Vasilevskiy. *Raman spectroscopy of optical phonons confined in semiconductor quantum dots and nanocrystals*. Journal of Raman Spectroscopy. 38 (**2007**) 618–633

[19] B.J. Landi, C.M. Evans, J.J. Worman, S.L. Castro, S.G. Bailey, R.P. Raffaelle. *Noncovalent attachment of CdSe quantum dots to single wall carbon nanotubes*. Materials Letters. 60 (**2006**) 3502

[20] A. Myers Kelley Quanqin Dai, J. Zhong-jie, J. A. Baker, D.F. Kelley. *Resonance Raman spectra of wurtzite and zincblende CdSe nanocrystals*. Chemical Physics. 422 (**2013**) 272–276

[21] V. M. Dzhagan, I. Lokteva, M. Y. Valakh et al. *Spectral features above LO phonon frequency in resonant Raman scattering spectra of small CdSe nanocrystals*. Journal of Applied Physics. 106 (**2009**) 084318

[22] T. Torchynska, Yu. Vorobiev. *Semiconductor II-VI Quantum Dots with Interface States and Their Biomedical Applications*. Advanced Biomedical Engineering, Gaeta-no D. Gargiulo and Alistair McEwan (Eds.), InTech Publisher, Croatia, pp. (**2011**) 143-182

[23] Khan A. Alim, Vladimir A. Fonoberov, Manu Shamsa, and Alexander A. Balandin. Micro-Raman investigation of optical phonons in ZnO nanocrystals. Journal of Applied Physics. 97 (124313) (**2005**)

[24] H. Li. *Synthesis and Characterization of Aqueous Quantum Dots for Biomedical Applications*. Ph.D Thesis (**2008**).

[25] .A. Ekpekpo and L. Akpojivi. *Synthesis and Characterization of CdS and CdSe Quantum Dots by UV-VIS Spectroscopy*. Journal of Emerging Trends in Engineering and Applied Sciences (JETEAS) 4 (2) (**2013**) 273-280

[26] K. Tadd, A.S. Laura, J.R. Sandra. Journal of Chemical Education. 79 (**2002**) 1200.

[27] E. M. Boatman and G.E. Lisensky. *A safer, easier, faster synthesis for CdSe Quantum Dot Nanocrystal*. Journal of Chemical Education. 82 (**2005**) 1697-1699\

[28] W. Yu, L. Qu, Lio, W. Guo, We, X. Peng. *Experimental Determination of the Extinction Coefficient of CdTe, CdSe, and CdS Nanocrystals*. Chemistry of Matterials.15 (**2003**) 2854–2860.

Chapter 5
Conclusions and Recommendations

5.1. Synthesis of CdSe QDs using the hot injection method

The hot injection method is a very facile and useful method to prepare CdSe QDs with high luminescence. There were three main stages during synthesis. First, a Se precursor was prepared by dissolving Se powder in DMF. Secondly, a Cd precursor was prepared at an elevated temperature. Lastly, the prepared Se was injected into the hot Cd precursor under vigorous stirring. Growth of the QDs was controlled by varying the reaction temperature. By utilising this technique CdSe QDs with different sizes and optical properties were fabricated in this work.

5.2. Fourier Transform Infrared Spectroscopy (FTIR)

The FTIR spectra of CdSe QDs synthesised using the hot injection method revealed peaks at 738, 738, 738, 738, 735, 735 and 733 cm^{-1} for 150℃, 175℃, 200℃, 225℃, 250℃, 275℃, and 300℃ synthesis temperature, respectively which were the characteristic peaks for Cd-Se bond. The presence of these peaks confirmed the successful fabrication of CdSe QDs. Additionally, the absence of the S-H peaks at 2654-2556 cm^{-1} indicated that the capping agent, 2-mercaptoethanol, was attached to the QD surface. In conclusion FTIR analysis confirmed the synthesis of successful fabrication of high quality CdSe QDs.

5.3. X-Ray Diffraction (XRD)

The XRD analysis of the as prepared CdSe QDs showed diffraction peaks at 2θ angles of 16.66°, 25.20°, 34.77°, 40.9°, 45.39° and 49.10° for the QDs synthesized at $150°C$; 17.40°, 25.22°, 34.85°, 41.7°, 44.45° and 47.5° for $175°C$; 17.07°, 25.19°, 34.85°, 41.34°, 44.41° and 48.86° for $200°C$; 16.34°, 25.20°, 34.76°, 40.6°, 44.74° and 49.48° for $225°C$; 17.44°, 25.17°, 34.19°, 41.70°, 44.45°, 49.24° for $250°C$; 16.70°, 25.16°, 34.85°, 40.32°, 45.10° and 49.1°7 for $275°C$;and 17.35°, 25.18°, 35.13°, 41.63°, 45.70°, 49.48° for $300°C$ indexed to crystal planes (100), (002), (102), (220), (103) and (112), belonging to hexagonal Wurtzite CdSe crystal structure. Additionally, XRD analysis revealed that the synthesized CdSe QDs had crystallite sizes of 1.77, 1.82, 1.91, 1.96, 1.97, 3.11 and 3.14 nm for synthesis temperatures 150, 175, 200, 225, 250, 275 and 300℃, respectively, which increased with increasing synthesis temperature. Furthermore, XRD analysis has revealed a shift to higher 2θ values as synthesis temperature was increase indicating growth in QD size.

5.4. High Resolution Transmission Electron Microscopy

The HRTEM of CdSe QDs synthesised by the hot injection method revealed that the as synthesized CdSe are spherical in shape and well dispersed. The analysis also revealed that CdSe QDs have lattice fringes which correspond to crystal planes of Miller indices (100), (002) and (101) for hexagonal Wurtzite structure. These results are in mutual agreement with the XRD results. Additionally, the selected area electron diffraction (SAED) of all the synthesized CdSe QDs samples showed concentrated electron diffraction patterns which confirmed that the as synthesised CdSe QDs have a Wurtzite crystal structure. The QDs size estimated using HRTEM was 1.79 nm, 1.81 nm, 2.06 nm, 2.08 nm, 2.11 nm, 3.10 nm and 3.12 nm for the QDs synthesized at 150 ºC, 175 ºC, 200 ºC, 225 ºC, 250 ºC, 275 ºC and 300 ºC, respectively. These results are in

close agreement from the QDs sizes calculated from XRD. In conclusion HRTEM and XRD confirmed that CdSe QDs synthesised by the hot injection method have a hexagonal Wurtzite structure and that QD size can be controlled by varying the reaction temperature.

5.5. Raman Spectroscopy

Raman spectroscopy of CdSe QDs showed characteristic peaks of CdSe at 288.16, 292.56, 295, 296.75, 292.35, 294.66 and 294.13 cm^{-1}, corresponding to the LO phonons, and 581.36, 588.08, 593.20, 590.65, 588.30, 592.68, and 590.80 cm^{-1}, corresponding to the 2LO phonons for samples taken at 150℃ , 175 ℃, 200 ℃, 225 ℃, 250 ℃, 275 ℃ and 300 ℃, respectively. The LO and 2LO phonon modes were blue shifted as compared to the bulk because of phonon confinement. Additionally, peak broadening was observed whereby as the QDs decreased in their size more broadening of the peak width was observed in their Raman spectra. Furthermore, RS and FTIR confirmed the fabrication of CdSe QDs.

5.6. Optical Properties

The UV-Vis spectroscopy showed that the peaks of CdSe QDs synthesised by the hot injection method shifted towards the high wavelengths as reaction temperature was increased. This indicated QD size growth. In addition, the QD size calculated from UV-Vis using the Yu *et al* equation was 1.79, 1.91, 1.93, 1.94, 1.95, 3.13 and 3.17 nm for 150, 175, 200, 225, 250, 275 and 300℃, respectively. These results agree with the estimated QD size from HRTEM and the calculated QD sizes using the Debye Scherrer equation in XRD. It was also observed that the energy band gap decreases with increasing QD size confirming the notion that QD size and band gap can be tuned by controlling the reaction temperature. Moreover, we also observed colour

changes in QDs synthesised at different temperatures, indicating the difference in QD size as temperature was increased.

5.7. Recommendations

Even though high quality CdSe QDs have been synthesised since the early 90s by the hot injection method, the use of extremely toxic materials during the synthesis process and difficulty in achieving precise reaction conditions motivates for exploring more user friendly approaches to make QDs. Generally, CdSe QDs have already proven to have numerous applications in many different fields. Still, many aspects of this material need to be explored in order to make them more suitable for more specific applications like solar cells. Some of these explorations include investigating its purity, tuning the core thickness of the QD in order to make them emit in certain wavelengths. Some of the aspects in this work that can be further explored is capping the QD with another semiconductor which will influence the overall optical and structural properties of the final QD. Thus, investigating the effect of using a semiconductor to coat CdSe QDs on the overall properties of the QD is recommended. Additionally, it was found from the HRTEM and XRD analysis that CdSe QDs size can be tuned and from UV-Vis results that CdSe QDs absorb in the useful region of the solar spectrum. For future work, the fabrication and characterisation of a quantum dot solar cell (QDSSC) using CdSe QDs as the absorber is recommended so we can evaluate the electrical properties of the solar cell device.

Appendix A
Research Outputs

The appendix presents a list of research outputs of the candidate which includes local poster presentations, oral presentations as well as future conferences that are going to come from this work.

A.1. Presented Abstracts

The candidate has attended and presented at the following conferences:

1. S. Makinana, R Taziwa and E Meyer (**2016**). Synthesis and Characterization of Cadmium Selenide quantum dots (QDs) for QDs sensitized solar cells. *Renewable and Sustainable Energy Symposium REPS 2016*, University of Fort Hare, 5^{th}-8^{th} September 2016.
2. Sinovuyo Makinana, Raymond Taziwa and Edson Meyer (**2017**), Synthesis and Characterisation of Cadmium Selenide Quantum Dots. *62^{nd} annual conference of the South Africa Institute of Physics, University of Stellenbosch*, South Africa. 03-07 July 2017.
3. Sinovuyo Makinana, Edson Meyer and Raymond Taziwa (**2017**), Morphological, Structural and Optical Characterization of CdSe Quantum Dots. *8^{th} Renewable and Sustainable Energy Symposium*, Stellenbosch University, South Africa. 12-14July, 2017.

A.3. Manuscripts in progress of peer reviewed journals

1. Sinovuyo Makinana, Raymond Taziwa, Edson Meyer and Omobola Okoh. *Synthesis and Characterisation of Cadmium Selenide Quantum Dots*. Journal of Materials Science and Technology. (**2017**).

A.4. Published Abstracts

VA3–09: Synthesis and Characterization of Cadmium Selenide quantum dots (QDs) for QDs sensitized solar cells (M)

Sinovuyo Makinana[1,2], E Meyer[1], R Taziwa[1,2], and O. Okoh[1,2]
[1]Fort Hare Institute of Technology, University of Fort Hare, Alice
[2]Chemistry Department, University of Fort Hare, Alice

Abstract: Efforts to design ordered nano-structures, paved the way for designing next generation solar cells devices. Quantum dots (QDs) such as CdSe can also serve as sensitizers because they can transfer electrons to wide semiconductors such as TiO_2. Anchoring QDs onto TiO_2 is a very important strategy to enhance solar efficiency of Gräztel type of solar cell to beyond 13%. This work focuses on synthesis and characterization of CdSe QDs. CdSe QDs have been synthesized using 2-mercaptoethanol as a capping agent employing cadmium acetate as Cd precursor and selenium powder as selenide precursor. Structural and Optical properties of the synthesized QDs have been evaluated using SEM, XRD, FTIR, RS, UV-Vis and HRTEM. FTIR analysis has revealed that the fabricated QDs are capped with mercapto group in which it is shown by the – SH stretch along the 2620-2550 range. SEM and TEM analysis has revealed that the synthesized QDs are spherical in nature with a particle size range of 2.1 – 6.5 nm. UV-Vis spectra revealed different absorption properties for the fabricated QDs.
Keywords: Nano-structures, Quantum dots, CdSe, Solar cells

Poster Session 2 - Board 16 / 323

Synthesis and Characterization of Cadmium Selenide Quantum Dots

Author: Ms. MAKINANA, Sinovuyo [1]

Co-Authors: Prof. MEYER, Edson [1]; Dr. TAZIWA, Raymond [1]

[1] *1Fort Hare Institute of Technology (FHIT), University of Fort Hare, Private Bag X1314, Alice, 5700, Republic of South Africa. 2Chemistry department, University of Fort Hare, Private Bag X1314, Alice, 5700, Republic of South Africa*

Corresponding Author: sinovuyomakinana@gmail.com

CdSe quantum dots (QDs) with different particle sizes were successfully synthesized using the hot-injection method. The CdSe QDS were synthesized by reacting cadmium acetate dihydrate [Cd (CH3COO) 2·2H2O] and selenium (Se) powder in the presence of 2-mercaptoethanol as the capping agent. CdSe QDs of different crystallite sizes were prepared at different reaction temperatures of 150°C to 175°C, 200°C, 225°C, 250°C, 275°C and 300°C.The morphological, structural and optical properties of the as synthesized CdSe QDs were evaluated using SEM, XRD, HRTEM, and UV-Vis spectroscopy. From the UV-Vis, it was found that the crystallite size of CdSe QDs increases with the increase in reaction temperatures. The Kippeny method was used to calculate the crystallite size of CdSe QDs and it was found to be in the range of 0.82 – 2.46 nm. Furthermore, the data analysis has revealed that CdSe QDs crystallite size is dependent upon the reaction temperature.

8th RENEWABLE ENERGY POSTGRADUATE SYMPOSIUM

and

5th Annual STERG SolarPACES SYMPOSIUM

Programme

12, 13, 14 JULY 2017

Knowledge Centre, Faculty of Engineering
Stellenbosch University

STERG
SOLAR THERMAL ENERGY RESEARCH GROUP

science & technology

National Research Foundation

08h00 - 08h30	Registration, Tea & Coffee	
	Session 1 – Solar PV **Chair: Prof E van Dyk – Room: K302**	
08h30 - 08h45	Opening Session	Prof JL van Niekerk
08h45 - 09h15	*Keynote Address* - An insight into the future of the Centre for Renewable and Sustainable Energy Studies at Stellenbosch University	Prof S Mamphweli
09h15 - 09h30	Questions/discussion	
09h30 - 09h50	Application of Genetic Algorithm Parameter Optimisation on Current-Voltage data of poly-crystalline Silicon solar cells	RM Dix-Peek
09h50 - 10h10	Confocal Raman characterization of sputter coated TiO2 nanotubes on functional substrate	S Zinya
10h10 - 10h30	Synthesis and characterization of C-TIO2 nanotubes using a template-assisted sol-gel technique.	N Takata
10h30 - 10h50	Morphological, Structural and Optical Characterization of CdSe quantum dots	S Makinana
10h50 - 11h10	Mono-crystalline silicon cell degradion analysis	G Osayemwenre
11h10 - 11h30	Tea & Coffee	
	Session 2 – Solar thermal **Chair: Prof S Mamphweli – Room: K302**	
11h30 - 11h50	Correlative data Acquisition System for a building integrated Photovoltaic system	C Buma